NASA CONTRACTOR REPORT

NASA-CR-128

NASA CR-284

INTEGRAL METHODS IN COMPRESSIBLE LAMINAR BOUNDARY LAYERS AND THEIR APPLICATION TO HYPERSONIC PRESSURE INTERACTIONS

by Yat-Yung Chan

Prepared under Grant No. NsG-633 *by*
UNIVERSITY OF TORONTO
Toronto, Canada
for

NATIONAL AERONAUTICS AND SPACE ADMINISTRATION • WASHINGTON, D. C. • SEPTEMBER 1965

NASA CR-284

INTEGRAL METHODS IN COMPRESSIBLE LAMINAR BOUNDARY LAYERS AND THEIR APPLICATION TO HYPERSONIC PRESSURE INTERACTIONS

By Yat-Yung Chan

Prepared under Grant No. NsG-633 by
UNIVERSITY OF TORONTO
Toronto, Canada

for

NATIONAL AERONAUTICS AND SPACE ADMINISTRATION

For sale by the Clearinghouse for Federal Scientific and Technical Information
Springfield, Virginia 22151 – Price $3.00

SUMMARY

A method is presented for calculating the properties of compressible laminar boundary layers with heat transfer and arbitrary pressure gradients. The method is based on the concept of combining integral relations and similarity solutions. It differs, however, from the classical technique in that both the momentum and the energy integral equations are used.

The method is applied to calculate the self-induced pressure interaction problem in hypersonic flows. The solutions cover the complete range of interaction and show good agreement with other more exact theoretical results as well as experimental data.

The pressure interaction problem is also considered for real gases using weakly dissociated boundary layers. Calculations are presented for a flat plate with a fully catalytic surface in a stream of oxygen. The results show that under these conditions the boundary layer characteristics vary only slightly from the perfect gas case.

TABLE OF CONTENTS

		Page
	NOTATION	vii
1.	INTRODUCTION	1
2.	INTEGRAL METHOD FOR TWO-DIMENSIONAL AND AXI-SYMMETRIC LAMINAR BOUNDARY LAYERS IN COMPRESSIBLE FLOWS	3
	2.1 Boundary Layer Equations	3
	2.2 Transformation	4
	2.3 Integral Equations	6
	2.4 Methods of Solution	7
	2.5 Method of One-Parameter Correlation	9
	2.5.1 Correlation Parameters and Reduced Integral Equation	9
	2.5.2 Two-Dimensional Flows	10
	2.5.3 Axisymmetric Flows	13
3.	APPLICATION TO HYPERSONIC LAMINAR BOUNDARY LAYERS	14
	3.1 Basic Equations	14
	3.2 Displacement Thickness	15
	3.3 Skin Friction Coefficient and Heat Transfer Coefficient	16
4.	HYPERSONIC LEADING EDGE SELF-INDUCED PRESSURE INTERACTION	17
	4.1 Fundamental Equations for Boundary Layer and Inviscid Flow	17
	4.2 Asymptotic Solutions	20
	4.3 Complete Solutions and Examples	23
	4.4 Axisymmetric Flows	25
5.	HYPERSONIC LEADING EDGE SELF-INDUCED PRESSURE INTERACTION WITH WEAK DISSOCIATION AND INFINITE CATALYCITY	26
	5.1 Introduction and Assumption	26
	5.2 Boundary Layer Equations	28
	5.3 Chemical Reaction Term	31
	5.4 Skin Friction, Heat Transfer, and Displacement Thickness	33
	5.5 Method of Solution	35
	5.6 Boundary Layer Self-Induced Pressure	40
	5.7 Example and Discussion	41

6. CONCLUDING REMARKS 44

REFERENCES 46

TABLES

FIGURES

APPENDIX A: Momentum Integral Method A1

APPENDIX B: Solution of the Pressure Interaction Problem by Iteration B1

APPENDIX C: Method of Local Similarity C1

NOTATION

a_n	coefficient of polynomial velocity profile (Eq. 5.41a)
$\overline{A}$	value of $\overline{L}$ at $\overline{m} = 0$ (A.7)
A	value of L at m = 0 (2.29)
b_n	coefficient of polynomial partial enthalpy profile (5.41b)
$\overline{B}$	slope of linearized $\overline{L} \sim \overline{m}$ relation (A.7)
B	slope of linearized $L \sim m$ relation (2.29)
B'	$\frac{He}{he} B$ (2.31)
c_n	coefficient of polynomial atom mass fraction profile (5.41c)
C	constant in linear viscosity - temperature relation $\frac{\mu_b}{\mu_\infty} = C \frac{T_b}{T_\infty}$ (3.6)
c_A	atom mass fraction (5.4)
c_e	atom mass fraction at external stream (5.5)
c_E	atom mass fraction at equilibrium (5.25)
C_p	specific heat at constant pressure
C_f	skin friction coefficient (3.7)
C_h	heat transfer coefficient (3.9)
D_{12}	binary diffusion coefficient (5.3)
f	dimensionless stream function variable defining velocity boundary layer (2.8)
G	transverse curvature parameter (2.38)
g	dimensionless total enthalpy, H/He (2.8)
h	specific enthalpy (per unit mass)
h_A^o	specific dissociation energy of atomic products (5.12a)
H	specific total enthalpy

H_T	specific partial enthalpy (5. 15)
H_F	boundary layer form factor Δ/θ (2. 22)
I	integral defined (5. 59a)
j	integer specifying number of dimensions (2. 1) (j = 0 two-dimensional case, j = 1 axisymmetric case)
k	thermal conductivity
k_d	dissociation rate constant (5. 21)
k_r	recombination rate constant (5. 21)
K	hypersonic similarity parameter (4. 10)
K_c	equilibrium constant based on mass concentration $K_c = kd/kr$ (5. 25)
K_p	equilibrium constant based on partial pressure (5. 27)
l	skin friction correlation parameter (2. 25)
Le	Lewis-Semenov number (5. 3)
$\overline{L}$	correlation parameter (A. 6)
L	correlation parameter (2. 28)
$\overline{m}$	velocity gradient parameter defined in (A. 1)
m	velocity gradient parameter (2. 24)
m_A	mass of atom (5. 23)
M	local Mach number
N	ratio $\frac{\rho\mu}{\rho_b\mu_b}$ (2. 11)
n	exponent in pressure relation $p \propto x^n$
P	pressure ratio p_e/p_s (2. 34)
p	pressure
P_r	Prandtl number
$\dot{q}$	heat transfer rate to body (3. 9)

Q	ratio of enthalpy defect thickness to momentum thickness $\bar{\Lambda}/\theta$ (2.23)
r	distance from axis in axisymmetric problems (2.1)
$\bar{r}$	heat transfer correlation parameter (2.26)
$\mathcal{R}$	universal gas constant
R	gas constant per unit mass
Re	Reynolds number
T	absolute temperature
t	characteristic chemical reaction time (5.30)
u	velocity component in x direction (2.1)
v	velocity component in y direction (2.1)
$\dot{w}$	mass production rate in dissociating flow (5.4)
x	boundary layer coordinate, distance along the surface (2.1)
y	boundary layer coordinate, distance normal to the surface (2.1)
z	atom mass fraction ratio $\frac{c_A}{c_e}$ (5.11)
$\bar{\alpha}$	exponent in the integral equation for $\bar{m}$ (A.13)
α	exponent in the integral equation for m (2.34)
$\bar{\beta}$	exponent in the integral equation for $\bar{m}$ (A.13)
β	exponent in the integral equation for m (2.33)
γ	specific heat ratio $\frac{c_p}{c_v}$
Γ	parameter governing transverse curvature in axisymmetric problem (2.12)
$\bar{\delta}$	transformed boundary layer thickness (5.41b)
δ^*	boundary layer displacement thickness (3.4)
Δ^*	dimensionless displacement thickness (4.6)

Δ	transformed displacement thickness (2.14a)
$\bar{\Delta}$	thickness defined in (5.20)
ζ	dimensionless η coordinate, $\frac{\eta}{\delta}$ (5.41a)
η	transformed y coordinate (2.7a)
θ	local angle of flow inclination (2.12)
Θ	transformed momentum thickness (2.14b)
$\varkappa$	parameter for temperature field (p. 11)
λ	parameter for velocity field (p. 11)
$\bar{\lambda}$	pressure distribution parameter (C.5)
Λ	transformed enthalpy defect thickness (2.14c)
$\bar{\Lambda}$	modified enthalpy defect thickness (2.18)
μ	viscosity coefficient
ξ	transformed x coordinate (2.7a)
ρ	density
σ	characteristic ratio of flow time to reaction time (5.30)
τ_b	shear stress on wall (3.7)
$\bar{\chi}$	hypersonic viscous interaction parameter (4.5)
ω	exponent for viscosity $\propto$ temperature relation $\mu \propto T^{\omega}$

Subscripts

A	atom
b	conditions at body surface
c	conditions at cone surface in an inviscid flow
e	conditions at the outer edge of the boundary layer
o	reference conditions
s	stagnation condition
∞	free stream condition

1. INTRODUCTION

The development of boundary layer theory has continued since it was first introduced by Prandtl in 1904. The theory allows one to obtain approximate solutions to the Navier-Stokes equations for the viscous flow around moving bodies. The flow field around a body is divided into two parts. In the external part, the effect of the viscosity of the fluid is neglected and the Navier-Stokes equations reduce to the Euler equations. In the inner part of the flow field, which is called the boundary layer, viscosity has a strong influence; but certain terms in the Navier-Stokes equations can be neglected to give the boundary layer equations. At high Reynolds numbers the boundary layer is very thin and the displacement of the external flow is negligible. This enables one to solve for the external flow field over the body by means of the Euler equations. These solutions are then used as external boundary conditions for the boundary layer equations. The boundary layer equations are still complex; they are a set of nonlinear partial differential equations.

In practical engineering applications, boundary layer theory provides a method for predicting with accuracy the shear stress and the heat transfer at the surface of bodies moving in fluids. It also provides an explanation of the mechanism of flow separation. Because of its usefulness in practice and its mathematical complexity, boundary layer theory is still one of the most interesting subjects in the field of fluid mechanics.

Thorough discussions of boundary layer theory are given in many standard works (for instance, Refs. 5 to 9). Due to the great mathematical difficulties encountered in solving the boundary layer equations, especially when the effects of compressibility, pressure gradients, and heat transfer are included, only very few precise numerical solutions have been obtained. Under certain conditions, such as specific types of free-stream pressure or surface temperature distributions, the boundary layer equations can be reduced to a system of ordinary differential equations by means of a similarity transformation. These are called similar solutions.

Because of the difficulties in obtaining exact solutions for general conditions and because similar solutions are restricted to certain specific types of conditions, approximate methods have been developed. A class of such methods is based on von Karman's momentum integral. These integral methods make certain assumptions as to the form of the unknown functions, which reduces the problem to solution of a set of ordinary differential equations. Pohlhausen developed a method for incompressible flow by assuming a quartic velocity profile. By satisfying suitable boundary conditions at the wall, the velocity profile is reduced to a function of one independent parameter. The x dependency of this parameter is then determined by solving the von Karman momentum integral equation .

This method can also be extended to the compressible boundary layer. In this case, the energy equation is also introduced in the

integral form. Similarly, a simple polynomial profile of the total enthalpy is assumed. Each of the boundary layer profiles are then reduced to a function of one independent parameter by satisfying the boundary conditions. These parameters are then determined by the simultaneous solutions of the two integral equations.

The concept of the combination of the integral method and similar solutions was first introduced by Thwaites (Ref. 1) for the case of incompressible flow with an arbitrary pressure gradient. His approach was to obtain a functional relationship between the shear stress at the wall, the local pressure gradient and the ratio of displacement thickness to momentum thickness. Instead of assuming a type of profile for the unknown functions, this relationship was obtained from the known incompressible similar solutions.

Rott and Crabtree (Ref. 2) have extended this concept to the case of compressible flow over an insulated body, and Cohen and Reshotko (Ref. 3) to the case of bodies with heat transfer. These two works are essentially applications of the classical momentum-integral technique. In the case of bodies with heat transfer, the consequence of this approach is that the momentum-integral equation and energy-integral equation cannot be satisfied simultaneously, and the energy equation is usually ignored. The heat transfer is obtained from the similar solutions through the correlation parameter which is determined from the momentum integral equation alone. The energy integral equation could also be used, however, the two answers disagree in general. With the energy integral equation ignored, in certain circumstances, the method may give the velocity field accurately while predicting the temperature field with only low accuracy.

In order to improve the accuracy of the computation of heat transfer, the energy integral equation must also be considered in the formulation of the integral relations. The first portion of this paper is concerned with developing such a method. The present approach is still based on the simple one-parameter correlation concept. However, the energy integral equation is considered simultaneously with the momentum integral equation such that the variation of the ratio of the energy defect thickness to momentum defect thickness, which has a strong effect on the computation of heat transfer, is taken into account. The results show that higher accuracy is obtained in predicting heat transfer from the leading edge to the separation point. However, the skin friction coefficient is predicted with greater accuracy towards the leading edge but the values are poorer near the separation point than those obtained from the momentum integral alone.

The present method is then applied to calculate the self-induced pressure interaction problem in hypersonic flows. The pressure interaction between the viscous boundary layer and the inviscid flow on a body moving at hypersonic speeds results from the relatively large outward streamline deflection induced by a thick boundary layer. The present

integral method makes it possible to construct a solution which is valid through the complete interaction range.

In high-speed boundary-layer flow, the temperature inside the boundary layer may become very high because of the large viscous dissipation and real gas effects can thus alter the properties of the flow. The effects of a weakly dissociating diatomic gas like oxygen are examined for the pressure-interaction problem on a fully catalytic flat plate. It is found that under these conditions the boundary layer properties depart only slightly from those of a perfect gas.

2. INTEGRAL METHOD FOR TWO-DIMENSIONAL AND AXISYMMETRIC LAMINAR BOUNDARY LAYERS IN COMPRESSIBLE FLOWS

2.1 Boundary Layer Equations

Consider the steady flow of a perfect gas over an unyawed body, using the coordinate system (x, y) where x is measured along the body surface from the nose or leading edge and y is measured along the outward normal from the body surface. Making the usual assumption that the boundary layer thickness is small compared to the longitudinal body radius of curvature and that the centrifugal forces are negligible, the equations of the steady, compressible laminar boundary layer for a perfect gas are

Continuity:

$$\frac{\partial \rho u r^j}{\partial x} + \frac{\partial \rho v r^j}{\partial y} = 0 \tag{2.1}$$

x - Momentum:

$$\rho u \frac{\partial u}{\partial x} + \rho v \frac{\partial u}{\partial y} = -\frac{\partial p}{\partial x} + \frac{1}{r^j}\frac{\partial}{\partial y}\left(\mu r^j \frac{\partial u}{\partial y}\right) \tag{2.2}$$

y - Momentum:

$$\frac{\partial p}{\partial y} = 0 \tag{2.3}$$

Energy:

$$\rho u \frac{\partial H}{\partial x} + \rho v \frac{\partial H}{\partial y} = \frac{1}{r^j}\frac{\partial}{\partial y}\left(\frac{\mu}{Pr} r^j \frac{\partial H}{\partial y}\right) + \frac{1}{r^j}\frac{\partial}{\partial y}\left[\mu\left(1-\frac{1}{Pr}\right) r^j \frac{\partial}{\partial y}\left(\frac{u^2}{2}\right)\right] \tag{2.4}$$

where u and v denote the velocity components in the x and y directions, respectively and H is the total enthalpy,

$$H = h + \tfrac{1}{2}u^2$$

j = 0 is for two-dimensional flow and j = 1 for axisymmetric flow. The distance r = r (x, y) is the cylindrical radius from the axis of symmetry to any point in the boundary layer.

The gas is assumed to be thermally perfect. The equation of state is given by

$$\frac{p}{\rho} = RT \tag{2.5}$$

Equations (2.1) to (2.5) constitute the system of equations for steady, laminar-boundary-layer flow of a perfect gas over an unyawed body. These equations are similar to those appearing in Ref. 5, except that in the latter the radius r is approximated by r_b, the radius from the axis of symmetry to the body surface. The present equations contain transverse curvature terms specified by r for axisymmetric flows. (Refs. 25, 29.)

The boundary condition on the velocity at the wall follows from the requirement of no slip, and the temperature may satisfy the condition that there is no heat transfer at the wall, or the surface temperature may be specified. The low Reynolds number effects such as velocity slip and temperature jump on the surface are not considered. Hence at y = 0, without suction or blowing from the surface,

$$u = v = 0 \tag{2.6a}$$

and

either $\frac{\partial T}{\partial y} = 0$

or $T = T_b(x)$

At the outer edge of the boundary layer, the values of u and T are specified by the inviscid flow solution. Hence at $y = \infty$

$$u = u_e \tag{2.6b}$$

$$T = T_e$$

or $H = H_e$

2.2 Transformation

The transformation of coordinates which we introduce is the generalized form of the usual Lees-Levy-Dorodnitsyn transformation. The transformation can be written (Ref. 5, 25)

$$\xi(x) = \int_0^x \rho_b \mu_b u_e r_b^{2j}\, dx \tag{2.7a}$$

$$\eta(x,y) = \frac{u_e}{\sqrt{2\xi}} \int_0^y \rho r^j\, dy$$

from which

$$\frac{d\xi}{dx} = \rho_b \mu_b u_e r_b^{2j} \tag{2.7b}$$

$$\frac{\partial \eta}{\partial y} = \frac{\rho u_e r^j}{\sqrt{2\xi}}$$

We further define the following dimensionless quantities as dependent variables

$$f = \int_0 \frac{u}{u_e}\, d\eta \quad , \qquad \frac{\partial f}{\partial \eta} = \frac{u}{u_e}$$
$$g = \frac{H}{H_e} \tag{2.8}$$

Applying the coordinate transformation (2.7) and the non-dimensional quantities (2.8), and assuming that the Prandtl number is constant, the momentum and the energy equations can be transformed with the aid of the continuity equation into the form

$$\frac{\partial}{\partial \eta}\left(N\Gamma^j \frac{\partial^2 f}{\partial \eta^2}\right) + f\frac{\partial^2 f}{\partial \eta^2} + 2\,\frac{d\ln u_e}{d\ln \xi}\left[\frac{\rho_e}{\rho} - \left(\frac{\partial f}{\partial \eta}\right)^2\right] = 2\xi\left(\frac{\partial f}{\partial \eta}\frac{\partial^2 f}{\partial \eta \partial \xi} - \frac{\partial f}{\partial \xi}\frac{\partial^2 f}{\partial \eta^2}\right) \tag{2.9}$$

$$\frac{\partial}{\partial \eta}\left(\frac{N\Gamma^j}{Pr}\frac{\partial g}{\partial \eta}\right) + f\frac{\partial g}{\partial \eta} + \frac{u_e^2}{H_e}\frac{\partial}{\partial \eta}\left[N\Gamma^j\left(1-\frac{1}{Pr}\right)\frac{\partial f}{\partial \eta}\frac{\partial^2 f}{\partial \eta^2}\right] = 2\xi\left(\frac{\partial f}{\partial \eta}\frac{\partial g}{\partial \xi} - \frac{\partial f}{\partial \xi}\frac{\partial g}{\partial \eta}\right) \tag{2.10}$$

where

$$N = \frac{\rho\mu}{\rho_b \mu_b} \tag{2.11}$$

$$\Gamma = \frac{r^2}{r_b^2} = 1 + \frac{2\cos\theta\sqrt{2\xi}}{\rho_e u_e r_b^2}\int_0^y \frac{\rho_e}{\rho}\, d\eta \tag{2.12}$$

The function Γ which appears in the axisymmetric case governs the effect of transverse curvature and θ is the local slope of the body.

The boundary conditions are reduced to

$$f(0) = 0\,,$$
$$f_\eta(0) = 0\,, \tag{2.13a}$$

either $g(0) = g_b(\xi)$,

or $g_\eta(0) = 0$;

and $f_\eta \to 1$

$g \to 1$ at $\eta \to \infty$ (2.13b)

The subscript η indicates partial differentiation with respect to η .

Equations (2.9) to (2.12) are the fundamental equations for a compressible laminar boundary layer to be solved under the boundary conditions (2.13). They are in general nonlinear partial differential equations. Under certain mathematical restrictions, these equations can be reduced to ordinary differential equations. The solutions of the latter which show similitude under these restrictions are called similar solutions (Ref. 5). Similar solutions have been obtained for two-dimensional flows (for example, Ref. 10 and 14) and for axisymmetric flows (Ref. 25).

2.3 Integral Equations

We now formulate our approximation method using integral relations, following the classical concept of the von Karman momentum integral. If we integrate the transformed equations of momentum and energy (2.9) and (2.10), with respect to η through the boundary layer, and introduce the following integrals, namely the dimensionless displacement, momentum, and enthalpy-defect thicknesses respectively,

$$\Delta = \int_0^\infty (g - f_\eta)\, d\eta \tag{2.14a}$$

$$\Theta = \int_0^\infty f_\eta (1 - f_\eta)\, d\eta \tag{2.14b}$$

$$\Lambda = \int_0^\infty f_\eta (1 - g)\, d\eta \tag{2.14c}$$

we have

$$f_{\eta\eta_b} = \Theta + 2\xi \frac{d\Theta}{d\xi} + \frac{H_e}{h_e} \frac{2\xi}{u_e} \frac{du_e}{d\xi} (\Delta + \Theta) \tag{2.15}$$

$$\frac{g_{\eta_b}}{Pr} = \Lambda + 2\xi \frac{d\Lambda}{d\xi} \tag{2.16}$$

Here we have used the relation

$$\frac{\rho_e}{\rho} - f_\eta^2 = \frac{H_e}{h_e} (g - f_\eta^2) \tag{2.17}$$

which holds for a perfect gas.

For constant wall temperature distribution, the energy integral equation can be written as

$$\frac{1}{Pr}\frac{g_{\eta_b}}{1-g_b} = \bar{\Lambda} + 2\xi\frac{d\bar{\Lambda}}{d\xi} \tag{2.18}$$

where

$$\bar{\Lambda} = \int_0^\infty f_\eta \left(\frac{1-g}{1-g_b}\right) d\eta \tag{2.19}$$

Note: This is equivalent to define a new nondimensional variable for the enthalpy

$$I = \frac{H - H_b}{H_e - H_b}$$

and the energy integral equation becomes

$$\frac{I_{\eta_b}}{Pr} = \bar{\Lambda} + 2\xi\frac{d\bar{\Lambda}}{d\xi} \tag{2.18a}$$

with

$$\bar{\Lambda} = \int_0^\infty f_\eta I\, d\eta \tag{2.19a}$$

The integral equations, Eqs. (2.15) and (2.16) are exactly the same for two-dimensional flows and axisymmetric flows. The effect of transverse curvature for axisymmetric flows does not appear explicitly in the equations (Ref. 25).

2.4 Methods of Solution

The momentum and the energy equations in integrated forms are given by Eqs. (2.15) and (2.18) with thicknesses defined by Eq. (2.14). These two equations can be rewritten as follows

$$\frac{d}{d\xi}(\xi\Theta^2) = \Theta f_{\eta\eta_b} - \frac{H_e}{h_e}\frac{2\xi}{u_e}\frac{du_e}{d\xi}\Theta^2(1+H_F) \tag{2.20}$$

$$\frac{d}{d\xi}(\xi\bar{\Lambda}^2) = \frac{\bar{\Lambda}\, g_{\eta_b}}{Pr(1-g_b)} \tag{2.21}$$

The fundamental requirement for a solution of these two equations is a correlation for the terms on the right hand sides. If some relation is assumed, then these equations can be integrated. In Pohlhausen's method (Refs. 6, 8), the assumption of the forms of the velocity profile and the total enthalpy profile serves this purpose. By satisfying a suitable number of boundary conditions at the wall and at the edge of the boundary layer, each of these profiles can be reduced to a function of one independent parameter. Therefore, the correlations of the Eqs. (2.20) and (2.21) are now depended on two parameters, namely, λ for the velocity profile and κ for the total enthalpy profile. For any correlation

quantity Q, one can obtain a functional relation $Q(\lambda, \varkappa)$ as illustrated in the sketch in Fig. 1. Once these correlations are assumed, the Eqs. (2.20) and (2.21) can be solved simultaneously to yield a unique relation of λ and $\varkappa$. This relation is shown by the dashed line on the $Q(\lambda, \varkappa)$ surface in Fig. 1.

In Thwaites' method (Ref. 1), or the extension given by Cohen and Reshotko (Ref. 3), instead of assuming types of profiles, the functional relations from the exact similarity solutions determine the relations between λ and $\varkappa$. Thus for a specified surface temperature, a single curve results for the correlation $Q(\lambda, \varkappa)$ as shown in Fig. 1. If this correlation is applied to Eq. (2.20), or Eq. (2.21), only one equation is then required to obtain the ξ dependency of λ or $\varkappa$. This is the basic method of one-parameter correlation.

Though the one-parameter approach restricts the individual development of the parameters λ and $\varkappa$, however, it provides a simple method to solve the problem with reasonably high accuracy, especially for cases with favourable pressure gradients and cold walls (Ref. 3). For cases with adverse pressure gradients and heated walls, it still provides a fairly good first approximation to the two-parameter methods, such as the methods of Tani and Poots (Refs. 13 and 11). In view of these facts, the following discussion will be limited to the one-parameter method and its improvement.

The basic one-parameter approach of solving compressible laminar boundary layer equations is exemplified by the momentum integral method (Ref. 3), in which the momentum integral equation alone is used and the energy equation is ignored. The details of the formulation of this method is given in Appendix A. With the energy equation ignored, the resulting heat transfer is obtained from the correlation parameters which are derived from the similarity solutions. The energy integral equation, however, can also be used to compute heat transfer, and the results do not agree with that obtained from the foregoing correlation. It has been shown in Refs. 4 and 5 (see also Appendix A) that, only if the thicknesses $\bar{\Lambda}$ and Θ are proportional to each other over the entire range under consideration will these two results be consistent. In general, the ratio $\bar{\Lambda}/\Theta$ is not constant throughout the entire range and the variation of $\bar{\Lambda}/\Theta$ as a function of ξ will affect the computation of heat transfer. Hence if only the momentum integral equation is used then, in certain circumstances, the method may predict the velocity field with accuracy while the accuracy of the temperature field will suffer. The accuracy of predicting the heat transfer can indeed be improved if the variation of $\bar{\Lambda}/\Theta$ is taken into account. This can be done, within the basic approach of the one-parameter method, by considering both the momentum integral equation and the energy integral equation at the same time and derive a new correlation based on both equations, as will be shown subsequently.

2.5 Method of One-Parameter Correlation

2.5.1 Correlation Parameters and Reduced Integral Equation

The dimensionless parameters which are related to the terms appearing in the momentum integral Eq. (2.20) and the energy integral Eq. (2.21) can be defined and evaluated from the following expressions.

Ratio of displacement thickness to momentum thickness

$$H_F = \frac{\Delta}{\Theta} \tag{2.22}$$

Ratio of enthalpy-defect thickness to momentum thickness

$$Q = \frac{\bar{\Lambda}}{\Theta} \tag{2.23}$$

Velocity gradient parameter

$$m = \frac{He}{he}\frac{\xi}{ue}\frac{due}{d\xi}(\Theta^2 + \bar{\Lambda}^2) \tag{2.24}$$

Shear parameter

$$\ell = \Theta f_{\eta\eta b} \tag{2.25}$$

Heat transfer parameter

$$\bar{r} = \frac{\bar{\Lambda}}{Pr}\frac{g_{\eta b}}{1-g_b} \tag{2.26}$$

The correlation parameters defined above indicate the behaviour of the boundary layer. The velocity gradient parameter m relates the external flow conditions to that of the momentum defect and the enthalpy defect. The "shape" of the velocity field is indicated by the value of H_F. The relation between the momentum defect thickness and the enthalpy defect thickness are finally linked by the value of Q.

If the momentum integral equation (2.20) and the energy integral equation (2.21) are added together, we have

$$\Theta f_{\eta\eta b} + \frac{\bar{\Lambda}\, g_{\eta b}}{Pr(1-g_b)} = \frac{d}{d\xi}(\Theta^2\xi) + \frac{d}{d\xi}(\bar{\Lambda}^2\xi) + \frac{He}{he}\frac{2\xi}{ue}\frac{due}{d\xi}\Theta^2(1+H_F) \tag{2.27}$$

Substituting the correlation parameters into the resulting equations, we finally have the reduced integral equation

$$\frac{d}{d\xi}\left[(\Theta^2+\bar{\Lambda}^2)\xi\right] = L \tag{2.28}$$

where

$$L = \ell + \bar{r} - 2m\,\frac{1+H_F}{1+Q^2} \tag{2.28a}$$

This is the fundamental equation of the present approach. Its solution, resulting in a determination of the parameter m is the first stage in solving for the boundary layer characteristics. Then the parameter ℓ is used to determine the skin friction and the parameter $\bar{r}$ is used to determine the heat transfer. The use of parameters ℓ and $\bar{r}$ here means that this approach is still confined within the limit of the one-parameter correlation. Therefore the determination of skin friction and heat transfer depends solely on the prediction of the parameter m.

Since the integral equations Eqs. (2.20) and (2.21) are in the same form for both the two-dimensional and the axisymmetric flows, therefore Eq. (2.28) applies to both cases. However, the correlation parameters which are based on the solutions of Eqs. (2.9) and (2.10) will be different for two-dimensional and axisymmetric flows. In the following sections these two cases will be discussed separately.

2.5.2 Two-Dimensional Flows

The fundamental requirement for a solution of Eq. (2.28) is a relation between the parameters L and m. If some relation is assumed, then Eq. (2.28) can be integrated. In the one-parameter correlation method this functional relation is determined from the known similarity solutions. Based on the concept of correlation, it is assumed that the parameters ℓ, $\bar{r}$, H_F, and Q are functions of m and g_b only (Ref. 3).

Equation (2.28) can now be integrated to yield m as a function of the external flow distribution. If m is known at a given point on the surface, the boundary layer characteristics follow through the correlation parameters. Thus if $\ell(m)$ is a known function for the specified wall temperature, the wall shear is then obtained from the correlation Eq. (2.25). Similarly, if $\bar{r}(m)$ is known, the heat transfer can be found from the correlation Eq. (2.26).

The numerical techniques for integrating Eq. (2.28) were given in Refs. 1 and 3 and will not be repeated here. When the wall temperature is uniform, it is often possible to approximate the right hand side of Eq. (2.28) as a piecewise linear function of m, and an analytical solution of Eq. (2.28) is then possible (Ref. 1, 3).

If we write

$$L(m) = A - Bm \tag{2.29}$$

then by inserting Eqs. (2.29) and (2.24) into Eq. (2.28), a simple linear first order ordinary differential equation results.

$$\frac{d}{d\xi}\left(\frac{m u_e}{u_{e\xi}}\frac{h_e}{H_e}\right) = A - Bm \tag{2.30}$$

The equation (2.30) can be simply integrated to yield

$$m = \frac{H_e}{h_e}\frac{u_{e\xi}}{u_e}\left(\exp -\int_{u_0}^{u} B'\frac{du_e}{u_e}\right)\left[C + \int_{\xi_0}^{\xi} A\left(\exp\int_{u_0}^{u} B'\frac{du_e}{u_e}\right)d\xi\right] \tag{2.31}$$

where

$$B' = \frac{H_e}{h_e}B$$

The constant of integration C is determined at $\xi = \xi_0$ as

$$C = \left(\Theta_0^2 + \bar{\Lambda}_0^2\right)\xi_0 \tag{2.32}$$

If the integration starts from the leading edge of the body, then C = 0.

Thus for given external velocity and enthalpy distributions and if the values of A and B are known for a specific wall temperature, the value of m can be determined as a function of ξ from Eq. (2.31). The boundary layer characteristics follow immediately from the previously evaluated correlation parameters. Equation (2.31) in physical coordinates is in the form

$$m = -\frac{\gamma-1}{2r}\frac{1}{u_e}P^{-\alpha}\left(1-P^{\frac{\gamma-1}{\gamma}}\right)^{-\beta}\frac{dP}{dx}\left[\left(\Theta_0^2+\bar{\Lambda}_0^2\right)u_{e_0}x_0 P_0^{\alpha-1}\left(1-P_0^{\frac{\gamma-1}{\gamma}}\right)^{\beta-1} + \int_{x_0}^{x} A P^{\alpha-1}\left(1-P^{\frac{\gamma-1}{\gamma}}\right)^{\beta-1} u_e\, dx\right] \tag{2.33}$$

where
$$\alpha = 2 - \frac{\gamma-1}{2r}B$$
$$\beta = 1 + \frac{B}{2} \tag{2.34}$$
$$P = p_e/p_s .$$

In order to compare the results of the present approach with those of the momentum integral method, an example of a flow with an adverse pressure gradient on a heated surface is computed. The case chosen here was originally computed by Poots (Ref. 11). The exact numerical solution is given. In this case, the external temperature varies as

$$\frac{T_e}{T_\infty} = \frac{1 + \frac{\gamma-1}{2}M_\infty^2\left(1-\frac{1}{8}X\right)}{1+\frac{\gamma-1}{2}M_\infty^2} \tag{2.35}$$

and the external velocity varies as

$$\frac{u_e}{u_\infty} = \frac{a_e}{a_\infty}\left(1-\frac{1}{8}X\right) \tag{2.36}$$

where

$$\chi = \int_0^x \left(\frac{a_e}{a_\infty}\right)^{\frac{2\gamma-1}{\gamma-1}} dx \qquad (2.37)$$

with Pr = 1 and $H_b/H_\infty = 2$, i.e., a heated surface.

The correlation functions for this case are evaluated from the similarity solutions in Ref. 10 for Pr = 1 and the Chapman and Rubesin temperature - viscosity law. The correlation of the function L and m for the present approach is given in Fig. 2, and the correlation of $\bar{L}$ and $\bar{m}$ for the momentum integral method is shown in Fig. 3. The correlations for computation of skin friction and heat transfer are shown in Figs. 4a and 4b for both approaches. All these correlation functions are tabulated in Table I. The values of α and β defined in Eq. (2.34) are

$$\alpha = 1.90$$
$$\beta = 1.35$$

And the values of $\bar{\alpha}$ and $\bar{\beta}$ defined in Eq. (A.13) are

$$\bar{\alpha} = 1.286$$
$$\bar{\beta} = 3.50$$

These linear approximations for the correlations $L \sim m$, $\bar{L} \sim \bar{m}$ are chosen to give good over-all agreement for the entire range of adverse pressure gradients. In the case of L(m), the linear approximation is valid only to m = -.0228. Thus it is not possible to extend the computation to the separation point of the boundary layer. The case with reference Mach number, $M_\infty = 6$ is computed. The resulting skin friction and heat transfer as functions of the distance along the surface are shown in Fig. 5.

The exact numerical solutions computed in Ref. 11 are also shown in Fig. 5 for comparison. For the heat transfer results, the present approach gives a higher accuracy than the momentum integral method. The improvement in heat transfer is consistent with the discussion given in Section 2.4, i.e., the energy integral equation which takes into account of the variation of the ratio $\bar{\lambda}/\theta$ should also be considered.

For a small pressure gradient, that is, from the leading edge to about $x/x_s = 0.5$, the skin friction predicted using the present approach lies closely to the exact solution. As the pressure gradient increases and the separation point is approached, the predicted skin friction falls below the exact solution and becomes increasingly poorer, while that obtained by the moment integral method follows the exact solution closely. Since for the one-parameter method, the velocity field and the temperature field are bound together. Therefore an improvement of the heat transfer by "lowering" the heat transfer curve to the exact solution (see Fig. 5) may cause a similar "down drift" of the skin friction.

However, for application to vehicle in hypersonic flight, it is more important to predict heat transfer accurately rather than skin friction, because the drag of a hypersonic vehicle is caused mainly by the wave system which it generates, while that due to skin friction is relatively small. However, the heating of the surface of the vehicle affects the design of the entire structure. Consequently, method that will predict the heat transfer with high accuracy is well worth developing.

It should be realized that although the one-parameter correlation method indeed provides a good first approximation for cases with adverse pressure gradient, it is still rather arbitrary by its nature as discussed below. Firstly, it is well known in the work of incompressible boundary layers that the velocity field does not depend solely on the pressure gradient parameter m (or λ , as discussed in Section 2.4). Therefore, the correlation of L(m) does not necessarily provide the proper relation for every case (Ref. 7). Secondly, the velocity field and the temperature field should not be bound a priori, but should be allowed to develop separately. Thus a further improvement of the solution can only be done by relaxing all these restrictions as demonstrated by the two parameter methods (Refs. 13 and 11). It is also in doubt that the one-parameter correlation method can be applied to flows with a sudden change of pressure field preceded by a well developed boundary layer, such as some examples illustrated in Ref. 12. This is because the actual boundary layer cannot adjust itself quickly to behave like the similarity profiles which are used in the correlation. However, if the pressure gradient is favourable and is roughly linear, the use of the one-parameter correlation method should lead to results with high accuracy (Refs. 1, 3 and 7).

2.5.3 Axisymmetric Flows

For flows over an axisymmetric body, similar solutions of the boundary layer equation can be obtained in a similar way to those for two-dimensional flows but with one more mathematical constraint (Ref. 25). This condition appears in Eq. (2.12) and is directly related to the transverse curvature of the body. If the boundary layer is thin in comparison with the body radius, then Γ is approximately equal to unity. If Γ is approximated by unity, which is usual for general boundary-layer flows except those over an extremely slender body or at very high speed, then the equations of axisymmetric flow are in the same form as the two-dimensional ones. The results obtained from the two-dimensional equations can be applied to the axisymmetric case through a coordinate transformation (Ref. 6, 7).

If $\Gamma > 1$, the boundary layer is not thin in comparison with the body radius, then the additional constraint for obtaining similar solutions is

$$G = \frac{2\sqrt{2\xi}\cos\theta}{\rho_e u_e r_b^2} = \text{constant} \qquad (2.38)$$

The correlation parameters now are also a function of G in addition to the original parameters m and g_b. Equation (2.28) can now be integrated for axisymmetric flow if both g_b and G are constant.

Some similar solutions for axisymmetric flows with $\Gamma > 1$ have been given in Ref. 25. However, the solutions were obtained only for some particular conditions which do not provide adequate details that can be used to evaluate correlation parameters. Hence axisymmetric flows considered in the following sections will be limited to cases with $\Gamma = 1$ only.

3. APPLICATION TO HYPERSONIC LAMINAR BOUNDARY LAYERS

3.1 Basic Equations

For a slender body moving at hypersonic speed, the flow field outside the body can be divided into three regions: (1) in front of the shock wave extending from the leading edge or nose of the body, the flow is undisturbed; (2) a boundary layer of viscous flow on the surface of the body; (3) in between the shock wave and the boundary layer there exists a layer of inviscid flow. We will consider the body to be thin and the hypersonic small-disturbance theory applies to the inviscid flow outside the boundary layer.

The method developed in the previous section can be readily applied to compute hypersonic laminar boundary layers. The following formulation is for two-dimensional flows. (It will be specified if axisymmetric flows are considered.)

In hypersonic flow the following conditions apply,

$$\frac{\gamma-1}{2} M_\infty^2 \gg 1 \tag{3.1}$$

and for flow over a slender body,

$$u_e \simeq u_\infty \tag{3.2}$$

With these approximations Eq. (2.33) for calculating the velocity gradient parameter m can be reduced to the following form with the integration starting from the leading edge of the body.

$$m = -\frac{\gamma-1}{2r} A \left[\frac{d}{dx}\left(\frac{p_e}{p_\infty}\right)\right]\left(\frac{p_e}{p_\infty}\right)^{-\alpha}\int_0 \left(\frac{p_e}{p_\infty}\right)^{\alpha-1} dx \tag{3.3}$$

where

$$\alpha = 2 - \frac{\gamma-1}{2r} B$$

Equation (3.3) is now in terms of physical coordinates which is useful for practical problems.

The correlation parameters m, ℓ , $\bar{r}$, H_F and Q defined in Eqs. (2.22) to (2.26) are now evaluated from the similarity solutions of Ref. 14. These similar solutions are obtained under the conditions that the Prandtl number is 0.7 and in the limiting situation of a locally hypersonic flow where $u_e^2/2H_e \to 1$. The power law relation for viscosity and temperature is employed with $\omega = 0.7$. It has been shown recently that the Pr = 1 solutions do not represent closely an actual fluid flow especially in predicting the heat transfer, which is particularly important in practical applications to high speed flow (Ref. 15).

The quantities m, ℓ , $\bar{r}$, H_F and Q are listed in Table II. Additional parameters $\frac{(1+H_F)^2}{1+Q^2}$, $\frac{\sqrt{1+Q^2}}{Q}\bar{r}$, and C_f/C_h are also listed. These will be used for computation of displacement thickness, heat transfer and skin friction respectively in Sec. 3. These quantities are also plotted in Figs. 6 to 10.

The quantities A, B and α are evaluated from the correlation parameters given in Sec. 2.5.1 and are listed in Table III. For a given pressure distribution, if we know the value of A and α for the specified surface temperature, Eq. (3.3) will yield the value of m as function of x. In the following we will derive some boundary layer characteristics and the expressions for calculating skin friction and heat transfer.

3.2 Displacement Thickness

The displacement thickness plays a dominant role in some of the hypersonic boundary layer problems such as the self-induced pressure interaction. It is defined by

$$\delta^* = \int_0^\infty \left(1 - \frac{\rho u}{\rho_e u_e}\right) dy \tag{3.4}$$

Through the coordinate transformation and the integral thicknesses defined by Eq. (2.14) we can write

$$\delta^* = \frac{\sqrt{2\xi}}{\rho_e u_e} \frac{H_e}{h_e} \left[(\Delta + \Theta) - \frac{h_e}{H_e}\Theta\right] \tag{3.5}$$

Since in hypersonic flow, $\frac{H_e}{h_e} \gg 1$

therefore δ^* can be approximated as

$$\delta^* = \frac{\sqrt{2\xi}}{\rho_e u_e} \frac{H_e}{h_e} (\Delta + \Theta) \tag{3.5a}$$

This is the expression we will use for all computations. From Eq. (3.3) and the definition of m and H_F, Eq. (3.5) can be reduced to the form in physical coordinates

$$\delta^{*2} = \frac{C \times M_\infty^4}{Re_{x\infty}} \frac{(\gamma-1)^2}{2} A \frac{(1+H_F)^2}{1+Q^2} \left(\frac{\rho_e}{\rho_\infty}\right)^{-\alpha} \int_0^x \left(\frac{\rho_e}{\rho_\infty}\right)^{\alpha-1} dx \tag{3.6}$$

where

$$Re_{x\infty} = \frac{\rho_\infty u_\infty x}{\mu_\infty}$$

and

$$\frac{\mu_b}{\mu_\infty} = C \frac{T_b}{T_\infty}$$

The quantity $(1 + H_F)^2 / 1 + Q^2$ can be evaluated from the correlation parameters once the value m(x) is known and the displacement thickness is completely determined. The values of this quantity are listed in Table II and are also plotted in Fig. 7.

3.3 Skin Friction Coefficient and Heat Transfer Coefficient

The skin friction coefficient is defined as

$$C_f = \frac{2\tau_b}{\rho_\infty u_\infty^2} \tag{3.7}$$

where τ_b is the shear stress on the surface of the body.

In the transformed coordinates, we can write

$$C_f = \mu_b \sqrt{\frac{2}{\xi}} \left(\frac{\rho_b}{\rho_\infty}\right)\left(\frac{u_e}{u_\infty}\right)^2 f_{\eta\eta b} \tag{3.8}$$

Using the hypersonic approximation and the correlation parameters, it can be expressed in the form

$$C_f = \frac{\sqrt{C}}{\sqrt{Re_{x\infty}}} \left(\frac{\gamma-1}{\gamma}\right)^{\frac{1}{2}} \left[-\chi \frac{d}{d\chi}\left(\frac{\rho_e}{\rho_\infty}\right)\right]^{\frac{1}{2}} \frac{1}{\sqrt{m}} \sqrt{1+Q^2}\, \ell \tag{3.8a}$$

The quantity $\sqrt{1+Q^2}\,\ell$ depends on m(x) for a specified surface temperature and can be determined from the previously tabulated parameters.

The heat transfer coefficient is defined by

$$C_h = \frac{-\dot{q}_b}{\rho_\infty u_\infty (H_\infty - H_b)} \tag{3.9}$$

where $\dot{q}_b$ is the rate of heat transfer to the surface of the body. In the transformed coordinates

$$C_h = \frac{1}{\sqrt{2\xi}} \left(\frac{\rho_b}{\rho_\infty}\right)\left(\frac{u_e}{u_\infty}\right) \frac{\mu_b}{Pr} \frac{g_{\eta b}}{1-g_b} \tag{3.10}$$

The final form in terms of the correlation parameters is thus

$$C_h = \frac{\sqrt{C}}{2\sqrt{Re_{x\infty}}} \left(\frac{\gamma-1}{\gamma}\right)^{\frac{1}{2}} \left[-\chi \frac{d}{d\chi}\left(\frac{p_e}{p_\infty}\right)\right]^{\frac{1}{2}} \frac{1}{\sqrt{m}} \frac{\sqrt{1+Q^2}}{Q} \bar{r} \qquad (3.10a)$$

Again the quantity $\left(\sqrt{1+Q^2}/\,Q\right)\bar{r}$ can be determined as a function of m(x) for a specified surface temperature.

A form similar to Reynolds' analogy can be written through the correlation parameters as

$$\frac{C_f}{C_h} = \frac{2\ell Q}{\bar{r}} \qquad (3.11)$$

Equations (3.10) and (3.11) give explicit expressions for the calculations of skin friction and heat transfer in a hypersonic boundary layer for a specified pressure distribution. The quantities $\sqrt{1+Q^2}\,\bar{r}/Q$ and C_f/C_h are evaluated from the correlation parameters and are plotted in Figs. 8 and 9 respectively for convenience.

4. HYPERSONIC LEADING EDGE SELF-INDUCED PRESSURE INTERACTION

4.1 Fundamental Equations for Boundary Layer and Inviscid Flow

The self-induced pressure interaction between the viscous and the inviscid flows on a slender body moving at hypersonic speed results from the relatively large outward streamline deflection induced by the thick boundary layer. At hypersonic speed, the boundary layer displacement thickness as shown in Eq. (3.6) is proportional to the reciprocal of the square root of the Reynolds number and to the square of the Mach number.

$$\delta^* \sim \frac{M_\infty^2 \chi}{\sqrt{Re_{x\infty}}}$$

If the free stream deflection can be approximated by the slope of the displacement thickness of the boundary layer, the flow angle θ_e

$$\theta_e \simeq \frac{d\delta^*}{d\chi} \sim \frac{M_\infty^2}{\sqrt{Re_{x\infty}}}$$

is thus proportional to the square of the Mach number. The induced pressure due to the flow deflection is of the order of $M_\infty \theta_e$ (Ref. 5), thus

$$p \sim \frac{M_\infty^3}{\sqrt{Re_{x\infty}}}$$

is proportional to the cube of the free-stream Mach number. Hence for hypersonic flow, even at high Reynolds number, the pressure induced by the thickness of the boundary layer is no longer negligible in general.

The self-induced pressure interaction can be divided into asymptotic regions, namely the strong and the weak intereactions (see sketch in Fig. 13). In the weak interaction region, the effects produced by the self-induced pressure gradient are essentially perturbations superimposed on an already existing uniform flow. The strong interaction region is characterized by the fact that the streamline inclinations induced by the viscous layer are large and the pressure gradient and viscous stress gradient terms are of the same order of magnitude. Thus the strong interaction region is close to the leading edge, while the weak interaction region is farther downstream. Between them there is an intermediate region in which the interaction is neither weak nor strong and the solutions are not of an asymptotic nature.

A number of papers have been published concerning the interaction problem. A complete discussion of this problem with a review of previous investigations is given in Ref. 5. Most of the previous investigations deal predominantly with the asymptotic regions using either perturbation or approximate methods to solve the boundary layer equations with the pressure gradient in these equations determined from the effective body shape. Solutions valid through the complete interaction range have been obtained by either numerical integration of the complete boundary layer equations (Refs. 19 and 20 for example) or by approximations such as the Karman-Pohlhausen method (Refs. 16 and 17) or the local-similarity method (Ref. 14). In the following section, an attempt is made to obtain an approximate solution of this problem valid through the whole range. By using the method developed in the previous sections it is possible to provide a simple formulation which will give a higher accuracy to the solution than the local-similarity method and with much less effort than the exact numerical solutions.

A flow model similar to the one described in Section 3.1 is used. The leading edge or the nose of the body is assumed to be sharp so that the effect of bluntness is negligible. We assume further that an effective body can be constructed, the thickness of which equals the sum of that of the original body and the displacement thickness of the boundary layer. The pressure field of the external inviscid flow is then determined by the effective body shape. This assumption of an effective body does not in fact match the viscous and the inviscid flows. It does, however, provide a good approximation (Ref. 5) and allows the viscous and the inviscid flows to be treated separately.

The equations developed in Section 3.1 and 3.2 can readily be applied to this problem. We rewrite the pressure gradient parameter m and the displacement thickness δ^* as

$$m = -\frac{\gamma-1}{2r} A \left[\frac{d}{dx}\left(\frac{p_e}{p_\infty}\right)\right]\left(\frac{p_e}{p_\infty}\right)^{-\alpha}\int_0^x \left(\frac{p_e}{p_\infty}\right)^{\alpha-1} d\alpha \qquad (4.1)$$

$$\delta^{*2} = \frac{C \times M_\infty^4}{Re_{x\infty}} \frac{(\gamma-1)^2}{2} A \frac{(1+H_F)^2}{1+Q^2} \left(\frac{p_e}{p_\infty}\right)^{-\alpha} \int_0^x \left(\frac{p_e}{p_\infty}\right)^{\alpha-1} dx \tag{4.2}$$

The tangent-wedge relation is used as the solution to the external inviscid flow because of its simplicity and the explicit relation between the local pressure and the local flow inclination. Hence the pressure distribution is known once the effective shape of the body is given. The tangent-wedge formula (Ref. 5) is given by

$$\frac{p_e}{p_\infty} = 1 + \gamma M_\infty^2 \theta_e^2 \left[\sqrt{\left(\frac{\gamma+1}{4}\right)^2 + \frac{1}{M_\infty^2 \theta_e^2}} + \frac{\gamma+1}{4} \right] \tag{4.3}$$

where θ_e is the local slope of the effective body which consists of the geometric slope and the gradient of the displacement thickness

$$\theta_e = \theta_b + \frac{d\delta^*}{dx} \tag{4.4}$$

This approximation without a centrifugal correction is accurate to order $(M_\infty \theta_e)^2$. Since the curvature of the outer edge of the boundary layer on a slender body is small, the centrifugal effect on the external flow is negligible throughout most part of the interaction range, except very close to the leading edge of the body.

In general, the shape of the slender body is specified with known surface temperature. Then we have to solve Eqs. (4.1), (4.2) and (4.3) simultaneously to obtain the pressure distribution and consequently the boundary layer properties.

Before we proceed to the solution of these equations, some parameters are introduced so that the equations will be in non-dimensional form. If we introduce the interaction parameter $\bar{\chi}$

$$\bar{\chi} = \frac{M_\infty^3 \sqrt{C}}{\sqrt{Re_{x\infty}}} \tag{4.5}$$

The nondimensional form of the displacement thickness is thus

$$\Delta^* = \frac{p_\infty u_\infty}{C \mu_\infty M_\infty^5} \delta^* \tag{4.6}$$

Equations (3.3) and (3.6) then reduce to

$$m = -\frac{\gamma-1}{2\gamma} A \left[\bar{\chi}^3 \frac{d}{d\bar{\chi}}\left(\frac{p_e}{p_\infty}\right)\right] \left(\frac{p_e}{p_\infty}\right)^{-\alpha} \int_{\bar{\chi}_0} \left(\frac{p_e}{p_\infty}\right)^{\alpha-1} \frac{d\bar{\chi}}{\bar{\chi}^3} \tag{4.7}$$

$$\Delta^{*2} = -(\gamma-1)^2 A \frac{(1+H_F)^2}{1+Q^2} \left(\frac{p_e}{p_\infty}\right)^{-\alpha} \int_{\bar{\chi}_0} \left(\frac{p_e}{p_\infty}\right)^{\alpha-1} \frac{d\bar{\chi}}{\bar{\chi}^3} \tag{4.8}$$

and the tangent-wedge relation becomes

$$-\frac{1}{2}\bar{\chi}^3\frac{d\Delta^*}{d\bar{\chi}}=\sqrt{\frac{2}{\gamma(\gamma+1)}}\frac{\frac{p_e}{p_\infty}-1}{\sqrt{\frac{p_e}{p_\infty}+\frac{\gamma-1}{\gamma+1}}} \tag{4.9}$$

This set of equations forms a complicated integro-differential system for the variables p_e/p_∞ and Δ^*, and prevents further attempts to obtain analytical solutions. However, these equations are in a form which lends itself to a successive approximation scheme. They also provide a direct and simple method to obtain solutions to the asymptotic regions.

4.2 Asymptotic Solutions

In the weak interaction region, the flow deflection resulting from the growth of the boundary layer is small. Under this condition, the local hypersonic similarity parameter K must be less than or of the order of one, where K is defined as

$$K=M_\infty\left(\theta_b+\frac{d\delta^*}{dx}\right) \tag{4.10}$$

If $K<1$, the induced pressure expressed by the tangent-wedge formula can be expanded in a series for small values of K (Ref. 5)

$$\frac{p_e}{p_\infty}=1+\gamma K+\frac{\gamma(\gamma+1)}{4}K^2+O(K^3) \tag{4.11}$$

For sufficiently small pressure gradients, Eq. (4.2) shows that

$$\frac{\delta^*}{x}\sim\frac{\gamma-1}{2}\frac{M_\infty^2\sqrt{C}}{\sqrt{Re_{x\infty}}}$$

Therefore for the weak interaction on a flat plate ($\theta_b = 0$), the hypersonic similarity parameter K is found to be proportional to the interaction parameter $\bar{\chi}$

$$K=M_\infty\frac{d\delta^*}{dx}\sim\frac{\gamma-1}{2}\frac{M_\infty^3\sqrt{C}}{\sqrt{Re_{x\infty}}}\sim\bar{\chi} \tag{4.12}$$

This permits an expansion of pressure in terms of $\bar{\chi}$ as

$$\frac{p_e}{p_\infty}=1+a_1\bar{\chi}+a_2\bar{\chi}^2+\cdots \tag{4.13}$$

The coefficient a_1 and a_2 can then be determined by the Eqs. (4.8) and (4.9) and yield

$$a_1=\frac{\gamma(\gamma-1)}{2}\frac{1+H_F}{\sqrt{1+Q^2}}\sqrt{\frac{A}{2}} \tag{4.14a}$$

$$b_1 = \frac{\gamma(\gamma+1)(\gamma-1)^2}{32}\frac{(1+H_F)^2}{1+Q^2}A \qquad (4.14b)$$

The value of $(1 + H_F)^2/(1 + Q^2)$ is taken at m = 0. This is done because this quantity is a slowly varying function of m as shown in Fig. 7. Thus an appropriate value within the asymptotic range of the problem may be chosen without introducing significant error.

In the strong interaction region, the flow deflection resulting from the growth of the boundary layer is significant, and $K^2 \gg 1$. The tangent-wedge formula can be expanded for large values of K as (Ref. 5)

$$\frac{p_e}{p_\infty} = \frac{\gamma(\gamma+1)}{2}K^2 + \frac{3\gamma+1}{\gamma+1} - \frac{8\gamma}{(\gamma+1)^3}\frac{1}{K^2} + O\left(\frac{1}{K^4}\right) \qquad (4.15)$$

The pressure variation at this region is close to $p \propto x^n$. Equation (4.2) shows for this condition that

$$\sqrt{\frac{p_e}{p_\infty}}\frac{\delta^*}{x} \sim \frac{\gamma-1}{2}\frac{M_\infty^2\sqrt{C}}{\sqrt{Re_{x\infty}}}$$

Since $p_e/p_\infty \sim K^2$, therefore for the strong interaction on a flat plate the hypersonic similarity parameter K is proportional to the square root of the interaction parameter

$$K \sim \bar{x}^{\frac{1}{2}} \qquad (4.16)$$

This shows that the pressure varies as $x^{-\frac{1}{2}}$ at the leading edge. Hence we expand the pressure distribution in a series for $\bar{x}$

$$\frac{p_e}{p_\infty} = a_2\bar{x} + b_2 + \frac{c_2}{\bar{x}} + \cdots \qquad (4.17)$$

The coefficients a_2, b_2, c_2, ... can then be determined from Eqs. (4.8) and (4.9) and yield

$$a_2 = \frac{3}{4}\frac{\sqrt{\gamma(\gamma+1)}(\gamma-1)}{\sqrt{3-\alpha}}\sqrt{\frac{A}{2}}\frac{1+H_F}{\sqrt{1+Q^2}} \qquad (4.18a)$$

$$b_2 = \frac{(\alpha-4)(3\gamma+1)}{(\alpha-9)(\gamma+1)} \qquad (4.18b)$$

Here again, the quantity $(1 + H_p)^2/(1 + Q^2)$ is evaluated at the value of m corresponding to $p \propto x^{-\frac{1}{2}}$.

These coefficients for both the weak and the strong interactions are evaluated for Pr = 0.7 and are listed in Table IV. Comparison is also made with results obtained by other authors.

Once the asymptotic solutions of the strong and the weak interaction is known, the skin friction and heat transfer can be computed immediately. The pressure gradient parameter m in Eq. (4.2) and the heat transfer coefficient in Eq. (3.6) are used for the computation. The results are shown in the following.

For weak interactions

$$m = \frac{\gamma-1}{2\gamma} A \left(\frac{1}{2} a_1 \bar{\chi} + b_1 \bar{\chi}^2 + \cdots \right) \tag{4.19}$$

$$M_\infty^3 C_h = \frac{1}{2} \left[\frac{\gamma-1}{2\gamma} \left(a_1 + 2 b_1 \bar{\chi} + \cdots \right) \bar{\chi}^3 \right]^{\frac{1}{2}} \frac{\sqrt{1+Q^2}}{Q} \bar{r} \frac{1}{\sqrt{m}} \tag{4.20}$$

For strong interactions

$$m = \frac{\gamma-1}{2\gamma} A \left[\frac{1}{3-\alpha} - \frac{3}{(4-\alpha)(3-\alpha)} \frac{b_2}{a_2} \frac{1}{\bar{\chi}} + \cdots \right] \tag{4.21}$$

$$M_\infty^3 C_h = \frac{1}{2} \left[\frac{\gamma-1}{2\gamma} \left(a_2 \bar{\chi}^3 \right) \right]^{\frac{1}{2}} \frac{\sqrt{1+Q^2}}{Q} \bar{r} \frac{1}{\sqrt{m}} \tag{4.22}$$

The quantity $\left(\sqrt{1+Q^2} / Q \right) \bar{r}$ is given in Fig. 8 as a function of m for different surface temperatures. The cross-plot of the linear approximation of this correlation against g_b is given in Fig. 12. The skin friction coefficient can be computed from the Reynolds analogy C_f/C_h using the values of m and $M_\infty^3 Ch$. The Reynolds analogy is given in Fig. 9.

It is interesting to note that the equilibrium wall temperature for an insulated plate is altered even to the first order in $\bar{\chi}$ in the weak interaction region. This was first pointed out in Ref. 18 (see also Ref. 9), and can be shown by the present approach. For flows with small pressure gradient, the equilibrium temperature on an insulated surface is related to the parameter m as (see Table II)

$$\frac{T_b}{T_o} = 0.819 - 0.65\, m \tag{4.23}$$

These values are evaluated from similar solutions in this report and a linear approximation is used for the correlation. For the weak interaction on a flat plate, the value of m is given in Eq. (4.19). Therefore, the variation of the equilibrium temperature on the surface of an insulated flat plate is

$$\frac{T_b}{T_o} = 0.819 - 0.65 \frac{\gamma-1}{2\gamma} A \left(\frac{1}{2} a_1 \bar{\chi} + b_1 \bar{\chi}^2 + \cdots \right) \tag{4.24}$$

For $\gamma = 1.4$, $Pr = 0.7$ and $\omega = 0.7$.

$$\frac{T_b}{T_o} = 0.819 - 0.0037\bar{\chi} + \cdots \qquad (4.25)$$

The result given by Ref. 18 is for Pr = 0.72 and $\omega = 1$

$$\frac{T_b}{T_o} = 0.848 - 0.005\bar{\chi} + \cdots$$

The slight difference in numerical value of these two results is due to the effect of the viscosity-temperature relationship.

4.3 Complete Solutions and Examples

In the previous sections the equations for calculating the displacement thickness and the pressure gradient parameter are formulated (see Eqs. 4.2 and 4.3). The tangent-wedge formula is used to govern the local pressure and flow inclination at the edge of the boundary layer. These equations are then solved numerically by an iteration scheme for different surface temperatures. The details of the numerical technique is given in Appendix B. These equations yield the pressure distribution and the pressure gradient parameter m as a function of the interaction parameter $\bar{\chi}$. Once these are known, the skin friction coefficients and the heat transfer coefficients follow immediately as described in the previous sections.

Several examples are calculated in order to compare the results obtained from the present method with experimental measurements and other theories.

The other theoretical results which we use for comparison are those due to Flügge-Lotz and Blottner (Ref. 19), who solved the boundary layer equations exactly by numerical methods. Like the present work they assumed an effective body and then used the tangent-wedge formula to compute the external local pressure. Their work was chosen for comparison because their flow model is the same as in this case, and the boundary layer solution is exact in their case.

Solutions in closed form can be obtained by combining the present integral method and the local similarity technique. The details of the derivations are given in Appendix C. The results obtained by this method are also shown in most cases for comparison.

Figure 14 shows a comparison of the surface pressure distribution on an insulated flat plate with a sharp leading edge with experimental data obtained by Kendall (Ref. 21) and Bertram (Ref. 22 and 23). Bertram's results obtained on a plate with a slight temperature gradient and heat transfer, and were corrected approximately to an insulated case. In general, the present results follow the trend of the experimental data closely and lie a little lower than the data. The asymptotic solutions obtained by the present method are also shown. The numerical solution by Flügge-

Lotz and Blottner gives higher values than the present solution. The local similarity solutions give lower values than the integral method. This deviation gets larger as the leading edge is approached, i.e., at large values of $\bar{\chi}$.

In Fig. 15, the pressure distribution on a cold flat plate obtained by the present method is compared with experimental measurement obtained by Hall and Golian (Ref. 24). The present results follow the experimental data closely, except near the leading edge where the predicted values are higher than the experimental data. It is interesting to note that the present solution nearly falls on the Flügge-Lotz and Blottner exact solution for Pr = 0.72. The solution using the local similarity method, like the previous case, predicts lower values than the integral method and becomes worse as the leading edge is approached. This is expected since the local similarity method is based on the assumption that $p \propto x^n$, and n is a constant locally. Thus, it neglects the upstream influence due to the change of the value of n. Since the displacement thickness increases as n decreases, (see Eq. (4.2), in this case, the pressure gradient is negative). The value of n is always larger upstream from the point under consideration. Therefore, the displacement thickness predicted by the local similarity method is smaller than the actual value. Consequently, the induced pressure due to the displacement effect is lower. However, since it provides a closed form solution and is simple to calculate, an approximate solution to the problem can readily be obtained if high accuracy is not required.

The skin friction coefficient for this case is shown in Fig. 16. Only the solution of Flügge-Lotz and Blottner is shown for comparison. No experimental data has been obtained for this case. Again, the present result agrees very well with the more exact solution.

The heat transfer coefficient for the same case is shown in Fig. 17. The experimental results were obtained by Hall and Golian in the same series of experiments. In general, the present results predict lower heat transfer rates than those obtained experimentally. The agreement with experiment is better at the strong and weak interaction regions. Beside the results of Flügge-Lotz and Blottner, the zero pressure gradient solution for Pr = 0.72 and Whalen's solution given in Ref. 24 for strong interaction are also shown. The present solution approaches these more exact solutions asymptotically. The solution using the local similarity method gives higher values than the integral method and thus lies closer to the experimental data. This interesting point was also illustrated in Ref. 14. This is again a consequence of the assumption of locally similarity flow which neglects any upstream influence. The heat transfer coefficient defined in Eq. (3.10) is proportional to the gradient of total enthalpy at the wall $g_{\eta b}$. This quantity is given explicitly by the energy integral Eq. (2.16),

$$\frac{g_{\eta b}}{Pr} = \Lambda \left[1 + \frac{2\xi}{\Lambda} \frac{d\Lambda}{d\xi} \right] \qquad (2.16)$$

With the local similarity assumption, the ξ dependency of Λ is neglected. Thus

$$\frac{g_{\eta b}}{P_r} = \Lambda \tag{4.26}$$

The error due to the omission of the second term in the right hand side of Eq. (2.16) can be estimated with the help of the similarity solutions as discussed in Appendix C. This term can be written in a similar way to Eq. (C.4),

$$\frac{\xi}{\Lambda}\frac{d\Lambda}{d\xi} = \left(\frac{\xi}{\beta}\frac{d\beta}{d\xi}\right)\left(\frac{\beta}{\Lambda}\frac{d\Lambda}{d\beta}\right) \tag{4.27}$$

Since the pressure gradient is decreasing from the leading edge, $d\beta/d\xi$ is negative. However, the similarity solutions show that $d\Lambda/d\beta$ is positive, (see Table II, where $\bar{r} = [\Lambda/(1-g_b)P_r]^2$) . Therefore, the term neglected in Eq. (2.16) is negative. Hence if the upstream influence is considered, the value of $g_{\eta b}$ will be smaller than that of the local similarity solutions. Therefore, the heat transfer calculation from the local similarity method will give higher values than the integral method and the other solutions in which the upstream influence is considered.

4.4 Axisymmetric Flows

In the previous discussion of axisymmetric flows, it was pointed out that a general formulation including transverse curvature effects cannot be obtained because of the inadequate number of similarity solutions for $\Gamma > 1$. Thus we are limited to deal with cases where Γ can be approximated by unity.

If $\Gamma = 1$, the axisymmetric equation can be reduced to the two-dimensional form through the well known Mangler transformation (Refs. 6 and 9). This transformation is a particular case of our original transformation (2.7a), if r is replaced by r_b, for the y coordinate transform. The main consequence of this transformation is that the assumption $r_b \gg \delta$ holds.

The pressure gradient parameter and the displacement thickness can be written in the form (for $\Gamma = 1$)

$$m = -\frac{\gamma-1}{2\gamma}\frac{A}{r_b^2}\left[\frac{d}{dx}\left(\frac{p_e}{p_\infty}\right)\right]\left(\frac{p_e}{p_\infty}\right)^{-\alpha}\int_0\left(\frac{p_e}{p_\infty}\right)^{\alpha-1} r_b^2\, dx \tag{4.28}$$

and

$$\delta^{*2} = \frac{C\chi M_\infty^4}{Re_\infty}\frac{(\gamma-1)^2}{2}\frac{A}{r_b^2}\frac{(1+H_F)^2}{1+Q^2}\left(\frac{p_e}{p_\infty}\right)^{-\alpha}\int_0\left(\frac{p_e}{p_\infty}\right)^{\alpha-1} r_b^2\, dx \tag{4.29}$$

The induced pressure due to the local flow inclination can be approximated by the tangent cone formula, if

$$K_e = M_\infty \theta_e = M_\infty \left(\theta_c + \frac{d\delta^*}{dx} \right) \tag{4.30}$$

where θ_c is the half cone angle. Then for $K_e \gg 1$, Lees' result for slender cones when the conical shock wave is not too far away from the cone surface can be used (Ref. 26)

$$\frac{p_e}{p_\infty} - 1 = \frac{2\gamma}{\gamma+1}\left(K_s^2 - 1\right) + \gamma\left(K_s - K_e\right)^2 \left[\frac{\gamma+1}{(\gamma-1) + \frac{2}{K_s^2}} \right] \tag{4.31a}$$

$$K_s = \frac{\gamma+1}{\gamma+3} K_e + \sqrt{\left(\frac{\gamma+1}{\gamma+3} K_e\right)^2 + \frac{2}{\gamma+3}} \tag{4.31b}$$

where $K_s = M_\infty \theta_s$ is the half angle of the conical shock and $K_e = M_\infty \theta_e$. The relation of K_s and K_e can be approximated by the form

$$\frac{K_s}{K_e} = \sqrt{\frac{\gamma+1}{2} + \frac{1}{K_e^2}} \tag{4.31c}$$

An example is shown in Fig. 18 in order to compare the theoretical prediction of heat transfer with experimental measurements obtain by Wittliff and Wilson (Ref. 28) on a 10° slender cone. The theoretical prediction in general lies lower than the average of the experimental data. For a slender cone at high Mach numbers, $M_\infty = 11 \sim 13$, this discrepancy can be accounted for as arising from the neglect of the transverse curvature effect. A correction based on the result of Probstein and Elliot (Ref. 29) for slender cones with zero pressure gradient is given as

$$M_c^3 C_h = M_c^3 C_{hm} \left\{ \left[0.517 + 0.913 \left(\frac{T_b}{T_c} \right) + 0.121 (\gamma-1) M_c^2 \right] \cdot \bar{\chi} \frac{1}{\sqrt{3} \tan\theta_c M_c^3} + 1 \right\} \tag{4.32}$$

where C_{hm} is the heat transfer coefficient obtained through the Mangler transformation. Strictly speaking, this result holds only for Pr = 1 (and zero pressure gradient), but is used here just to show the effect of transverse curvature. The corrected curve is also shown in Fig. 18.

5. HYPERSONIC LEADING EDGE SELF-INDUCED PRESSURE INTERACTION WITH WEAK DISSOCIATION AND INFINITE CATALYCITY

5.1 Introduction and Assumption

In hypersonic flight, real gas effects due to the inherent high temperatures begin to play an important role. Dissociation occurs, for instance, across the strong bow shock wave formed in front of a blunt body. The chemical reaction then carries on downstream into the boundary

layer and on to the surface of the body. The shock wave formed by a slender body, on the other hand, is not so strong that chemical reactions are likely to be present in the inviscid flow. The gas phase reaction present is predominantly that of dissociation in the boundary layer because of the high viscous dissipation. In the boundary layer, the relative magnitudes of the convection and reaction rates are generally different and their coupling is further complicated by diffusion of the chemical species. Thus one may expect that the boundary layer associated with these flows will exhibit varying degrees of chemical nonequilibrium.

Nonequilibrium boundary layer flows have been investigated by several authors. Chung and Anderson (Ref. 31) used integral methods and obtained solutions for dissociated oxygen over an adiabatic flat plate with a noncatalytic surface. Solutions obtained by numerical integration of the complete boundary layer equations were given by Blottner (Ref. 32). An analytical solution is given by Rae (Ref. 35) based on a perturbation of the frozen solution at the leading edge. This approach was later used by Inger (Ref. 36) to study a flat plate boundary layer with a self-induced pressure field and zero catalycity on the surface.

The presence of dissociation inside the boundary layer may change the properties of the boundary layer greatly from those with perfect gases. The energy distribution will be changed as the molecules are dissociated into atoms and energy is partitioned during the process. On the other hand, the self-induced pressure field may change the chemical process since the reaction rate is controlled both by temperature and pressure. This interplay between the pressure field and the nonequilibrium reaction may modify the aerodynamic heat transfer.

In this section, the integral method associated with the local similarity concept is used to examine the nonequilibrium boundary layer with a self-induced pressure field over a flat plate. The gas is assumed to be a diatomic gas mixture composed of atoms and molecules. The Prandtl number and the Lewis number are assumed constant. This assumption tends to break down for a highly dissociated gas because these parameters are affected strongly by dissociation. For a weakly dissociated gas, we further assume that the specific heat is approximately that of the molecules. Thermal diffusion is also assumed to be negligible. These assumptions appear to be a satisfactory engineering approximation in analyzing boundary layer flow over a non-ablating and highly cooled surface, unless the finer details of the temperature and composition profiles are of interest. (Refs. 31, 35).

The specific heat of molecules for a diatomic gas depends on temperature when the rotational and vibrational modes are considered. In the following computation, this temperature dependence is neglected. Although this assumption is unnecessary in the formulation, it is adopted in order to facilitate a later comparison with some other work that does incorporate it.

5.2 Boundary Layer Equations

A weakly dissociated diatomic gas such as oxygen is assumed to flow over a flat plate at hypersonic Mach number where considerable viscous heating occurs within the boundary layer. The external flow is considered to be such that the dissociation level at the edge of the boundary layer does not change. Interaction effects that may arise from the self-induced pressure field due to the rapid growth of the boundary layer near the leading edge are considered.

The conservation equations given in Sec. 2.1 are generalized to include molecular dissociation. The effectsof radiation and thermal diffusion are neglected, and only two-dimensional cases are considered.

Continuity:

$$\frac{\partial \rho u}{\partial x} + \frac{\partial \rho v}{\partial y} = 0 \tag{5.1}$$

x-momentum

$$\rho u \frac{\partial u}{\partial x} + \rho v \frac{\partial u}{\partial y} = - \frac{\partial p}{\partial x} + \frac{\partial}{\partial y}\left(\mu \frac{\partial u}{\partial y}\right) \tag{5.2}$$

energy:

$$\rho u \frac{\partial H}{\partial x} + \rho v \frac{\partial H}{\partial y} = \frac{\partial}{\partial y}\left(\frac{\mu}{Pr} \frac{\partial H}{\partial y}\right) + \frac{\partial}{\partial y}\left[\mu\left(1 - \frac{1}{Pr}\right)\frac{\partial}{\partial y}\left(\frac{u^2}{2}\right)\right] + \frac{\partial}{\partial y}\left[\rho D_{12}\left(1 - \frac{1}{Le}\right)\sum_{i=1}^{2} h_i \frac{\partial c_i}{\partial y}\right] \tag{5.3}$$

Species continuity: (Ref. 30)

$$\rho u \frac{\partial c_i}{\partial x} + \rho v \frac{\partial c_i}{\partial y} = \frac{\partial}{\partial y}\left(\rho D_{12} \frac{\partial c_i}{\partial y}\right) + \dot{w}_i \tag{5.4}$$

where c_i is the mass fraction of the species. For a binary gas only, the species continuity equation for the mass fraction of atoms is required.

The boundary conditions are:

at y = 0

	$u = 0$		
	$v = 0$		
either	$H = H_b$	for the heat transfer case	
or	$\frac{\partial H}{\partial y} = 0$	for the adiabatic wall	(5.5)
either	$c_A = 0$	for the fully catalytic wall	
or	$\frac{\partial c_A}{\partial y} = 0$	for the fully non-catalytic wall	

at $y = \infty$

$$u = u_\infty$$
$$H = H_\infty$$
$$C_A = c_e$$

The equation of state for the mixture is

$$\frac{p}{\rho} = \frac{\mathcal{R}}{2 m_A}(1 + c_A)\, T \tag{5.6}$$

The coordinate transformation (2.7) for the two-dimensional flow is

$$\xi(x) = \int_0^x \rho_b \mu_b u_e \, dx$$
$$\eta(x,y) = \frac{u_e}{\sqrt{2\xi}} \int_0^y \rho \, dy \tag{5.7}$$

The equations for the conservation of momentum, energy, and chemical species then have the form

Momentum:

$$\frac{\partial}{\partial \eta}\left(N \frac{\partial^2 f}{\partial \eta^2}\right) + f \frac{\partial^2 f}{\partial \eta^2} + 2 \frac{d \ln u_e}{d \ln \xi}\left[\frac{\rho_e}{\rho} - \left(\frac{\partial f}{\partial \eta}\right)^2\right] = 2\xi\left[\frac{\partial f}{\partial \eta}\frac{\partial^2 f}{\partial \xi \, \partial \eta} - \frac{\partial f}{\partial \xi}\frac{\partial^2 f}{\partial \eta^2}\right] \tag{5.8}$$

Energy

$$\frac{\partial}{\partial \eta}\left(\frac{N}{Pr}\frac{\partial g}{\partial \eta}\right) + f \frac{\partial g}{\partial \eta} + \frac{u_e^2}{H_e}\frac{\partial}{\partial \eta}\left[\left(1 - \frac{1}{Pr}\right) N \frac{\partial f}{\partial \eta}\frac{\partial^2 f}{\partial \eta^2}\right] + \frac{\partial}{\partial \eta}\left[\frac{N}{Pr}(Le - 1)\frac{h_m - h_A}{H_e}\frac{\partial c_A}{\partial \eta}\right] = 2\xi\left(\frac{\partial f}{\partial \eta}\frac{\partial g}{\partial \xi} - \frac{\partial f}{\partial \xi}\frac{\partial g}{\partial \eta}\right) \tag{5.9}$$

Species:

$$\frac{\partial}{\partial \eta}\left(\frac{N Le}{Pr}\frac{\partial z}{\partial \eta}\right) + f \frac{\partial z}{\partial \eta} - 2z \frac{\partial f}{\partial \eta}\frac{d \ln c_e}{d \ln \xi} + \frac{2\xi}{c_e u_e}\frac{dx}{d\xi}\frac{\dot{\omega}}{\rho} = 2\xi\left(\frac{\partial f}{\partial \eta}\frac{\partial z}{\partial \xi} - \frac{\partial f}{\partial \xi}\frac{\partial z}{\partial \eta}\right) \tag{5.10}$$

where
$$f = \int_0 \frac{u}{u_e} d\eta$$
$$g = \frac{H}{H_e}$$
$$z = \frac{c_A}{c_e} \tag{5.11}$$
$$N = \frac{\rho \mu}{\rho_b \mu_b}$$

It is more convenient to use the following approach by formulating an energy equation which does not include the dissociation energy (Ref. 37). The total enthalpy is given by:

$$H = \sum_{i=1}^{2} h_i c_i + \frac{1}{2} u^2 \qquad (5.12)$$

where, in general, when C_p is a function of temperature and for constant pressure across the boundary layer

$$h_A = \int_0^T c_{pA}\, dT + h_A^\circ \qquad (5.12a)$$

$$h_m = \int_0^T c_{pm}\, dT \qquad (5.12b)$$

Now

$$H = c_A h_A + (1 - c_A) h_m + \frac{1}{2} u^2$$

$$= c_A (h_A - h_m) + h_m + \frac{1}{2} u^2$$

Since

$$h_A - h_m = h_A^\circ + \int_0^T (c_{pA} - c_{pm})\, dT$$

and

$$h_A^\circ \gg \int_0^T (c_{pA} - c_{pm})\, dT$$

therefore

$$h_A - h_m \simeq h_A^\circ \qquad (5.13)$$

Thus we have for the total enthalpy

$$H = h_m + c_A h_A^\circ + \frac{1}{2} u^2 \qquad (5.14)$$

The partial enthalpy is defined as

$$H_T = h_m + \frac{1}{2} u^2 \qquad (5.15)$$

The partial enthalpy equation can then be derived by multiplying the species equation by $h_A^\circ c_e$ and subtracting the resulting equation from the energy equation; the final form is

$$\frac{\partial}{\partial\eta}\left(\frac{N}{Pr}\frac{\partial g_T}{\partial\eta}\right) + f\frac{\partial g_T}{\partial\eta} + \frac{u_e^2}{H_{Te}}\frac{\partial}{\partial\eta}\left[N\left(1-\frac{1}{Pr}\right)\frac{\partial f}{\partial\eta}\frac{\partial^2 f}{\partial\eta^2}\right] - \frac{2\xi}{u_e}\frac{dx}{d\xi}\frac{\dot{\omega}}{\rho}\frac{h_A^\circ}{H_{Te}} = 2\xi\left(\frac{\partial f}{\partial\eta}\frac{\partial g_T}{\partial\xi} - \frac{\partial f}{\partial\xi}\frac{\partial g_T}{\partial\eta}\right) \tag{5.16}$$

where $g_T = \frac{H_T}{H_{Te}}$

With our assumptions, we can now integrate the momentum, the partial energy, and the species equations across the boundary layer. The following integro-differential equations are obtained:

$$f_{\eta\eta_b} = \theta + 2\xi\frac{d\Theta}{d\xi} + \frac{2\xi}{u_e}\frac{du_e}{d\xi}(\bar{\Delta} + \Theta) \tag{5.17}$$

$$\frac{g_{T\eta_b}}{Pr} = \Lambda + 2\xi\frac{d\Lambda}{d\xi} - \frac{h_A^\circ}{H_{Te}}\frac{2\xi}{u_e}\frac{dx}{d\xi}\int_0^\infty \frac{\dot{\omega}}{\rho}\,d\eta \tag{5.18}$$

$$\frac{Le}{Pr}z_{\eta_b} = \Lambda^* + 2\xi\frac{d\Lambda^*}{d\xi} + \frac{2\xi}{u_e}\frac{dx}{d\xi}\frac{1}{Ce}\int_0^\infty \frac{\dot{\omega}}{\rho}\,d\eta \tag{5.19}$$

where
$$\bar{\Delta} = \int_0^\infty\left(\frac{\rho_e}{\rho} - f_\eta^2\right)d\eta$$
$$\Theta = \int_0^\infty f_\eta(1-f_\eta)\,d\eta$$
$$\Lambda = \int_0^\infty f_\eta(1-g_T)\,d\eta \tag{5.20}$$
$$\Lambda^* = \int_0^\infty f_\eta(1-z)\,d\eta$$

The subscript η refers to partial differentiation with respect to η .

5.3 Chemical Reaction Term

The chemical kinetics are taken to follow the reaction

$$A_2 + X \underset{k_r}{\overset{k_d}{\rightleftharpoons}} A_1 + A_1 + X \tag{5.21}$$

where A_1, A_2, and X represent the atoms, molecules, and inert collision partners, respectively. The law of mass action yields the rate of change of concentration of atoms per mole of the mixture for the above reaction (Ref. 38)

$$\frac{\partial[A_1]}{\partial t} = 2k_d[A_2][X] - 2k_r[A_1]^2[X] \tag{5.22}$$

where $[A_1]$, $[A_2]$, and $[X]$ represent the mole concentration of the atoms, molecules, and inert collision partners, respectively. When the mole concentrations are written in terms of the mass fraction of atoms, c_A, we have

$$[A_1] = \frac{\rho c_A}{m_A}$$
$$[A_2] = \frac{(1-c_A)\rho}{2m_A} \qquad (5.23)$$
$$[X] = \frac{(1+c_A)\rho}{2m_A}$$

Thus we have

$$\dot{w} = \frac{\partial(\rho c_A)}{\partial t} = \frac{k_r \rho^3 (1+c_A)}{m_A^2}\left[\frac{m_A}{2\rho}\frac{k_d}{k_r}(1-c_A) - c_A^2\right] \qquad (5.24)$$

The ratio k_d/k_r can be evaluated at the equilibrium condition, and is defined as the equilibrium constant based on mole concentration. At equilibrium, the net mass production rate is zero, thus

$$K_c = \frac{k_d}{k_r} = \frac{2\rho_E}{m_A}\frac{c_E^2}{1-c_E} \qquad (5.25)$$

where K_c is the equilibrium constant based on mole concentration. The mass production rate term is

$$\frac{\dot{w}}{\rho} = 4k_r\left(\frac{p}{RT}\right)^2\left[\frac{c_E^2}{1-c_E^2}(1-c_A) - \frac{c_A^2}{1+c_A}\right] \qquad (5.26)$$

In the examples we will compute below, oxygen is considered as the working medium. We follow Chung and Anderson (Ref. 31) by choosing the transport properties for oxygen as

$$2k_r = \frac{1.98\times10^{22}}{T^2}\left(\frac{cm^6}{mole^2\text{-}sec}\right)$$
$$\frac{c_E^2}{1-c_E^2} = \frac{K_p}{4p} \qquad (5.27)$$
$$K_p = \exp\left(15.8 - \frac{60{,}000}{T}\right)$$

where p is in atmospheres and T is in degrees Kelvin; K_p is the equilibrium constant based on partial pressure.

The final expression of the reaction term becomes

$$\frac{\dot{w}}{\rho} = \frac{3.96\times10^{22}}{T^4}\left(\frac{p}{R}\right)^2\left[\frac{1}{4p}\exp\left(15.8 - \frac{60{,}000}{T}\right)(1-c_A) - \frac{c_A^2}{1+c_A}\right] \qquad (5.28)$$

In the transformed coordinates, the reaction term appears both in the species equation and the partial energy equation in the form, from Eq. (5.26)

$$\frac{\xi}{u_e}\frac{dx}{d\xi}\frac{\dot{w}}{\rho} = \frac{\xi}{u_e^2 \rho_b \mu_b} 4 k_r \left(\frac{p}{RT}\right)^2 \left[\frac{c_E^2}{1-c_E^2}(1-c_A) - \frac{c_A^2}{1+c_A}\right] \tag{5.29}$$

The quantity $\frac{1}{\tau} = 4 k_r \left(\frac{p}{RT}\right)^2$ can be interpreted as the reciprocal of a characteristic time for the reaction. The quantity

$$\sigma = \frac{\xi \frac{1}{\tau}}{\rho_b \mu_b u_e^2} \simeq \frac{x/u_e}{\tau} \tag{5.30}$$

is a characteristic ratio of flow time to reaction time. Thus $\sigma \to 0$ denotes that the reaction is nearly chemically frozen and $\sigma \to \infty$ corresponds to the near-equilibrium condition. On a slender body or a flat plate, the flow is chemically frozen at the leading edge ($\sigma \to 0$). Non-equilibrium processes develop as the flow proceeds downstream. The equilibrium condition can only be reached far downstream where the recombination rate is equal to the dissociation rate. The reaction term vanishes when the flow reaches equilibrium.

5.4 Skin Friction, Heat Transfer, and Displacement Thickness

The shear τ_b on the body surface is

$$\tau_b = \mu_b \left(\frac{\partial u}{\partial y}\right)_b \tag{5.31}$$

and the skin friction coefficient is defined again as in Eq. (3.7)

$$C_f = \frac{2\tau_b}{\rho_\infty u_\infty^2} \tag{3.7}$$

In the transformed coordinates

$$C_f = \frac{\sqrt{2}\, u_b}{\sqrt{\xi}} \left(\frac{\rho_b}{\rho_\infty}\right)\left(\frac{u_e}{u_\infty}\right)^2 \left(\frac{\partial^2 f}{\partial \eta^2}\right)_b \tag{3.8}$$

In the following case we will consider the degree of dissociation to be small, i.e., $c_A \ll 1$. With this simplification and with the self-induced pressure in mind, the skin friction coefficient can finally be put in the following form

$$C_f = \sqrt{\frac{p_e}{p_\infty}} \left[\frac{\frac{p_e}{p_\infty} x}{\int_0^x \frac{p_e}{p_\infty} dx}\right]^{\frac{1}{2}} \frac{\sqrt{2c}}{\sqrt{Re_{x\infty}}} f_{\eta\eta b} \tag{5.32}$$

where $Re_{x\infty} = \frac{\rho_\infty u_\infty x}{\mu_\infty}$

and $\frac{\mu_b}{\mu_\infty} = c\,\frac{T_b}{T_\infty}$

and we have used the hypersonic small disturbance theory where $u_e \simeq u_\infty$.

From Eq. (5.32) we can see that for a slightly dissociating gas the effect of dissociation on the skin friction appears through the gradient of the velocity profile for a specified pressure distribution since dissociation affects the momentum equation (5.8) through the density in the pressure gradient term only. For a slender body with a highly cooled surface this pressure gradient term is very small. Thus the velocity profile, and therefore the skin friction, is practically unaffected by slight dissociation.

The heat flux through the boundary layer to the wall for a dissociating gas is

$$-\dot{q}_b = \left[k\frac{\partial T}{\partial y} + \rho D_{12}(h_A - h_m)\frac{\partial c_A}{\partial y} \right]_b = \left[k\frac{\partial T}{\partial y} + \rho D_{12} h_A^\circ \frac{\partial c_A}{\partial y} \right]_b \tag{5.33}$$

When these terms are written in terms of the transformed coordinates and in nondimensional form we have

$$-\dot{q}_b = \frac{\mu_b \rho_b u_e}{\sqrt{2\xi}} \left[\frac{1}{P_r} H_{Te} \left(\frac{\partial g_r}{\partial \eta} \right) + \frac{Le}{P_r} h_A^\circ \left(\frac{\partial c_A}{\partial \eta} \right) \right]_b \tag{5.33a}$$

We define the heat transfer coefficient as

$$C_h = \frac{-\dot{q}_b}{\rho_\infty u_\infty (H_\infty - H_b)} \tag{3.9}$$

With the slight dissociation assumption, we can write

$$C_h = \frac{\sqrt{C}}{\sqrt{2\,Re_{x\infty}}\,P_r} \sqrt{\frac{\rho_e}{\rho_\infty}} \left[\frac{\frac{\rho_e}{\rho_\infty}\chi}{\int_0^x \frac{\rho_e}{\rho_\infty} d\chi} \right]^{\frac{1}{2}} \frac{H_{Te}}{H_\infty - H_w} \left[g_{T\eta} + Le\,\frac{h_A^\circ}{H_{Te}} c_{A\eta} \right]_b \tag{5.34}$$

We can see from Eq. (5.31) that the heat transfer to the body surface is accomplished by conduction due to the temperature gradient and the release of energy due to recombination of atoms diffused onto the surface of the body.

Since we are interested in the self-induced pressure effect, the displacement thickness which will be used in the following calculation is now written as

$$\delta^* = \frac{\sqrt{2C}}{\sqrt{Re_{x\infty}}} \frac{\left[x \int_0^x \frac{p_e}{p_\infty} dx\right]^{\frac{1}{2}}}{\frac{p_e}{p_\infty}} \int_0^\infty \left(\frac{T}{T_e}(1 + C_4) - f_\eta\right) d\eta \qquad (5.35)$$

Again we have made use of the slight dissociation simplification for the coordinate transformation.

5.5 Method of Solution

The solution of the three coupled partial differential equations (5.8), (5.9), and (5.10) can only be obtained by numerical integration. Blottner (Ref. 32) has demonstrated this approach and several particular solutions were obtained. Since the reaction term depends explicitly on the distance from the leading edge, similar solutions in the same sense as for a perfect gas do not exist even for a flat plate without pressure gradient. However, if the boundary layer characteristics depend only weakly on ξ, then we may assume a priori that the dependent terms are small in magnitude in comparison with the rest of the terms and can be dropped from the equations. Thus we obtain a set of ordinary differential equations with all ξ-dependent quantities evaluated locally. Solutions of these equations for a particular case were also obtained by Blottner (Ref. 33). These were compared with the exact solutions obtained by solving the complete set of partial differential equations. It is interesting to note that the gradients of the temperature profile and the atom mass fraction profile from the local similar solutions deviate by less than five percent from the exact solution at a distance of five feet from the leading edge for the case Blottner computed. Thus it is convincing that the local similar solutions still provide a fairly good approximation to the exact solutions.

With the local similarity assumption, we can now drop all terms containing derivatives with respect to ξ and make all ξ dependent quantities assume local values. Equations (5.17), (5.18), and (5.19) are simplified to

$$f_{\eta\eta_b} = \Theta + \frac{2\xi}{u_e}\frac{du_e}{d\xi}(\bar{\Delta} + \Theta) \qquad (5.36)$$

$$\frac{g_{\tau\eta_b}}{P_r} = \Lambda - \frac{h_A^\circ}{H_{Te}}\frac{2\xi}{u_e}\frac{dx}{d\xi}\int_0^\infty \frac{\dot{w}}{\rho} d\eta \qquad (5.37)$$

$$\frac{Le}{P_r} z_{\eta_b} = \Lambda^* + \frac{2\xi}{u_e}\frac{dx}{d\xi}\frac{1}{Le}\int_0^\infty \frac{\dot{w}}{\rho} d\eta \qquad (5.38)$$

The temperature profile which appears explicitly in the mass production term is determined from the partial enthalpy and the velocity profiles,

$$\frac{h_m}{h_{me}} = \frac{H_{Te}}{h_{me}}(g_\tau - f_\eta^2) + f_\eta^2 \qquad (5.39)$$

If C_{p_m} is assumed constant, then

$$\frac{T}{T_e} = \frac{H_{T_e}}{h_{me}}(g_T - f_\eta^2) + f_\eta^2 \tag{5.40}$$

It was already noted that this assumption is unnecessary in the calculation and that it was adopted for convenience in order to facilitate a later comparison with some other work that incorporated this assumption.

The first step in solving these equations is to assume appropriate profiles for the velocity, the partial enthalpy, and the atom mass fraction. A sixth degree polynomial is assumed for the velocity profile, and a seventh degree polynomial for the partial enthalpy and the atom mass fraction profiles (Refs. 31, 39). Thus

$$\begin{aligned} f_\eta &= \sum_{n=0}^{6} a_n \zeta^n \\ g_T &= \sum_{n=0}^{7} b_n \zeta^n \\ C_A &= \sum_{n=0}^{7} c_n \zeta^n \end{aligned} \tag{5.41}$$

where

$$\zeta = \frac{\eta}{\bar{\delta}} \tag{5.41a}$$

and

$$\bar{\delta} = \frac{\rho_e u_e}{\sqrt{2\xi}} \int_0^\delta \frac{\rho}{\rho_e}\, dy \tag{5.41b}$$

Five boundary conditions are required to determine the coefficients of the velocity profile polynomial. One coefficient is left to be determined by the equations. Similarily, six boundary conditions are required for the partial enthalpy and the atom mass fraction profiles, respectively, and the rest of the coefficients are determined by the equations. Besides the boundary conditions given in Sec. 5.2, additional conditions can be obtained by differentiating the equations with respect to η and satisfying them on the body surface.

Thus we have for the velocity

$$\begin{aligned} \zeta = 0 \quad & f = 0 \\ & f_\eta = 0 \\ \zeta = 1 : \quad & f_\eta = 1 \\ & f_{\eta\eta} = 0 \\ & f_{\eta\eta\eta} = 0 \end{aligned} \tag{5.42}$$

For partial enthalpy

$$\zeta = 0 : \quad g_T = g_{Tb}$$

$$\left(\frac{g_{T\eta}}{P_r}\right)_b = \frac{u_e^2}{H_{Te}}\left(\frac{1-P_r}{P_r}\right)(f_{\eta\eta})_b^2 + \frac{2\xi}{u_e}\frac{dx}{d\xi}\frac{h_A^\circ}{H_{Te}}\left(\frac{\dot{w}}{\rho}\right)_b \qquad (5.43)$$

$$(g_{T\eta\eta})_b = \frac{2\xi}{u_e}\frac{dx}{d\xi}\frac{h_A^\circ}{H_{Te}} P_r \frac{\partial}{\partial\eta}\left(\frac{\dot{w}}{\rho}\right)_b$$

$$\zeta = 1 \; ; \quad g_T = 1 , \quad g_{T\eta} = 0 , \quad g_{T\eta\eta} = 0$$

For atom mass fraction

$$\zeta = 0 : \quad z = 0 \qquad \text{for a fully catalytic surface}$$

$$(z_{\eta\eta})_b = -\frac{P_r}{Le}\frac{2\xi}{u_e}\frac{dx}{d\xi}\left(\frac{\dot{w}}{\rho}\right)_b \frac{1}{Ce} \qquad (5.44)$$

$$(z_{\eta\eta\eta})_b = -\frac{P_r}{Le}\frac{2\xi}{u_e}\frac{dx}{d\xi}\frac{1}{Ce}\frac{\partial}{\partial\eta}\left(\frac{\dot{w}}{\rho}\right)_b$$

$$\zeta = 1 \; ; \quad z = 1 , \quad z_\eta = 0 , \quad z_{\eta\eta} = 0$$

From the momentum equation, we can see that the pressure gradient parameter

$$a_2 = -\bar{\zeta}^2 \frac{\rho_e}{\rho_b}\frac{d\ln u_e}{d\ln \xi} \qquad (5.45)$$

can be written through the coordinate transformation

$$a_2 = -\delta^2 g_{Tb} \frac{\int_0^x \frac{p_e}{p_\infty}dx}{\left(\frac{p_e}{p_\infty}\right)^2}\frac{d\left(\frac{p_e}{p_\infty}\right)}{dx} \qquad (5.45a)$$

For a small pressure gradient and very cold body, $g_{T_b} \to 0$, a_2 has a very small value. In fact, the coefficients of a_2 in the equations are also small after the polynomial profile is determined. Thus all terms containing a_2 are very small in comparison with the others and can be neglected. Physically, this means that the pressure gradient effect is extremely small in these equations. With the pressure gradient term neglected, the momentum integral equation decouples from the other equations and reduces to a simple algebraic equation. The solution of this equation is of the form (Ref. 39)

$$f_\eta = 2\zeta - 5\zeta^4 + 6\zeta^5 - 2\zeta^6 \qquad (5.46)$$

and $\bar{\delta}$ is given as

$$\bar{\delta}^2 = \frac{18018}{983} \qquad (5.47)$$

$$\bar{\delta} = 4.28$$

By choosing b_1 and c_1 to be determined by the equations, the coefficients of the polynomial profiles for g_T and C_A are determined by the boundary conditions (Ref. 39)

$$
\begin{aligned}
b_0 &= z_b = 0 \\
b_2 &= -\frac{\xi}{u_e}\frac{dx}{d\xi}\frac{P_r}{L_e}\frac{\bar{s}^2}{C_e}\left(\frac{\dot{w}}{\rho}\right)_b \\
b_3 &= -\frac{1}{3}\frac{\xi}{u_e}\frac{dx}{d\xi}\frac{P_r}{L_e}\frac{\bar{s}^2}{C_e}\frac{\partial}{\partial\zeta}\left(\frac{\dot{w}}{\rho}\right)_b \\
b_4 &= 35(1-z_b) - 20\,b_1 - 10\,b_2 - 4\,b_3 \\
b_5 &= -84(1-z_b) + 45\,b_1 + 20\,b_2 + 6\,b_3 \\
b_6 &= 70(1-z_b) - 30\,b_1 - 15\,b_2 - 4\,b_3 \\
b_7 &= -20(1-z_b) + 10\,b_1 + 4\,b_2 + b_3
\end{aligned}
\qquad (5.48)
$$

and

$$
\begin{aligned}
c_0 &= g_{Tb} \\
c_2 &= \frac{u_e^2}{H_{Te}}(1-P_r)(f_{nn})_b^2 + \frac{\xi}{u_e}\frac{dx}{d\xi}\frac{h_A^\circ}{H_{Te}}P_r\,\bar{s}^2\left(\frac{\dot{w}}{\rho}\right)_b \\
c_3 &= \frac{1}{3}\frac{\xi}{u_e}\frac{dx}{d\xi}\frac{h_A^\circ}{H_{Te}}P_r\,\bar{s}^2\frac{\partial}{\partial\zeta}\left(\frac{\dot{w}}{\rho}\right)_b \\
c_4 &= 35(1-g_{Tb}) - 20\,c_1 - 10\,c_2 - 4\,c_3 \\
c_5 &= -84(1-g_{Tb}) + 45\,c_1 + 20\,c_2 + 6\,c_3 \\
c_6 &= 70(1-g_{Tb}) - 36\,c_1 - 15\,c_2 - 4\,c_3 \\
c_7 &= -20(1-g_{Tb}) + 10\,c_1 + 4\,c_2 + c_3
\end{aligned}
\qquad (5.49)
$$

Now the two integrals Λ and Λ^* which appear in Eqs. (5.37) and (5.38) respectively, become

$$
\Lambda = \frac{31}{126}(1-g_{Tb}) - \frac{953}{360360}c_3 - \frac{151}{9009}c_2 - \frac{821}{12012}c_1 \qquad (5.50)
$$

and

$$
\Lambda^* = \frac{31}{126}(1-z_b) - \frac{953}{360360}b_3 - \frac{151}{9009}b_2 - \frac{821}{12012}c_1 \qquad (5.51)
$$

The chemical reaction term

$$
\frac{\xi}{u_e}\frac{dx}{d\xi}\int_0^1 \frac{\dot{w}}{\rho}\,d\zeta
$$

can be written with the small dissociation assumption

$$\frac{\int_0^x \frac{p_e}{p_\infty}\,dx}{u_e \frac{p_e}{p_\infty}} \left(\frac{p_e}{R}\right)^2 3.96\times10^{22} \int_0^1 \frac{1}{T^4}\left[\frac{529.054}{p_e}(1-c_4)\exp\left(15.8-\frac{60000}{T}\right) - \frac{c_A^2}{1+c_A}\right] \tag{5.52}$$

A simple iteration scheme can be constructed to solve for b_1 and c_1 from Eqs. (5.37) and (5.38). By eliminating the chemical reaction integral from both equations, we obtain an algebraic relation for b_1 and c_1

$$\left(\frac{1}{\xi^2 P_r}+\frac{821}{12012}\right)c_1 = -\frac{h_A^\circ}{H_e}\left[\frac{953}{360360}b_3+\frac{151}{9009}b_2+\left(\frac{Le}{P_r\xi^2}+\frac{821}{12012}\right)b_1\right] + \left[\frac{31}{126}(1-g_{T_b})-\frac{953}{360360}c_3-\frac{151}{9009}c_2\right] \tag{5.53}$$

where $c_e = 0$ is assumed for the species integral equation (5.38).

The species equation gives

$$\left(\frac{Le}{\xi^2 P_r}+\frac{821}{12012}\right)b_1 = \frac{2\xi}{u_e}\frac{dx}{d\xi}\int_0^1 \left(\frac{\dot{w}}{\rho}\right)d\zeta - \frac{953}{360360}b_3 - \frac{151}{9009}b_2 \tag{5.54}$$

For a given pressure distribution $p_e(x)$, we can solve equations (5.53) and (5.54) for b_1 and c_1. Once this is done, boundary layer characteristics follow immediately. Although the pressure gradient is neglected in the computation of the velocity profile, the effect of pressure still appears explicitly through the chemical reaction term since the chemical reaction rate is governed by both temperature and pressure.

In Eq. (5.48), both the coefficients b_2 and b_3 are directly proportional to $(\xi/u_e)(dx/d\xi) \simeq x/u_e$ which is very small when the velocity u_e is very large. Thus b_2 and b_3 can be neglected in comparison with b_1, hence

$$b_2 \simeq 0$$
$$b_3 \simeq 0 \tag{5.55}$$

It follows directly that

$$c_1 \simeq \frac{u_e^2}{H_e}(1-P_r)\,f''^2_{\eta\eta_b} \tag{5.56}$$
$$c_3 \simeq 0$$

Equation (5.53) reduces to

$$\left(\frac{1}{\xi^2 P_r}+\frac{821}{12012}\right)c_1 = -\frac{h_A^\circ}{H_e}b_1\left(\frac{Le}{\xi^2 P_r}+\frac{821}{12012}\right)+\left[\frac{31}{120}(1-g_{b})-\frac{151}{9009}c_2\right] \tag{5.57}$$

Since g_b and c_2 are known, this equation gives a direct relation between b_1 and c_1. With $b_2 = b_3 = 0$, and for zero pressure gradient, Eq. (5.54) can be solved for x,

$$\chi = \frac{u_e}{2} \frac{\left(\frac{Le}{\delta^2 P_r} + \frac{821}{12012}\right) b_1}{\int_0^1 \frac{\dot{w}}{\rho} d\zeta} \tag{5.58}$$

The function $\frac{\dot{w}}{\rho}$ is given by Eq. (5.28). It consists of functions of T and c which can be computed once b_1 and c_1 are specified. Therefore, if b_1 is assumed, then c_1 follows from Eq. (5.57) and their x dependency is determined from Eq. (5.58).

5.6 Boundary Layer Self-Induced Pressure

From the previous sections, it is known that the dissociation rate depends strongly on pressure. Thus the induced pressure gradient due to the boundary layer displacement thickness may alter the dissociation rate considerably from that of a uniform pressure distribution.

The displacement thickness for a weakly dissociating boundary layer is given by Eq. (5.35) and rewritten here as

$$\delta^* = \frac{\sqrt{2C}}{\sqrt{Re_{x\infty}}} \frac{\left[\chi \int_0^\chi \frac{p_e}{p_\infty} d\chi\right]^{\frac{1}{2}}}{\frac{p_e}{p_\infty}} I \delta \tag{5.59}$$

where

$$I = \int_0^1 \left(\frac{T}{T_e}(1 + C_4) - f_\eta\right) d\zeta \tag{5.59a}$$

and

$$\frac{T}{T_e} = \frac{H_{Te}}{h_{me}}(g_T - f_\eta^2) + f_\eta^2 \tag{5.40}$$

The external flow is assumed to have a fixed degree of dissociation. For flow past a slender body, strong dissociation may occur in the inviscid flow only at a short distance from the leading edge where the shock wave is strong. This effect has been examined by Inger (Ref. 36). He shows that the failure to properly match the viscous flow reaction rate at the outer edge of the boundary layer to the inviscid flow rate will usually cause only a small error in solving the boundary layer equations. Thus except in the strong interaction region, the assumption that the dissociation level at the edge of the boundary layer does not change provides a good approximation.

For frozen flows, or flows without dissociation, the tangent-wedge relation again can be used to compute pressure distribution. As before, the tangent-wedge formula gives, Eq. (4.3)

$$\frac{p_e}{p_\infty} = 1 + \gamma M_\infty^2 \theta_e^2 \left[\sqrt{\left(\frac{\gamma+1}{4}\right)^2 + \frac{1}{M_\infty^2 \theta_e^2}} + \frac{\gamma+1}{4} \right] \tag{4.3}$$

where γ is the frozen specific heat of the external flow. This expression can be reversed to have θ_e in terms of p_e/p_∞. If this is done, it can be integrated to yield δ^* (see also Appendix B)

$$\delta^* = \sqrt{\frac{2}{\gamma(\gamma+1)}} \frac{1}{M_\infty} \int_0^x \frac{\frac{p_e}{p_\infty} - 1}{\sqrt{\frac{p_e}{p_\infty} + \frac{\gamma-1}{\gamma+1}}} d\chi \tag{5.60}$$

With the displacement thickness (5.59) we can formulate an expression suitable for computing the pressure distribution

$$\frac{p_e}{p_\infty} = \sqrt{\frac{\gamma(\gamma+1)}{Re_{x\infty}}} M_\infty \frac{\left[\chi \int_0^x \frac{p_e}{p_\infty} d\chi\right]^{\frac{1}{2}}}{\int_0^x \frac{\frac{p_e}{p_\infty} - 1}{\sqrt{\frac{p_e}{p_\infty} + \frac{\gamma-1}{\gamma+1}}} d\chi} I \bar{\delta} \tag{5.61}$$

This expression is suitable for an iteration scheme. Once the pressure distribution is obtained, we can then compute all required boundary layer characteristics such as skin friction and heat transfer.

5.7 Example and Discussion

From the previous outline, we know that for a nonequilibrium chemically reacting boundary layer similar solutions do not exist in general. The chemical reaction term depends strongly on the magnitude of the local pressure and the velocity of the external flow. Thus for each case which is computed, the pressure and the velocity of the external stream must be specified.

A special example was computed in order to show the magnitude of the effects for a nonequilibrium dissociating boundary layer. The case chosen was a flat plate with fully catalytic wall with the following conditions, (equivalent to the standard atmosphere at 100,000 ft. of altitude)

$p_\infty = 24.3$ psf,

$T_\infty = 392.4\,^\circ R$

$u_\infty = 25{,}000$ ft/sec

$\frac{T_b}{T_\infty} = 3, \quad Pr = 0.7, \quad Le = 1.4$

Both the Prandtl number and the Lewis number were assumed constant. A complete solution of the partial differential equations and the "similar" solutions of the corresponding ordinary differential equations was obtained in Refs. 32 and 33 for a flat plate with zero pressure gradient for the same conditions. Thus a direct comparison of the present results with these more exact solutions was possible.

The solutions obtained by the present approximation for a flat plate with and without self-induced pressure gradient are shown in Figs. 19a and b. Typical temperature and atom mass fraction profiles at distances of 0 ft, 1 ft and 10 ft from the leading edge of the flat plate are shown in Figs. 19c and d. At the leading edge, the boundary layer is chemically frozen. Since the external flow is assumed to be undissociated, no atoms are produced in or diffused into this region, therefore, the atom mass fraction is zero. When dissociation develops downstream, the atom mass fraction increases, and as energy is absorbed in the process, the temperature consequently decreases. It can be seen that the dissociation takes place mainly in the high temperature region where the viscous dissipation is large. Atoms then diffuse into the outer portion and the portion of the boundary layer near the wall and combine there. Figure 19a shows the temperature gradient at the wall up to 10 ft from the leading edge and Fig. 19b shows the gradient of atom mass fraction at the wall for the same distance. The "similar" solutions by Blottner are also shown in the figures. The solutions obtained by the present approximation are about 4 percent too high for the temperature gradient and 20 percent too high for the atom mass fraction gradient. This large error in the atom concentration gradient is believed to be caused by the polynomial approximation of the atom mass fraction profile. It is well known that a polynomial type of approximation can give reasonable results if the represented variable possesses a simple geometric profile which varies monotonically from zero to its maximum value, such as the velocity profile with a favourable pressure gradient or the total enthalpy profile. In this case, the polynomial approximation gives a reasonably accurate result for the partial enthalpy profile which possesses a simple form. However, poor results are obtained for the atom mass fraction profile which has a more complicated form. Thus one improvement of the present approach would be to employ the total energy equation and the partial energy equation instead of the atom concentration equation so that these two simple geometric profiles can be represented more accurately by polynomials. The atom mass fraction could be obtained from the difference of these two profiles.

The pressure gradient due to the self-induced pressure tends to increase the dissociation as shown in Fig. 19b. This can be seen through the atom mass production term Eq. (5.29). As the pressure increases, the collision rate of the species also increases. The net result is to decrease the characteristic time for the chemical reaction given in Eq. (5.30), and consequently, the equilibrium condition will be reached more quickly than at a lower pressure. An increase in the dissociation rate also causes a corresponding absorbtion of flow energy in the form of dissociation energy and a consequent decrease of temperature as shown in Fig. 19a.

It is important to note that the integral method can still yield good results for integrated properties although the detailed profile may not be satisfactory. This is demonstrated by Karman's original approach (see for example Ref. 6). Figure 20 shows the displacement thickness of the boundary layer with and without self-induced pressure gradient. Blottner's

exact solution is also shown up to 5 ft. The agreement of the present results with the exact solution is reasonably good. Since the displacement thickness determines the local pressure field, the close agreement of approximate and exact solutions is encouraging. The displacement thickness with self-induced pressure gradient is also shown in Fig. 20. It gives a slightly lower value than that with zero pressure gradient up to about 3 ft and then becomes higher downstream. The displacement thickness of a perfect gas without pressure gradient is also shown in the figure. It is thicker than the corresponding dissociating boundary layer. This is because the dissociating boundary layer has a higher average density, (i.e., a lower average temperature) due to the absorption of energy by dissociation and is consequently thinner than in the perfect gas case.

The induced pressure distribution for the dissociating case appears in Fig. 21. The pressure distribution obtained for a perfect gas is also shown. In general, the induced pressure is lower in the dissociating case than in the perfect gas case owing to the thinner displacement thickness in the dissociating case, as discussed above.

Figure 22 shows the heat transfer coefficient along the plate. The value for the perfect gas case is also shown. It is interesting to see that although the heat transfer is in general only slightly greater than for the perfect gas case, the difference is insignificant. This can be seen from the expression for the heat transfer coefficient in Eq. (5.34). If we recall the expression of total enthalpy Eq. (5.14), the gradient on the surface is

$$\left(\frac{\partial H}{\partial \eta}\right)_b = \left(\frac{\partial h_m}{\partial \eta}\right)_b + h_A^\circ \left(\frac{\partial c_A}{\partial \eta}\right)_b$$

and the heat transfer rate, Eq. (5.33a),

$$-\dot{q}_b = \frac{\mu_b \rho_e u_e}{\sqrt{2\xi}} \left[\frac{1}{P_r} H_{1e} \left(\frac{\partial g_1}{\partial \eta}\right) + \frac{Le}{P_r} h_A^\circ \frac{\partial c_A}{\partial \eta} \right]_b$$

Thus if Le = 1, then the heat flux is directly proportional to the total enthalpy flux as for a perfect gas. Thus the slight difference in these two cases comes from the effect of Lewis number or the diffusion effect. Since the Lewis number is only slightly different from unity, the heat transfer in both cases will be very similar. For a fully catalytic surface the atoms striking the cold surface recombine there immediately. The heat transfer is approximately the same as the energy transfer and is determined primarily by the difference in enthalpy between the hot gas and the cold surface. Whether the atoms recombine in the boundary layer or on the wall, the mechanism of heat transfer does not play a significant role in such a process. The energy is transported at approximately the same rate whether it is carried in the active modes as translational and rotational energy by a molecule, or in the inert modes as energy of dissociation by an atom (Ref. 5).

6. CONCLUDING REMARKS

An approximate method of solution of the compressible laminar boundary layer equations has been developed. The method is based on the concept of a combination of integral relations and similarity solutions, which was originally introduced by Thwaites for the case of incompressible flow. In the classical approach, the momentum integral equation is used while the energy equation is usually ignored. Therefore, under certain conditions this procedure yields the temperature field with low accuracy and predicts the velocity field more accurately. In order to improve the prediction of heat transfer, the energy integral equation must also be considered in the formulation of the integral relations. The basic difference between the present approach and the classical momentum integral methods is that the energy integral equation is also fully used in the derivation of the fundamental integral relation. Therefore the variation of the ratio of the energy defect thickness to the momentum defect thickness, which has a strong effect on the computation of heat transfer, is taken into account. This approach improves the accuracy of the prediction of heat transfer.

Using a linear approximation for the correlation parameters, the basic equation can be integrated analytically. Its solution, results in a determination of the velocity gradient parameter (m) for a given external velocity distribution and specified surface temperature. This is the first step in solving for the boundary layer characteristics, which then follow immediately from the correlation parameters. The resulting equation is then reduced to a form which is suitable for the computation of boundary layer properties in hypersonic flows.

The application of this formulation is illustrated by solution of the hypersonic self-induced pressure interaction problem. The external local pressure field and the local flow inclination are related by the tangent-wedge relation for two-dimensional flows and the tangent-cone relation for axisymmetric flows. The present method makes it possible to construct solutions valid throughout the complete interaction range. Solutions are compared with available experimental results and more exact solutions by other authors and the agreement is good. This shows that the use of the energy integral equation in the formulation of the boundary-layer integral relation is important, especially in the calculation of heat transfer.

The present method does not give explicit analytical solutions to the pressure interaction problem because of the complexity of the resulting integro-differential equation. However, this equation can be solved by using a successive approximation scheme that involves only simple numerical integrations.

With the present integral method and the local-similarity concept, closed form solutions to the pressure interaction problem can also be

obtained but with relatively low accuracy. However, the present method using the integro-differential equation does provide a simple approach that gives a higher accuracy solution than the local-similarity method and with much less effort than is required for the exact numerical solutions. This may have worthwhile practical applications.

Real gas effects arising from nonequilibrium dissociation in the boundary layer due to the high viscous dissipation at hypersonic speed are also examined for the pressure interaction problem. A weakly dissociating diatomic gas, such as oxygen, is used as a model. It is found that for a body with a fully-catalytic surface, the occurrence of dissociation tends to reduce the interaction effect slightly due to a decreased boundary layer displacement thickness. The increase in heat transfer due to the recombination of atoms at the wall is small in comparison with the perfect gas case. The simplified example used to illustrate this type of flow provides useful insight and it is possible to extend the method to actual cases by using correct thermodynamic conditions and dispensing with the local-similarity concept.

REFERENCES

1. Thwaites, B. — Approximate Calculation of the Laminar Boundary Layer. The Aeronautical Quarterly, Vol. 1, pp. 245-280, Nov. 1949.

2. Rott, N. Crabtree, L.E. — Simplified Laminar Boundary Layer Calculations for Bodies of Revolution and for Yawed Wings. J. Aero. Sciences, Vol. 19, No. 8, pp. 553-565, 1952.

3. Cohen, C.B. Reshotko, E. — The Compressible Laminar Boundary Layer with Heat Transfer and Arbitrary Pressure Gradient. NACA Rept. 1294, 1956.

4. Hayes, W. — On Laminar Boundary Layers with Heat Transfer. Jet Propulsion Vol. 26, No. 4, 1956.

5. Hayes, W.D. Probstein, R.F. — Hypersonic Flow Theory. Academic Press, 1959.

6. Schlichting, H. — Boundary Layer Theory, McGraw Hill, 1955.

7. Rosenhead, L. (editor) — Laminar Boundary Layers, Oxford University Pressure, 1963.

8. Curle, N. — The Laminar Boundary Layer Equations. Oxford University Press, 1962.

9. Stewartson, K. — The Theory of Laminar Boundary Layers in Compressible Fluids. Oxford University Press, 1964.

10. Cohen, C.B. Reshotko, E. — Similar Solutions for the Compressible Laminar Boundary Layer with Heat Transfer and Pressure Gradient. NACA Rept. 1293, 1956.

11. Poots, G. — A Solution of the Compressible Laminar Boundary Layer Equations with Heat Transfer and Adverse Pressure Gradient. Quart. J. Mech. Appl. Math. Vol. 13, pp. 57-84, 1960.

12. Baxter, D.C. Flügge-Lotz, I. — The Solution of Compressible Laminar Boundary Layer Problems by a Finite Difference Method Part 2. Further Discussion of the Method and Computation of Examples. Stanford Univ. Div. of Eng. Mech. Tech. Rept. No. 110, 1957.

13. Tani, I. — On the Approximate Solution of the Laminar Boundary-Layer Equation. J. Aero. Sciences, Vol. 21, No. 6, 1954.

14. Dewey, C.F., Jr. — Use of Local Similarity Concepts in Hypersonic Viscous Interaction Problems. AIAA Journal, Vol. 1, No. 1, 1963.

15. Dewey, C.F., Jr. Gross, J.F. — Similar Solutions of the Laminar Boundary Layer Equations with Variable Fluid Properties. Memo RM-3729-PR. The Rand Corp. 1963.

16. Nagakura, T. Naruse, H. — An Approximate Solution of the Hypersonic Laminar Boundary Layer Equations and Its Applications. J. Phy. Soc. of Japan. Vol. 12, No. 11, 1957.

17. Naruse, H. — Approximate Solutions of the Hypersonic Laminar Boundary Layer Equations with Heat Transfer and Arbitrary Pressure Gradient and Their Application. Aero. Res. Inst. Univ. of Tokyo, Rept. No. 361, 1961.

18. Riley, N. — Note on the Weak Interaction Region in a Hypersonic Flow. The Physics of Fluids. Vol. 6, No. 10, 1963.

19. Flügge-Lotz, I. Blottner, F.G. — Computation of the Compressible Laminar Boundary Lyaer Flow Including Displacement-Thickness Interaction Using Finite Difference Methods. Tech. Rept. No. 131, Division of Eng. Mech. Stanford Univ., Jan. 1962.

20. Mann, W.M., Jr. Bradley, R.G., Jr. — Hypersonic Viscid-Inviscid Interaction Solutions for Perfect Gas and Equilibrium Real-Air Boundary Layer Flow. American Astronautical Society, Advance in Astronautical Sciences, Vol. 8, 1961.

21. Kendall, J.M., Jr. — An Experimental Investigation of Leading-Edge Shock-Wave-Boundary-Layer Interaction at Mach 5.8. J. Aero. Sci. Vol. 24, No. 1, pp. 47-56, 1957.

22. Bertram, M.H. — Boundary Layer Displacement Effects in Air at Mach Number of 6.8 and 9.6. NACA TN 4133, 1958.

23. Bertram, M.H. Blackstock, T.A. — Some Simple Solutions to the Problem of Predicting Boundary-Layer Self-Induced Pressures. NASA TN D-798, 1961.

24. Hall, J.G. Golian, T.C. — Shock Tunnel Studies of Hypersonic Flat Plate Air Flows. Rept. No. AD-1052-A-10. Cornell Aero. Lab., 1960.

25. Yasuhara, M. — Axisymmetric Viscous Flow Past Very Slender Bodies of Revolution. J. Aero. Sci. Vol. 29, No. 6, 1962.

26. Chernyi, G.G. — Introduction to Hypersonic Flow. Transl. and edited by R. F. Probstein. Academic Press, 1961.

27. Kopal, Z. — Table of Supersonic Flow Around Cones. Tech. Rept. No. 1. Dept. of Elect. Eng. Mass. Inst. Tech. 1947.

28. Wittliff, C.E. Wilson, M.R. — Heat Transfer to Slender Cones in Hypersonic Air Flow. Including Effects of Yaw and Nose Bluntness. J. Aero. Sci. Vol. 29, No. 7, 1962.

29. Probstein, R.F. Elliott, D. — The Transverse Curvature Effect in Compressible Axially-Symmetrical Laminar Boundary-Layer Flow. Rept. 261, Dept. of Aero. Eng., Princeton Univ., 1954.

30. Dorrance, W.H. — Viscous Hypersonic Flow. McGraw-Hill, 1962.

31. Chung, P.M. Anderson, A.D. — Dissociative Relaxation of Oxygen Over an Adiabatic Flat Plate at Hypersonic Mach Numbers. NASA TN D-140, April 1960.

32. Blottner, F.G. — Chemical Nonequilibrium Boundary Layer. AIAA Journal, Vol. 2, No. 2, Feb. 1964.

33. Blottner, F.G. — Similar and Nonsimilar Solutions of the Nonequilibrium Laminar Boundary Layer. AIAA Journal, Vol. 1, No. 9, Sept. 1963.

34. Inger, G.R. — Nonequilibrium Dissociated Boundary Layers with a Reacting Inviscid Flow. AIAA Journal. Vol. 1. No. 9, 1963.

35. Rae, W.J. — A Solution for Nonequilibrium Flat-Plate Boundary Layer. AIAA Journal. Vol. 1, No. 10, October, 1963.

36. Inger, G.R. — Nonequilibrium Hypersonic Flat-Plate Boundary-Layer Flow with a Strong Induced Pressure Field. AIAA Journal Vol. 2, No. 3, March, 1964.

37. Lees, L. — Convective Heat Transfer with Mass Addition and Chemical Reactions. Combustion and Propulsion, Third AGARD Colloquium, March 17-28, 1958. Pergamon Press, New York.

38. Glass, I.I. Takano, A. — Nonequilibrium Expansion Flow of Dissociated Oxygen Around a Corner. UTIA Rept. No. 91, Institute of Aerophysics, Univ. of Toronto, 1963.

39. Libby, P.A. Morduchow, M. — Method for Calculation of Compressible Laminar Boundary Layer with Axial Pressure Gradient and Heat Transfer. NACA TN 3157, Jan. 1954.

TABLE I

Summary of Correlation Parameters
for $g_b = 2$, $Pr = 1$

β	m	L	$\bar{m}$	$\bar{L}$	$f_{\eta\eta_b}$	C_f/C_h
2.00	.4451	.4406	.0045	.0033	2.4878	7.5240
1.50	.3192	.4255	.0093	.0127	2.1402	6.6621
1.00	.2053	.4091	.0156	.0304	1.7318	5.6444
.50	.1009	.4026	.0188	.0748	1.2351	4.3174
.30	.0614	.4086	.0167	.1108	.9829	3.6023
0	0	.4410	0	.2205	.4696	2.0000
-.10	-.0228	.4567	-.0147	.2940	.1805	.8951
-.1295	-.0283	.4368	-.0209	.3220	0	0

Note: These results were calculated from the similarity solutions listed in Ref. 10.

TABLE II

Summary of Correlation Parameters

g_b	β	m	ℓ	$\bar{r}$	H_F	Q	L	$\frac{(1+H_F)^2}{1+Q^2}$	$\frac{\sqrt{1+Q^2}}{Q}\bar{r}$	C_f/C_h
0.15	0.0	0.0	0.1980	0.2008	0.3001	1.0072	0.3988	0.8391	0.2829	1.9882
	0.1	0.0198	0.2095	0.2098	0.2288	1.0604	0.3964	0.7107	0.2885	2.1180
	0.2	0.0395	0.2193	0.2175	0.1691	1.1063	0.3953	0.6146	0.2932	2.2307
	0.2857	0.0564	0.2268	0.2235	0.1248	1.1414	0.3952	0.5494	0.2973	2.3155
	0.4	0.0791	0.2356	0.2308	0.0736	1.1827	0.3959	0.4805	0.3023	2.4176
0.40	0.0	0.0	0.2336	0.1869	1.0000	0.8945	0.4205	2.2221	0.2806	2.2364
	0.1	0.0204	0.2531	0.1957	0.9169	0.9601	0.4081	1.9120	0.2825	2.4828
	0.2	0.0399	0.2686	0.2030	0.8518	1.0178	0.3990	1.6844	0.2845	2.6928
	0.2857	0.0561	0.2798	0.2083	0.8038	1.0621	0.3930	1.5289	0.2861	2.8536
	0.4	0.0774	0.2928	0.2147	0.7480	1.1164	0.3870	1.4382	0.2864	3.0444
0.60	0.0	0.0	0.2455	0.1208	1.5474	0.7017	0.3663	4.3482	0.2104	2.8515
	0.1	0.0171	0.2704	0.1241	1.4726	0.7568	0.3407	3.8875	0.2056	3.2972
	0.2	0.0321	0.2889	0.1263	1.4179	0.8054	0.3211	3.5459	0.2013	3.6843
	0.2857	0.0439	0.3018	0.1277	1.3779	0.8429	0.3074	3.3057	0.1982	3.9848
	0.4	0.0585	0.3157	0.1291	1.3341	0.8891	0.2923	3.0427	0.1943	4.3490
*0.8191	0.0	0.0	0.2532	0.0	2.1465	0.0	0.2532	9.9005	0.0	---
0.8123	0.1	0.0108	0.2830	0.0	2.0740	0.0	0.2166	9.4495	0.0	---
0.8066	0.2	0.0189	0.3135	0.0	2.0267	0.0	0.1891	9.1609	0.0	---
0.8025	0.2857	0.0244	0.3166	0.0	1.9976	0.0	0.1706	8.9856	0.0	---
0.7977	0.4	0.0301	0.3296	0.0	1.9701	0.0	0.1505	8.8215	0.0	---

Note: These results were calculated from the similar solutions of the laminar boundary layer equations under the conditions that Pr = 0.7, $u_e^2/2H_e \to 1$, listed in Ref. 14.

* Adiabatic wall condition

TABLE III

Summary of Linear Approximate Values for Correlation Parameters

g_b	A	B	α
0.15	0.3988	0.12	1.983
0.40	0.4205	0.60	1.914
0.60	0.3663	1.49	1.787
Adiabatic Wall	0.2532	3.39	1.516

TABLE IV

Summary of Coefficients for Asymptotic Solutions of Pressure Distribution

Weak Interaction

g_b	a_1	b_1	d*	d^+
0.0	-----	------	0.125**	0.145
0.15	0.115	0.0057	0.205	-----
0.40	0.192	0.0157	0.342	-----
0.60	0.250	0.0267	0.446	-----
Adiabatic Wall	0.314	0.0422	0.560	0.556

*d is defined as $d = \frac{a_1}{\gamma(\gamma-1)}$

** Extrapolated from other values, Pr = 0.7.

+ Results from Ref. 5 for Pr = 0.725.

Strong Interaction

g_b	a_2	b_2	a_2^{**}	b_2^{**}
0.0	0.100*	0.501*	0.149	------
0.15	0.177	0.503	-----	------
0.40	0.302	0.515	-----	------
0.60	0.390	0.537	-----	------
Adiabatic Wall	0.483	0.581	0.515	0.759

* Extrapolated from other values, Pr = 0.7.

** Results from Ref. 5 for Pr = 1.0.

TABLE V

Relations of K^2, n, p_e/p_∞ for a Flat Plate from Local Similar Solutions

K^2	K	n	p_e/p_∞
0.1	0.316	-0.171	1.54
0.2	0.448	-0.220	1.82
0.3	0.548	-0.252	2.06
0.4	0.633	-0.276	2.29
0.5	0.708	-0.295	2.50
0.6	0.775	-0.310	2.70
0.7	0.837	-0.322	2.90
0.8	0.895	-0.333	3.10
0.9	0.950	-0.342	3.28
1.0	1.000	-0.351	3.48
1.2	1.096	-0.365	3.84
1.4	1.183	-0.376	4.21
1.6	1.266	-0.386	4.57
2.0	1.415	-0.402	5.28
2.5	1.580	-0.414	6.15
3.0	1.733	-0.424	7.02
3.5	1.872	-0.433	7.88
4.0	2.000	-0.438	8.73

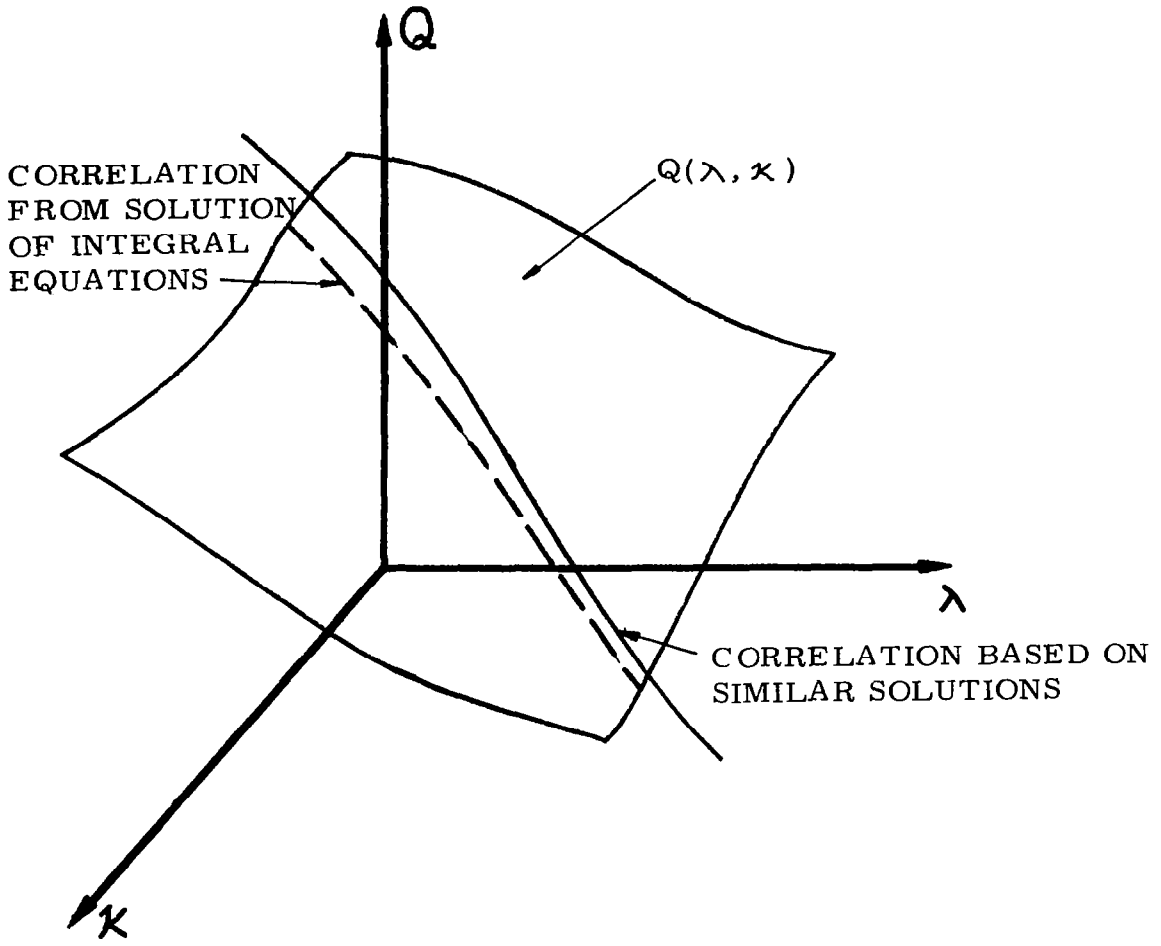

FIG. 1 SKETCH OF CORRELATION $Q(\lambda, \kappa)$

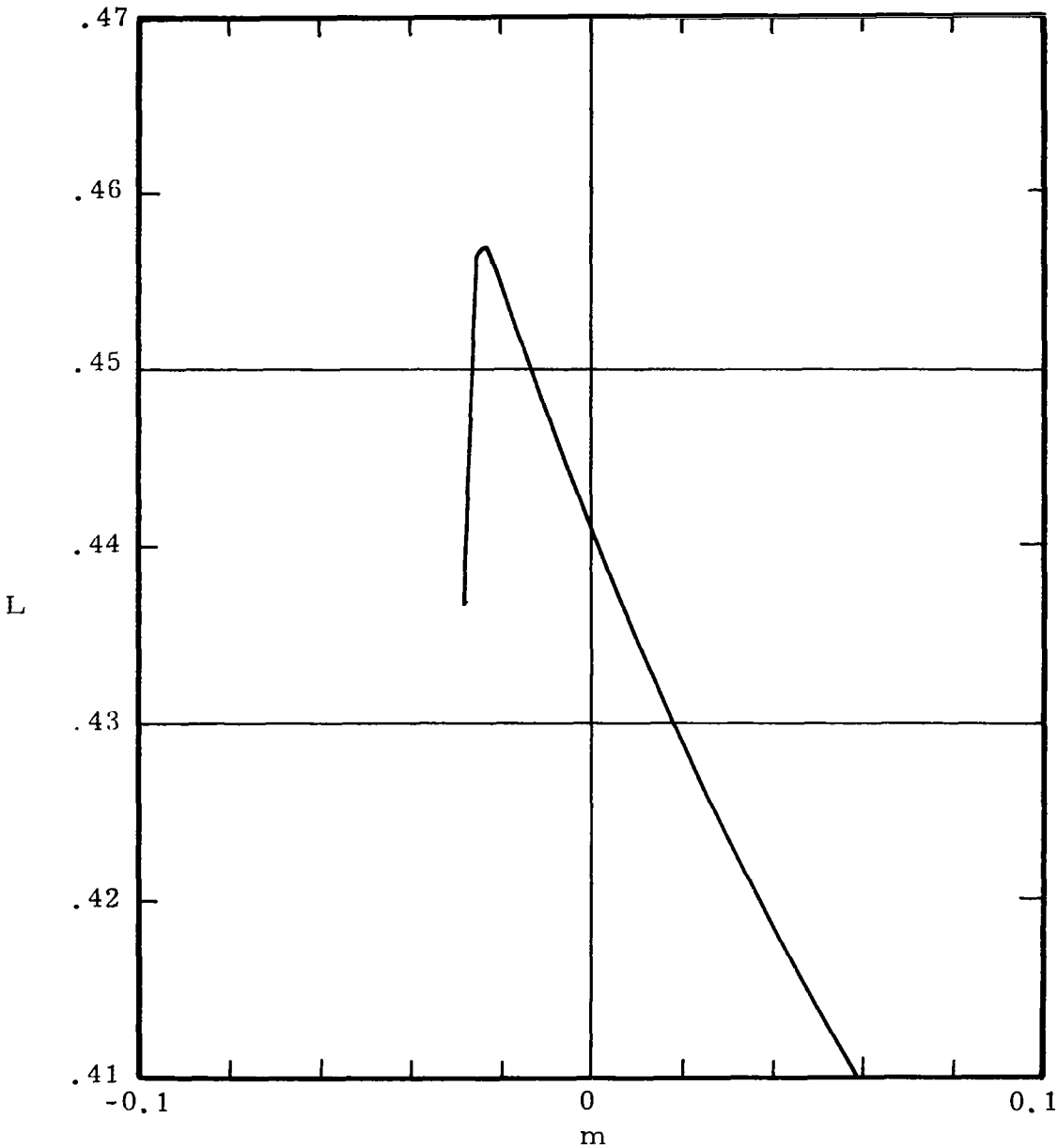

FIG. 2 CORRELATION OF PARAMETERS L AND m, g_b=2 , Pr=1.

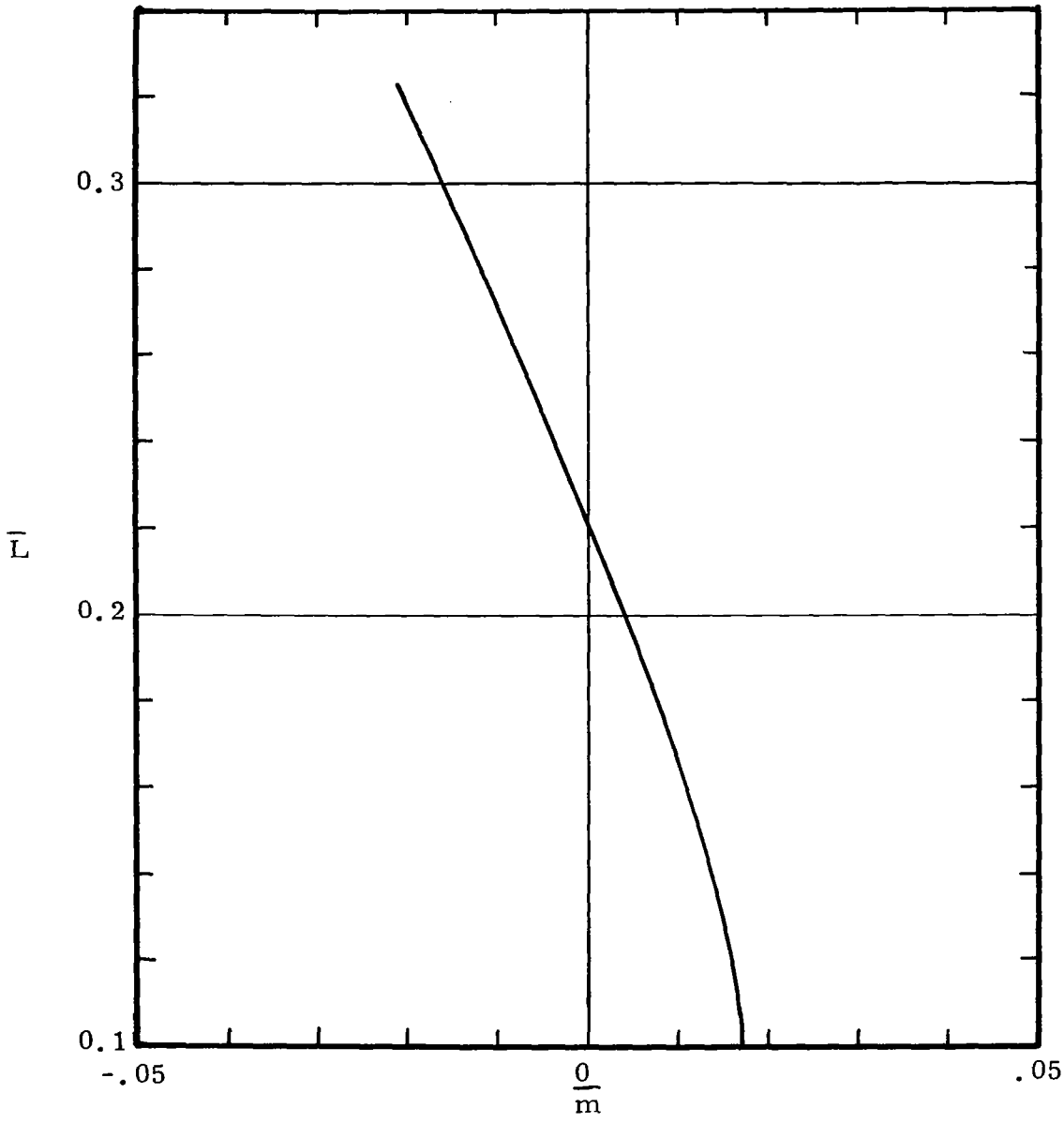

FIG. 3 CORRELATION OF PARAMETERS $\bar{L}$ AND $\bar{m}$, g_b=2, Pr=1.

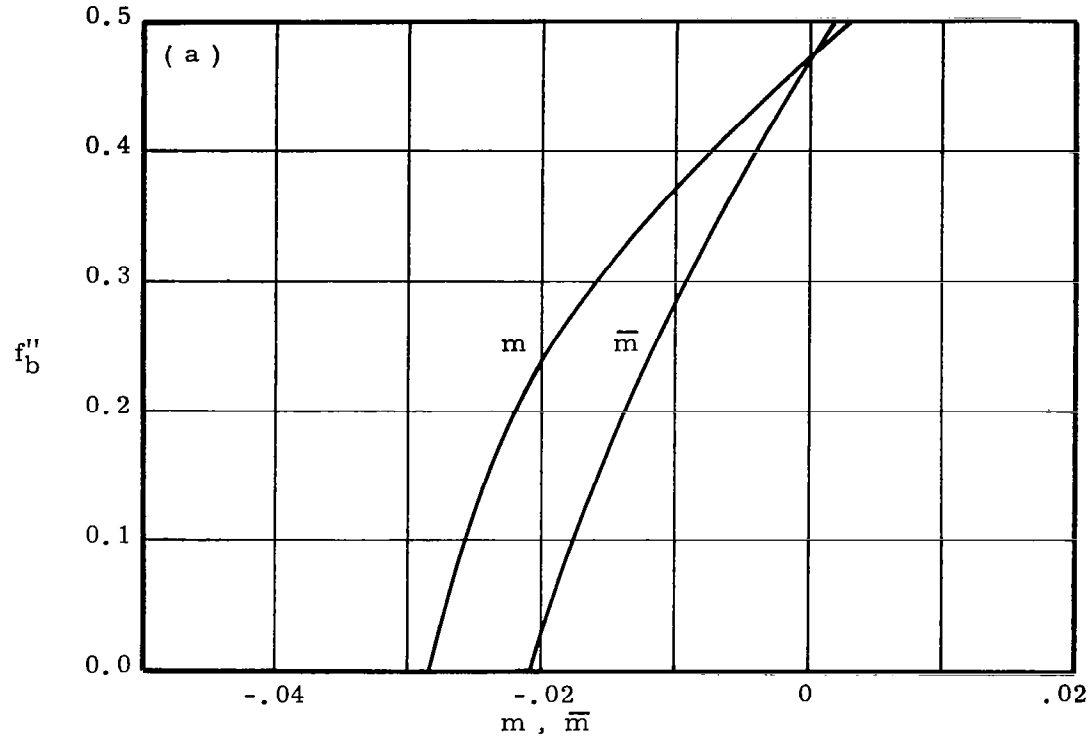

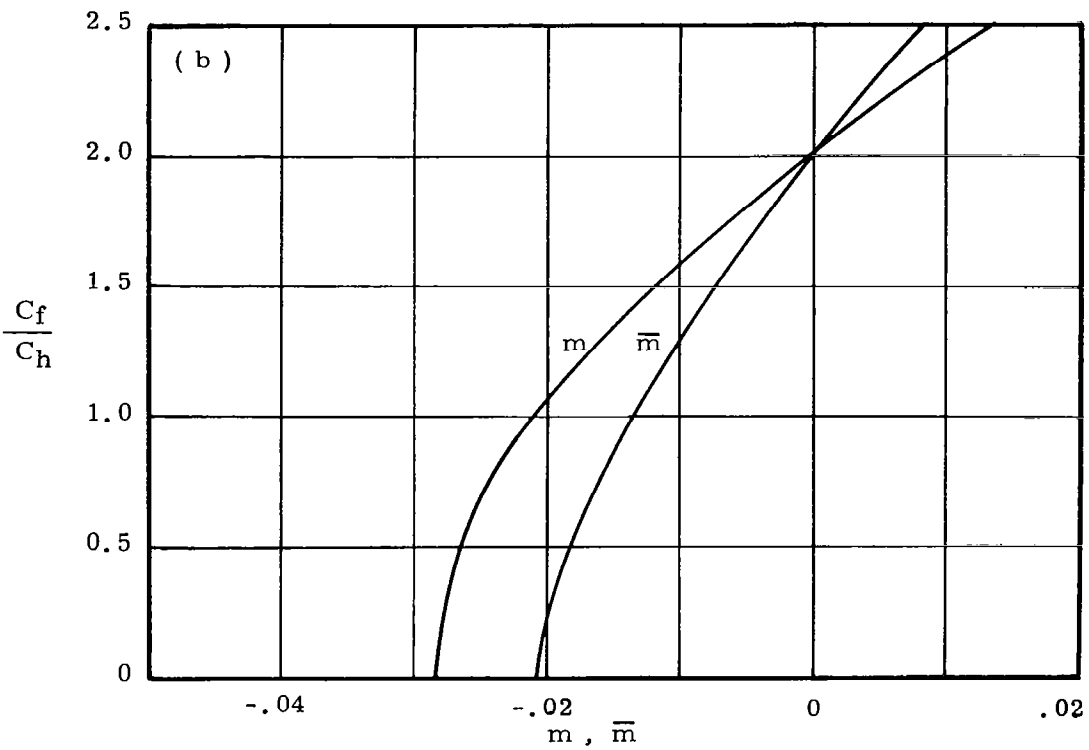

FIG. 4a, b CORRELATION OF SKIN FRICTION AND HEAT TRANSFER PARAMETERS WITH RESPECT TO m AND $\bar{m}$, g_b=2, Pr=1.

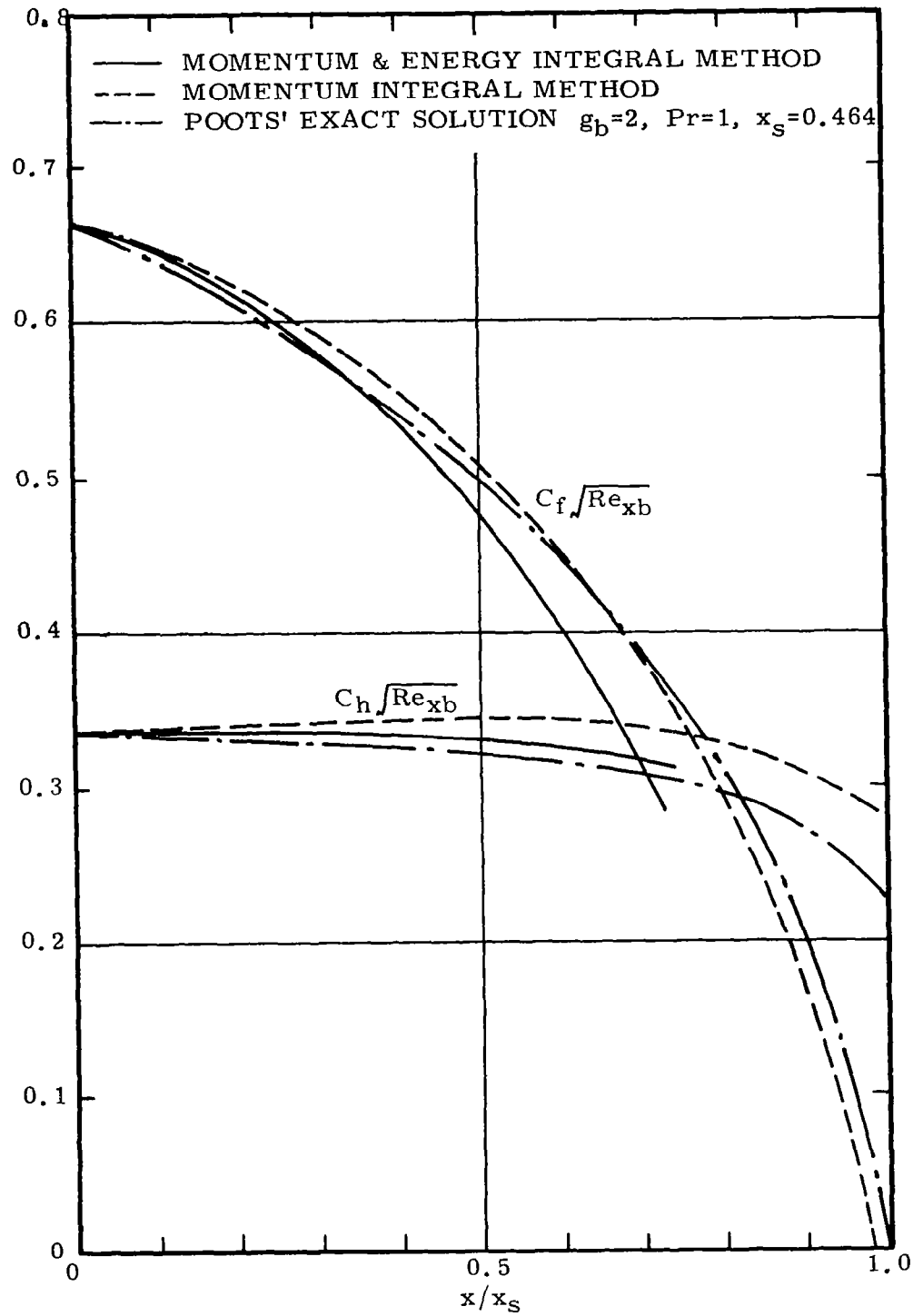

FIG. 5 COMPARISON OF SKIN FRICTION AND HEAT TRANSFER PREDICTED BY PRESENT APPROACH AND MOMENTUM INTEGRAL METHOD EXACT SOLUTIONS

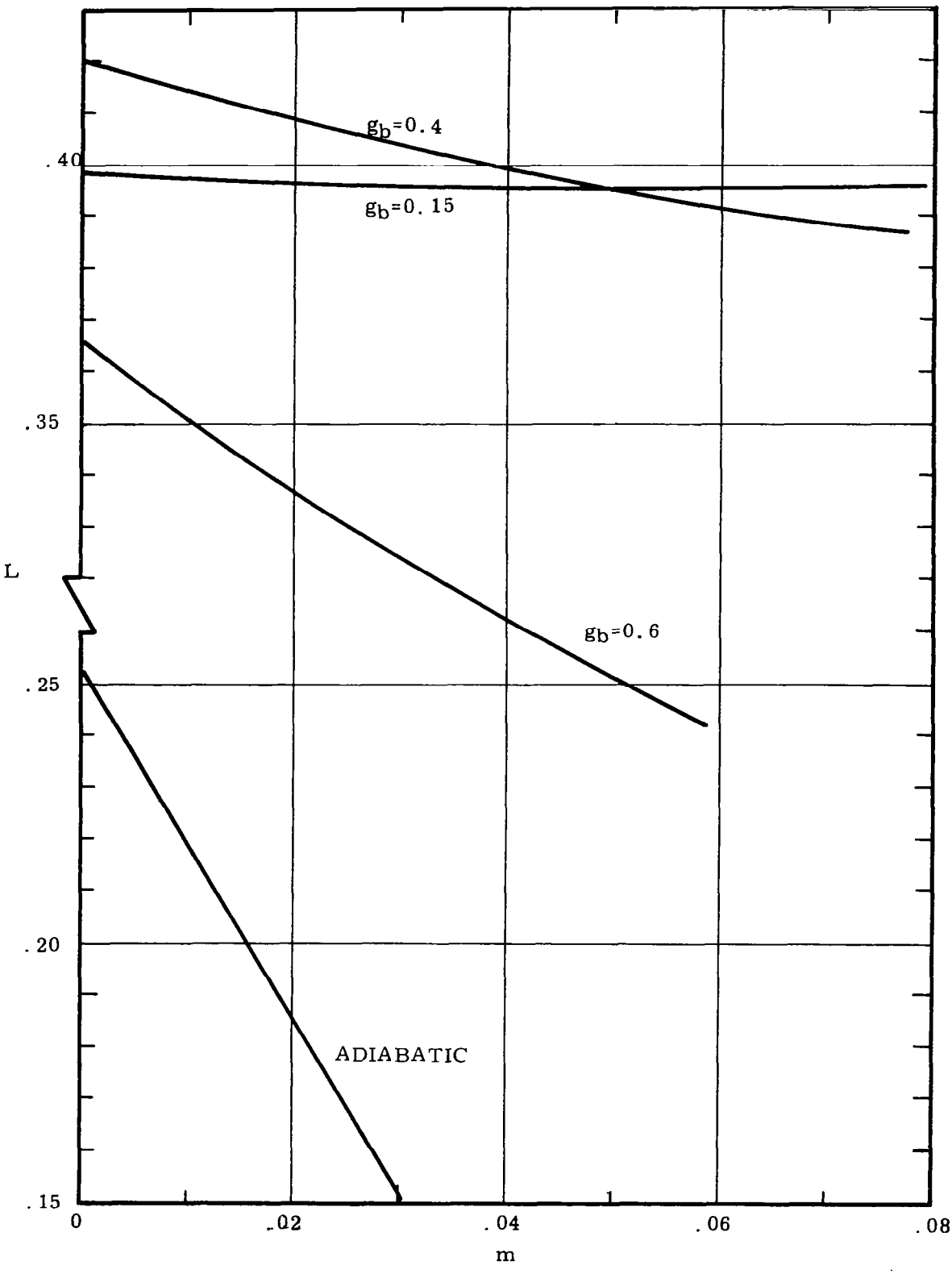

FIG. 6 CORRELATION OF PARAMETERS L AND m Pr=0.7

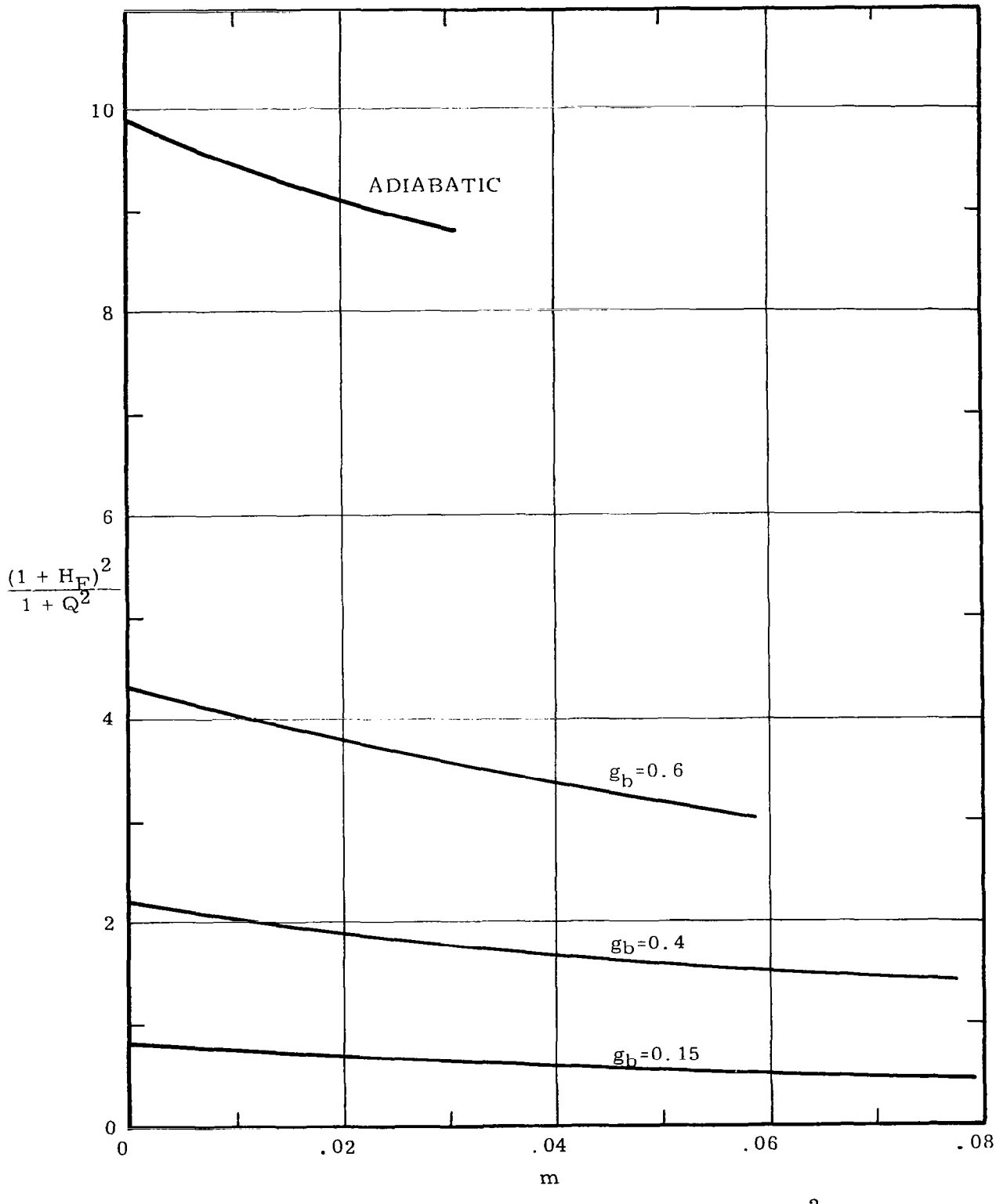

FIG. 7 CORRELATION OF PARAMETERS $\frac{(1 + H_F)^2}{1 + Q^2}$ AND m

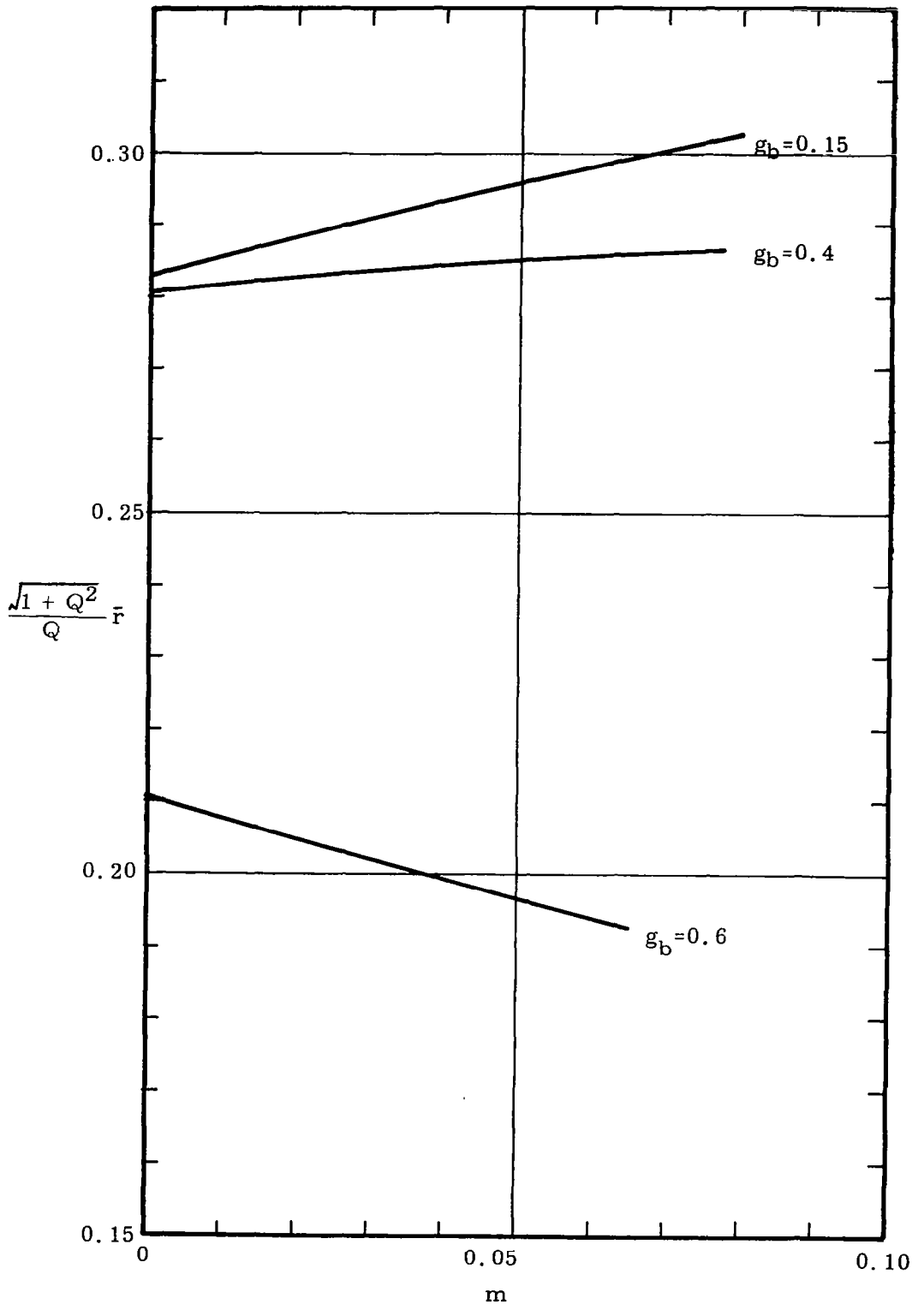

FIG. 8 CORRELATION OF PARAMETERS $\frac{\sqrt{1+Q^2}}{Q}\bar{r}$ AND m

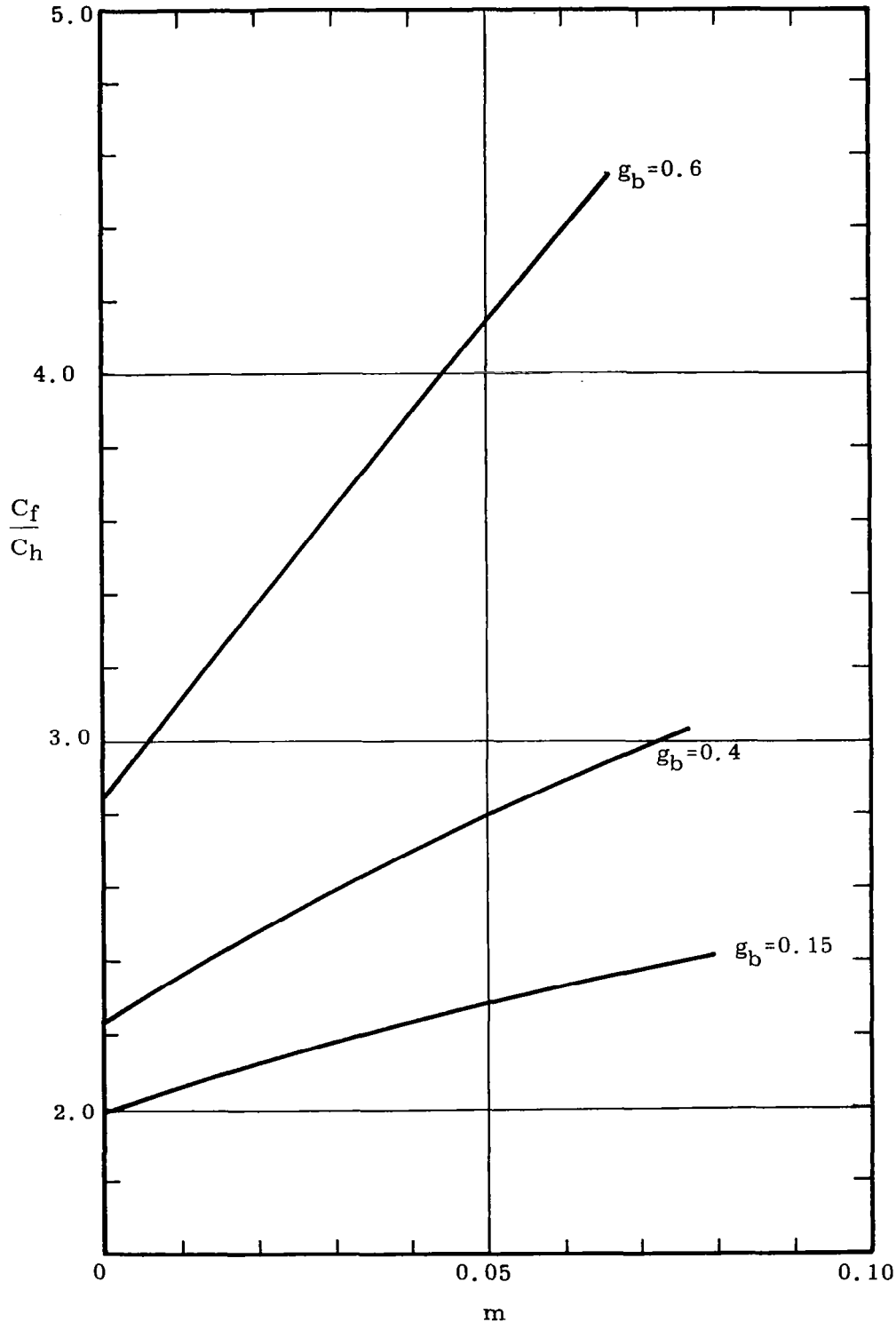

FIG. 9 CORRELATION OF REYNOLDS ANALOGY PARAMETER AND m

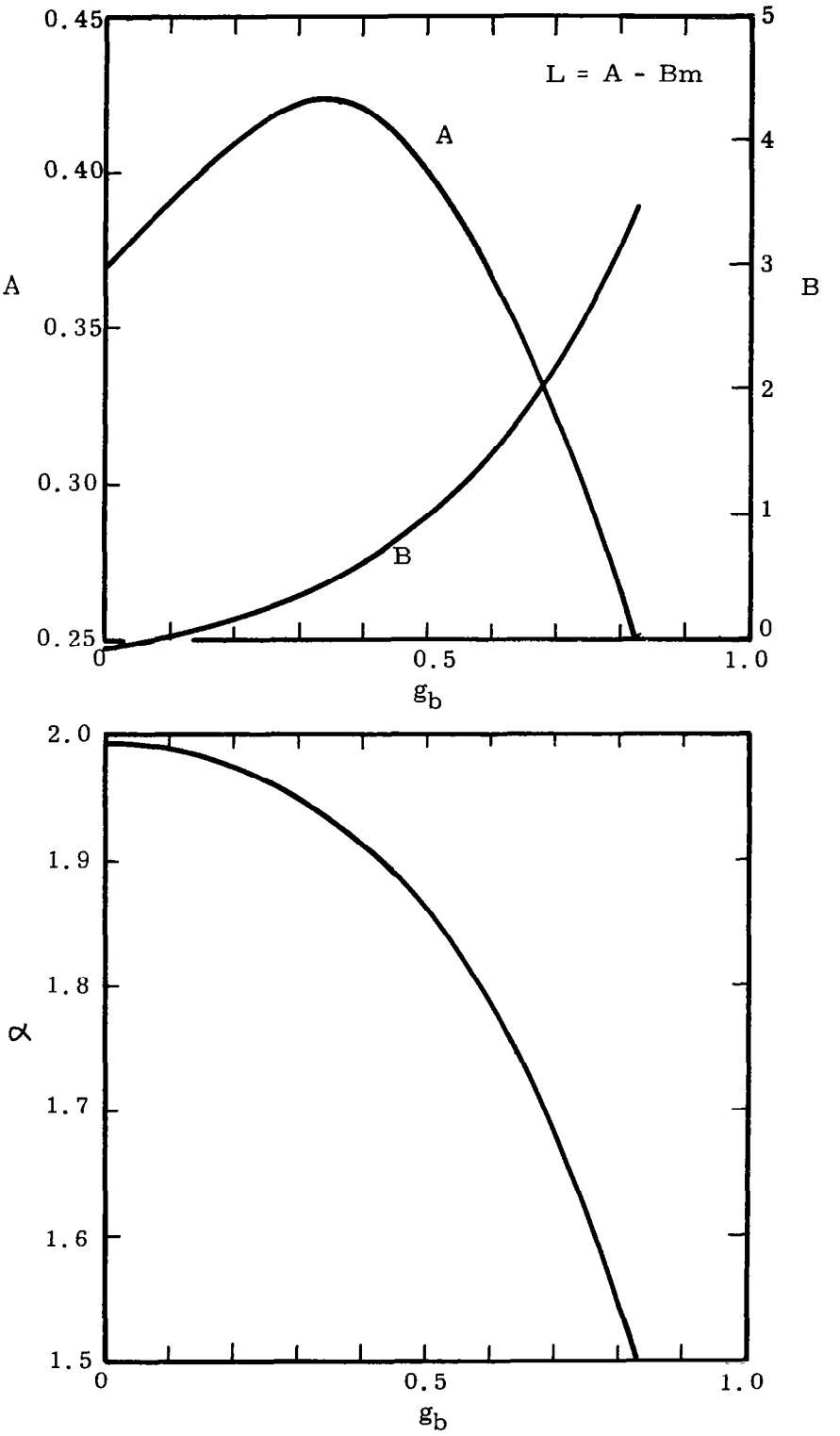

FIG. 10 VARIATION OF A, B AND α FOR USE IN LINEAR METHOD OF DETERMINING PARAMETER m

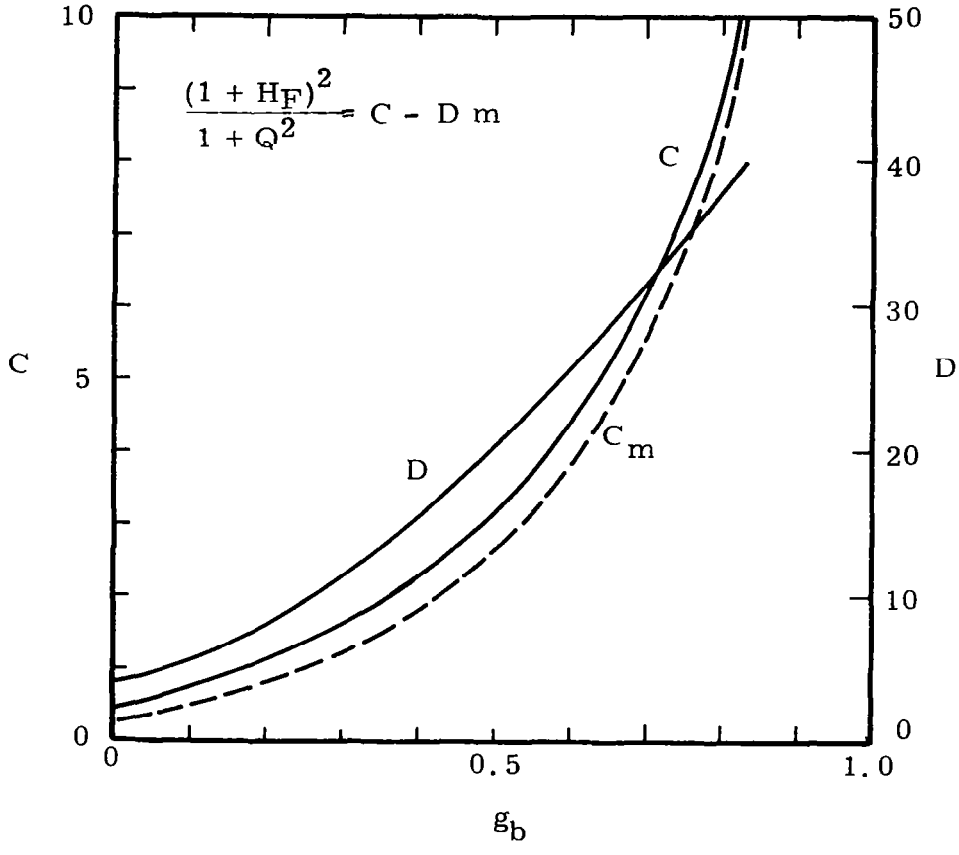

FIG. 11 VARIATION OF C, D AND C_m FOR USE IN LINEAR METHOD

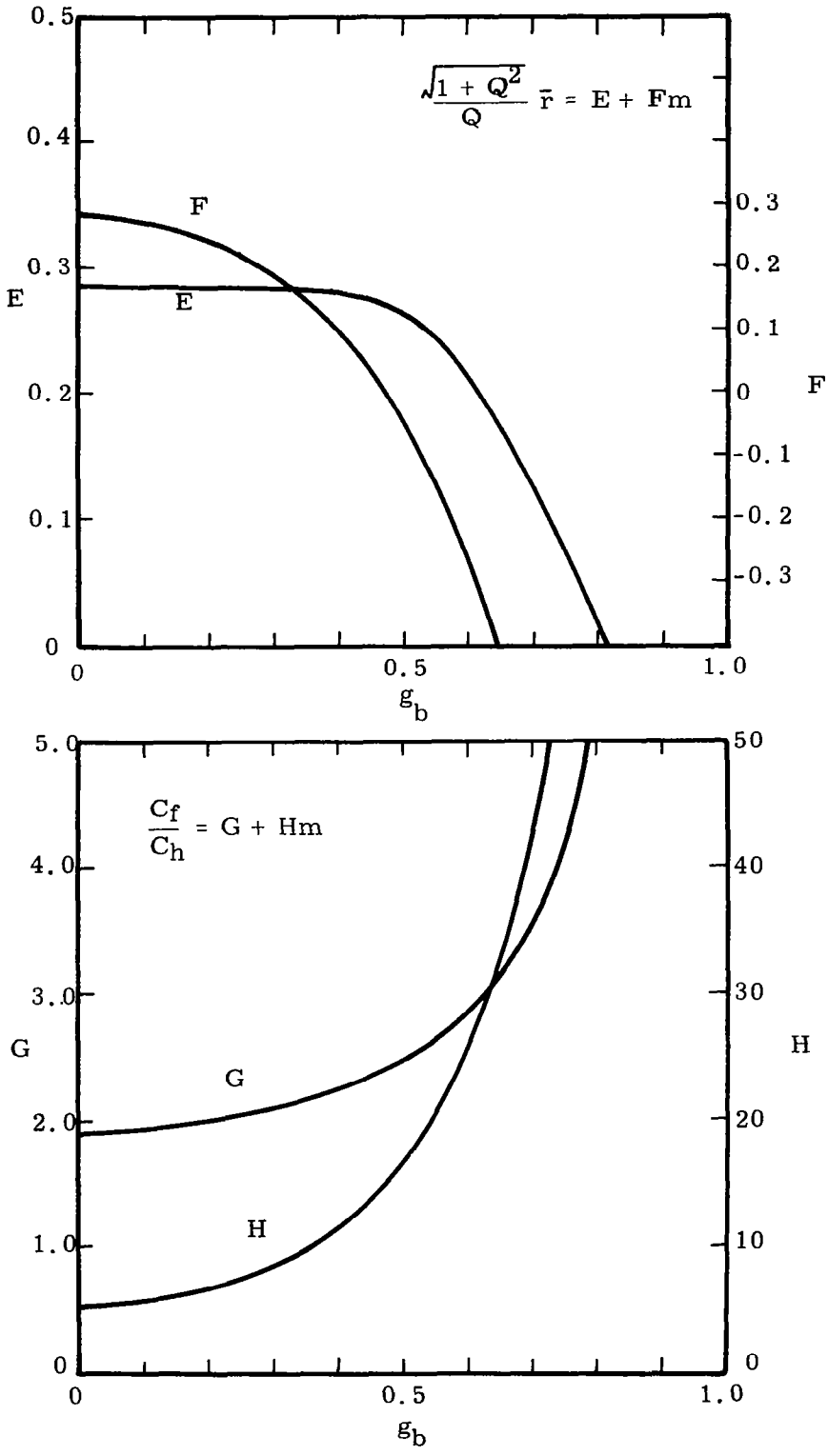

FIG. 12 VARIATION OF E, F, G, H FOR USE IN LINEAR METHOD IN DETERMINING SKIN FRICTION AND HEAT TRANSFER

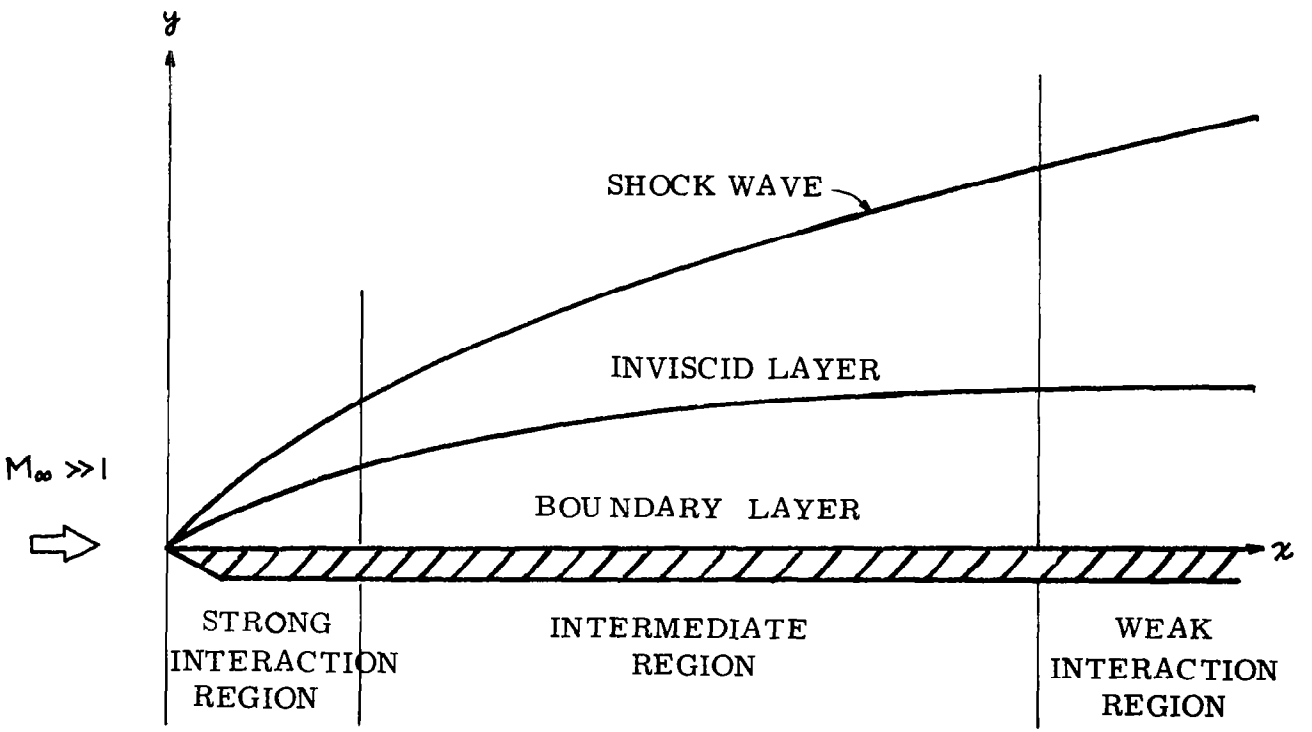

FIG. 13 SKETCH OF BOUNDARY LAYER INDUCED FLOW FIELD OVER A FLAT PLATE

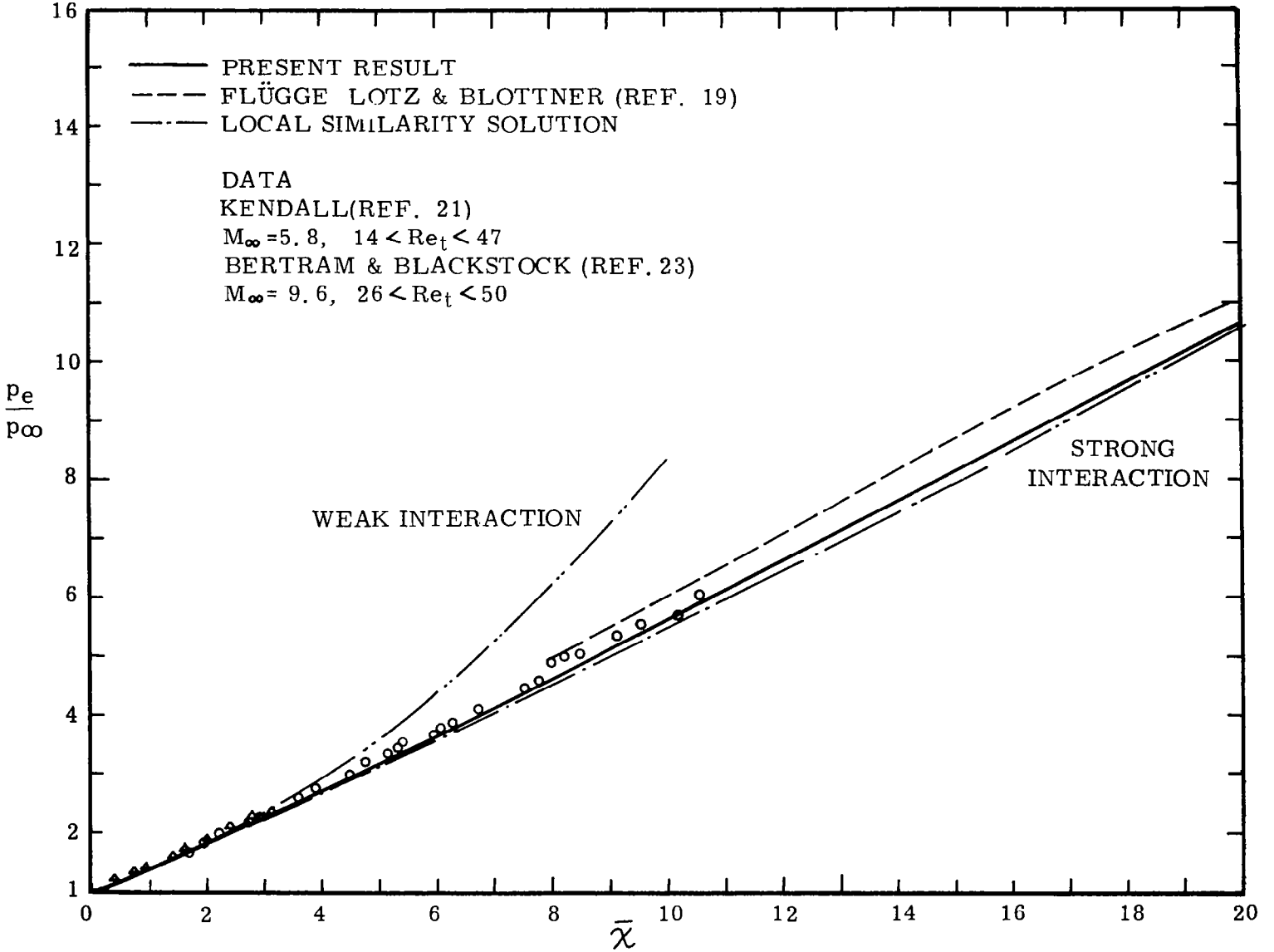

FIG. 14 COMPARISON OF THEORETICAL PREDICTIONS OF SELF-INDUCED PRESSURE INTERACTION WITH EXPERIMENTAL RESULTS OBTAINED BY KENDALL AND BERTRAM ON AN INSULATED FLAT PLATE

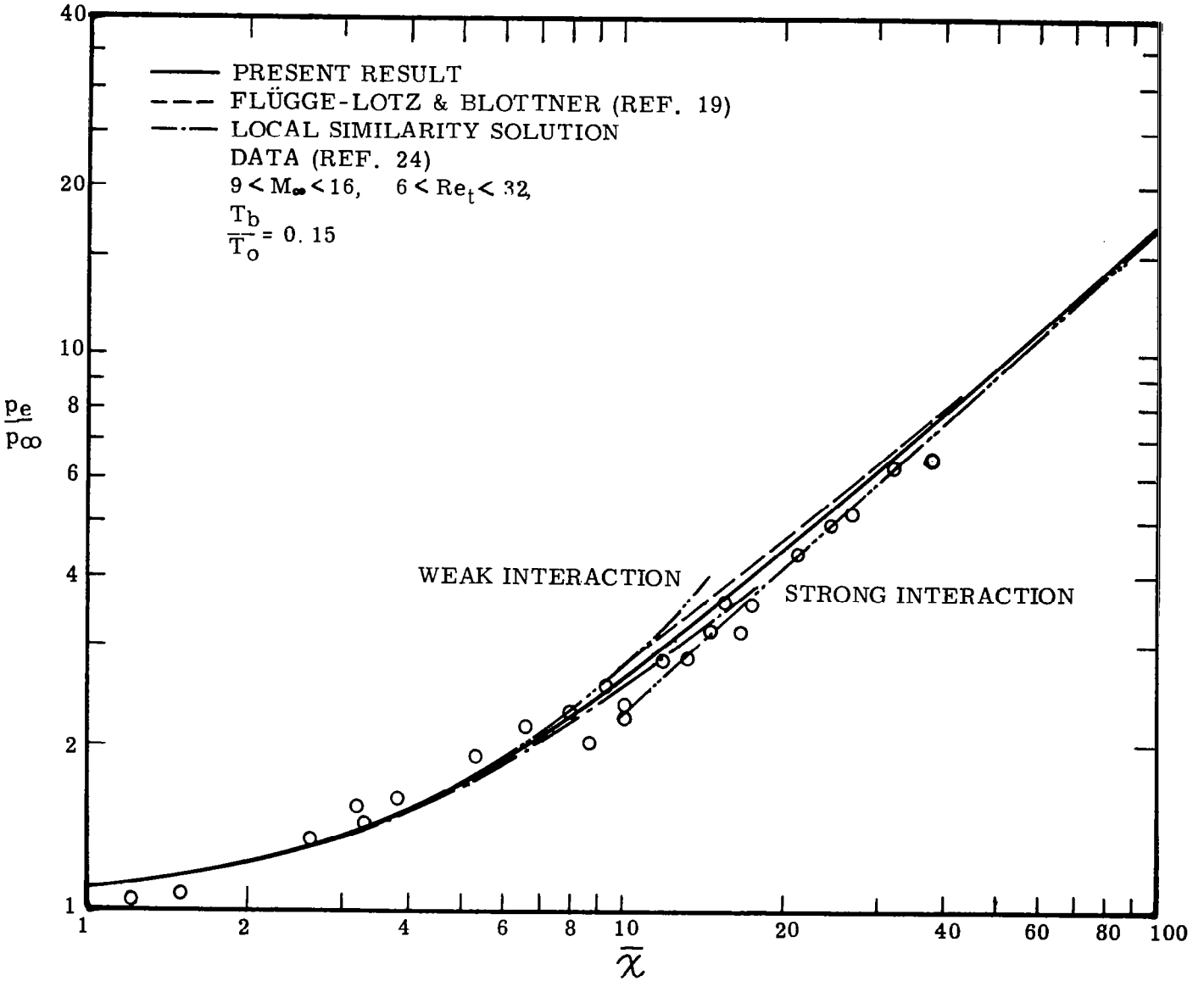

FIG. 15 COMPARISON OF THEORETICAL PREDICTIONS OF PRESSURE WITH EXPERIMENTAL RESULTS OBTAINED BY HALL AND GOLIAN ON A COLD FLAT PLATE

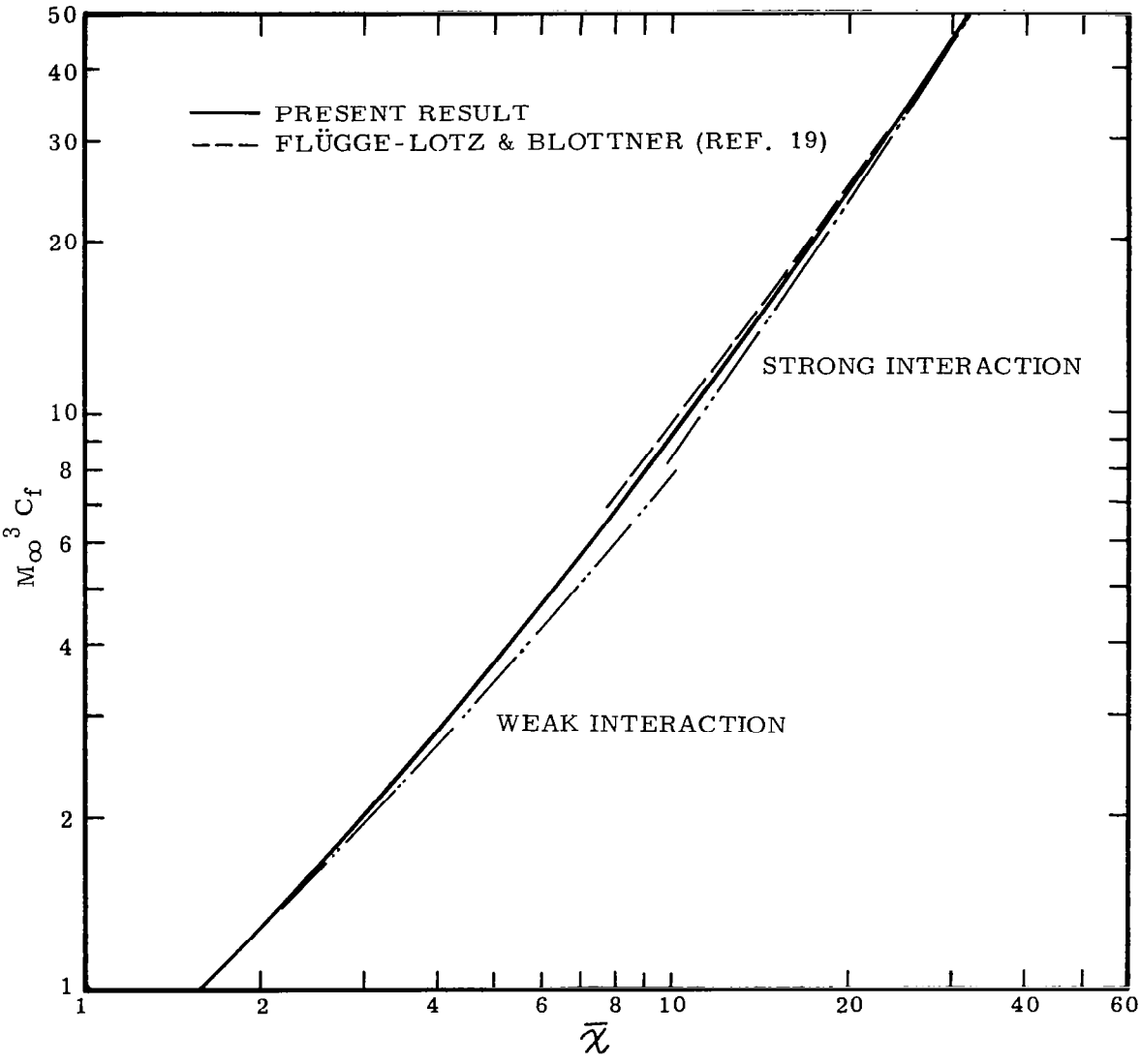

FIG. 16 THEORETICAL PREDICTIONS OF SKIN FRICTION ON A COLD FLAT PLATE

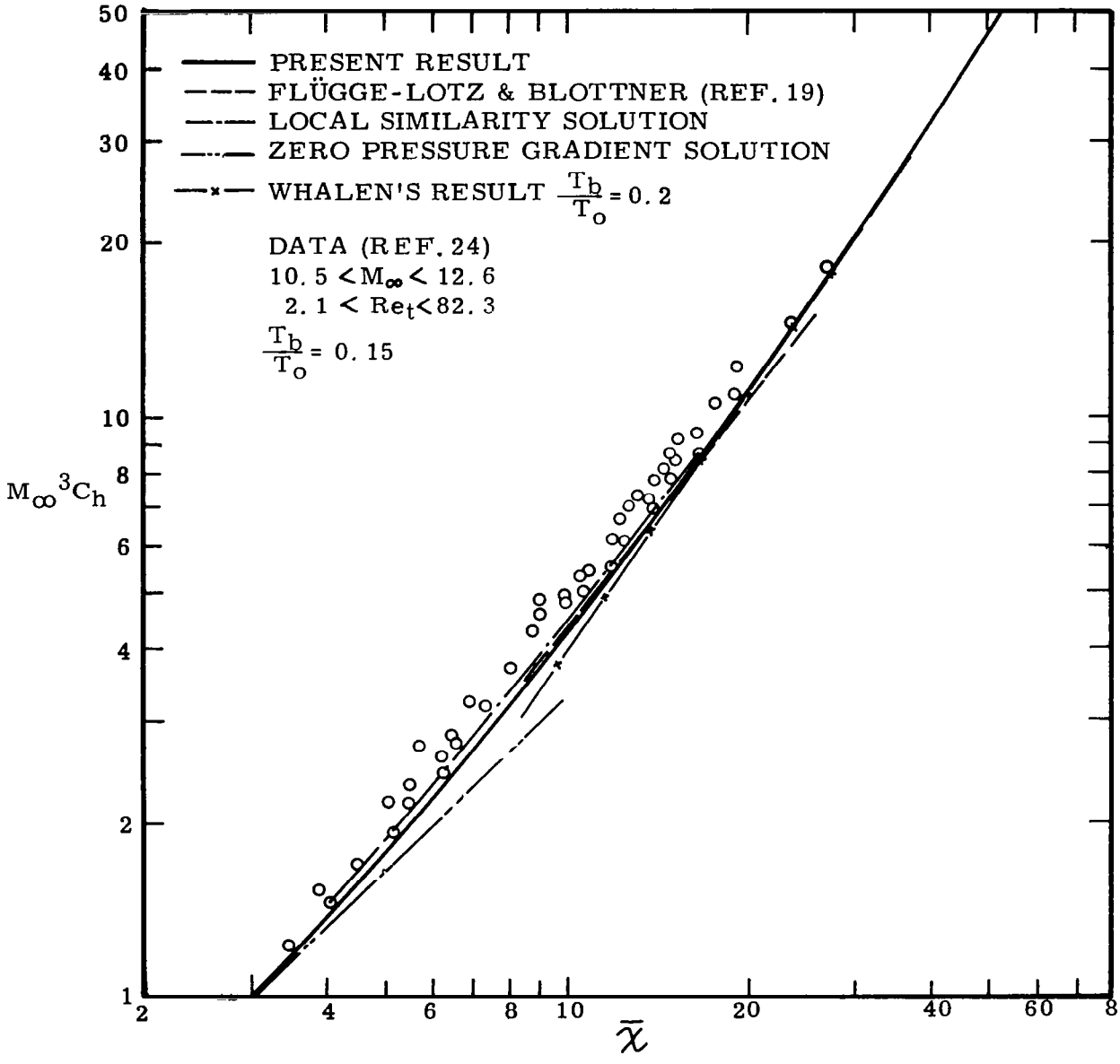

FIG. 17 COMPARISON OF THEORETICAL PREDICTIONS OF HEAT TRANSFER WITH EXPERIMENTAL RESULTS OBTAINED BY HALL AND GOLIAN ON A COLD FLAT PLATE

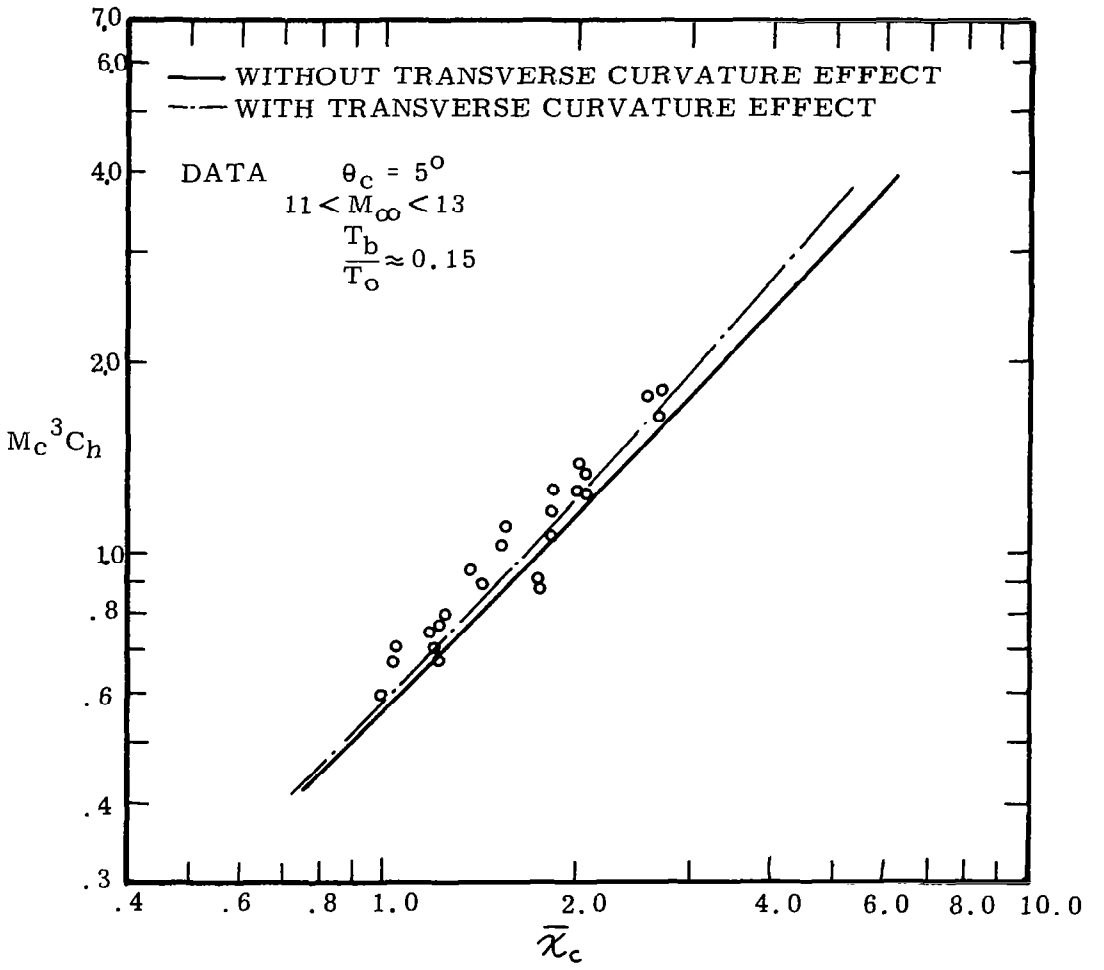

FIG. 18 COMPARISON OF THEORETICAL PREDICTIONS OF HEAT TRANSFER ON A COLD SLENDER CONE WITH EXPERIMENTAL RESULTS OBTAINED BY WITTLIFF AND WILSON (REF. 28)

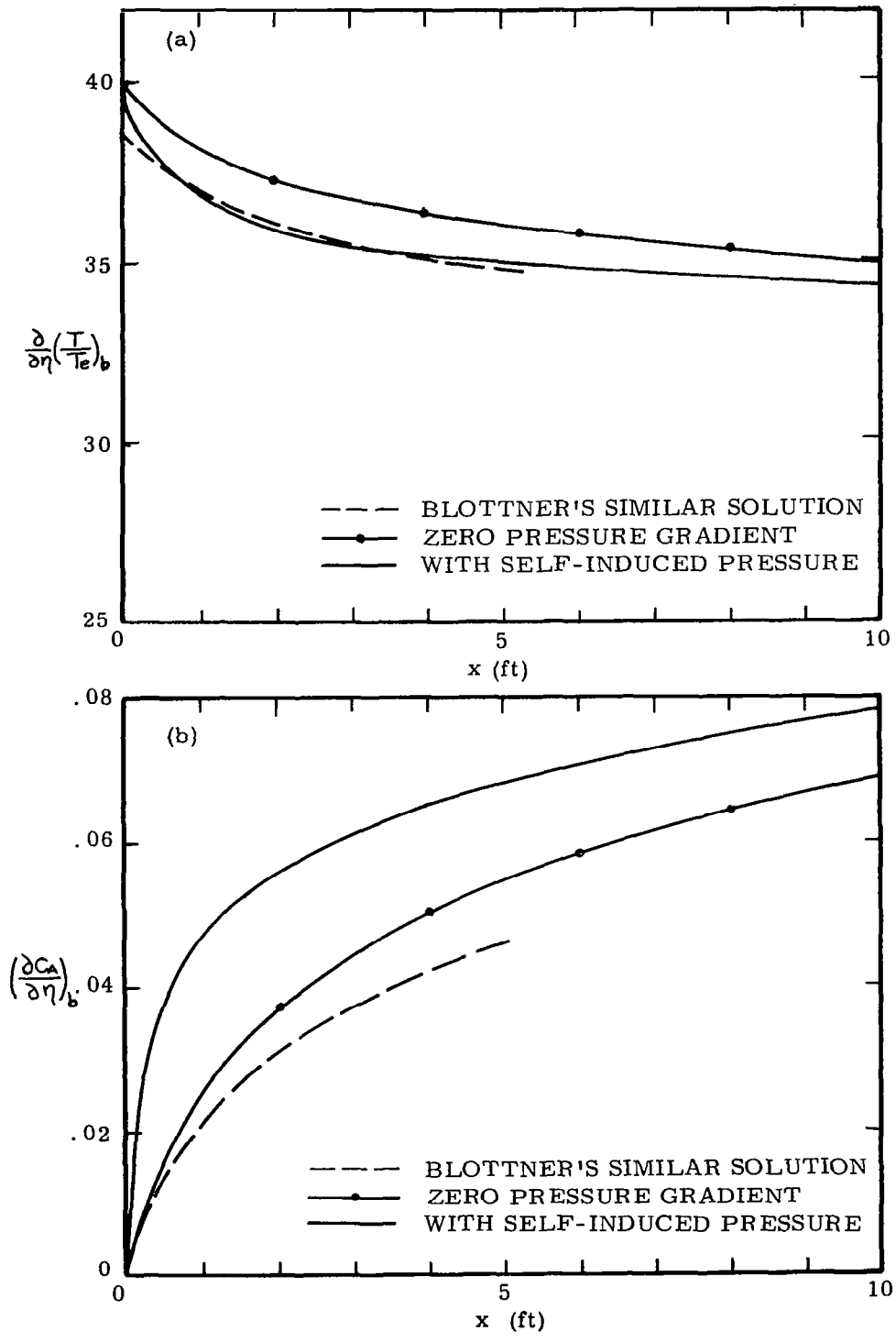

FIG. 19a, b TEMPERATURE GRADIENT AND ATOM MASS FRACTION AT THE WALL WITH FULL CATALICITY AT ZERO PRESSURE GRADIENT

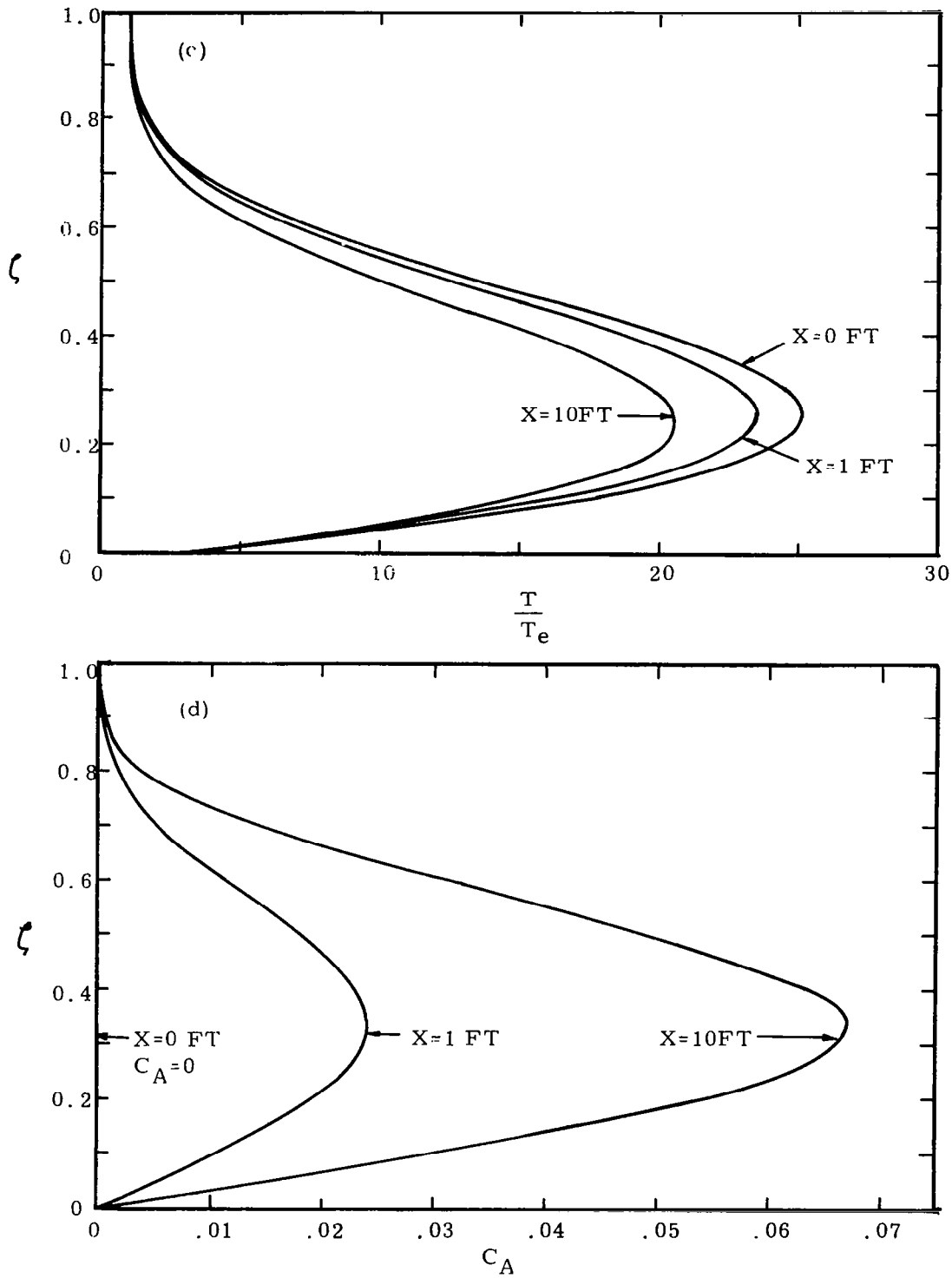

FIG. 19c, d TEMPERATURE AND ATOM MASS FRACTION PROFILES AT ZERO PRESSURE GRADIENT

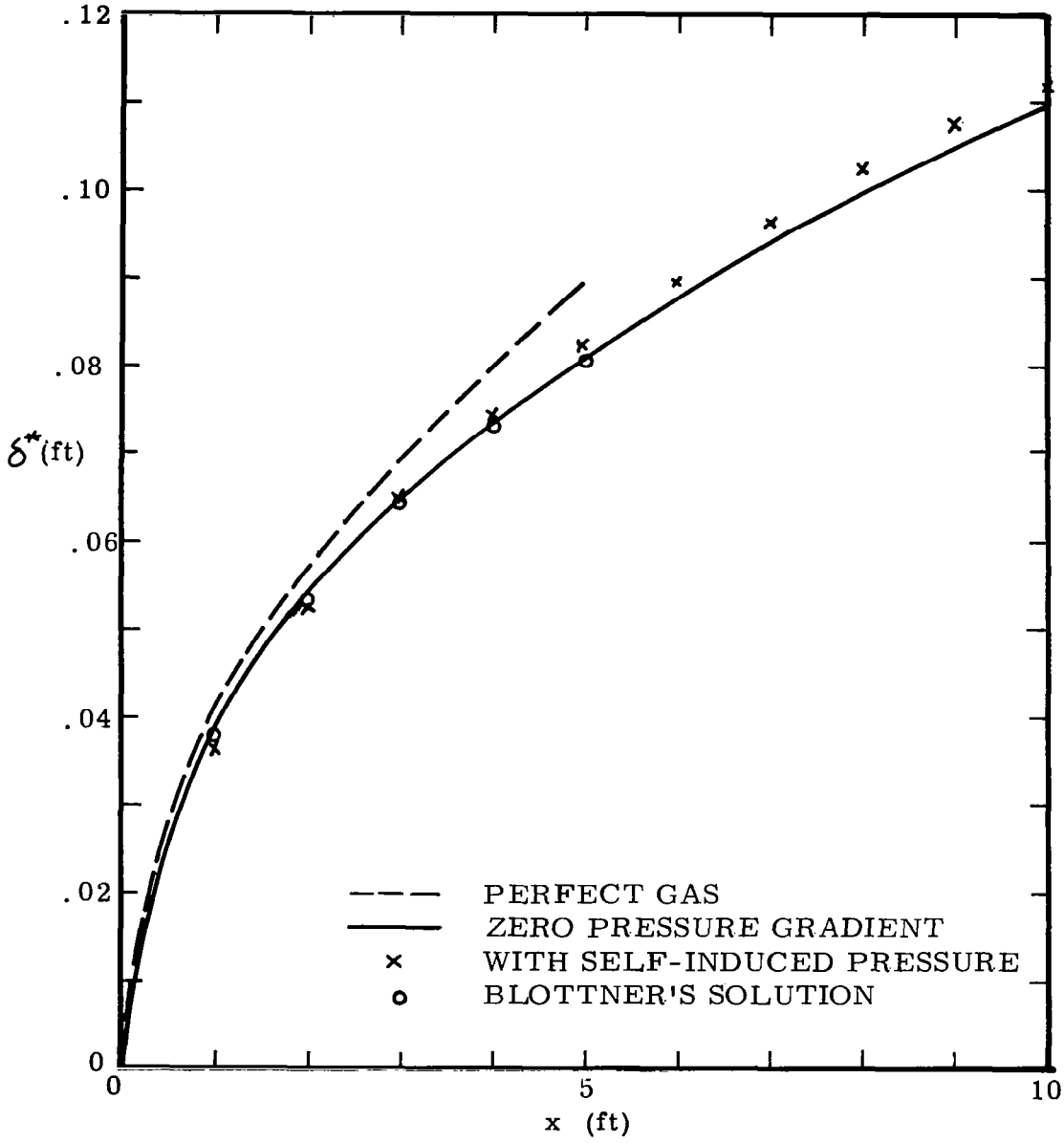

FIG. 20 DISPLACEMENT THICKNESS FOR FLOW ALONG A CATALYTIC FLAT PLATE

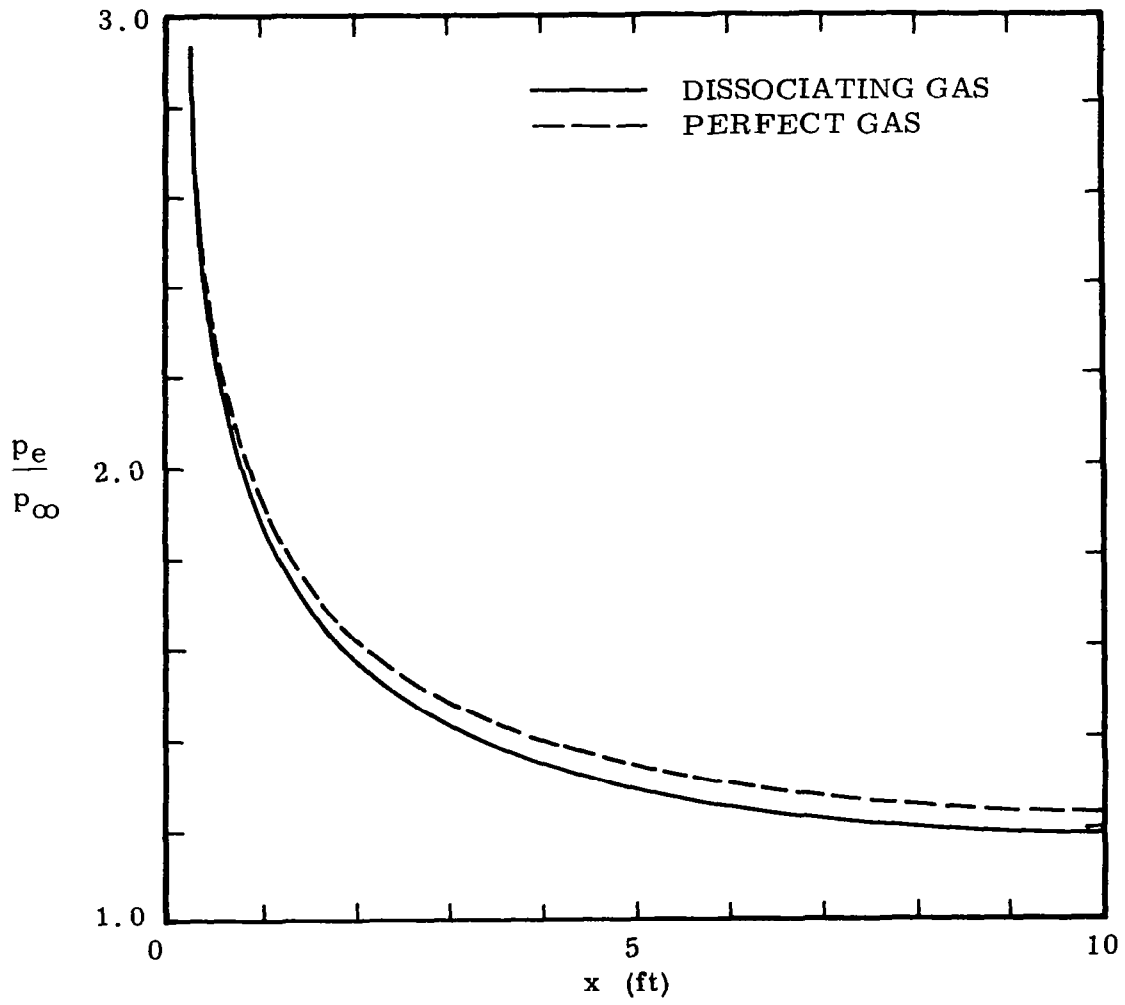

FIG. 21 VARIATION OF PRESSURE DUE TO DISPLACEMENT EFFECT ALONG A CATALYTIC FLAT PLATE

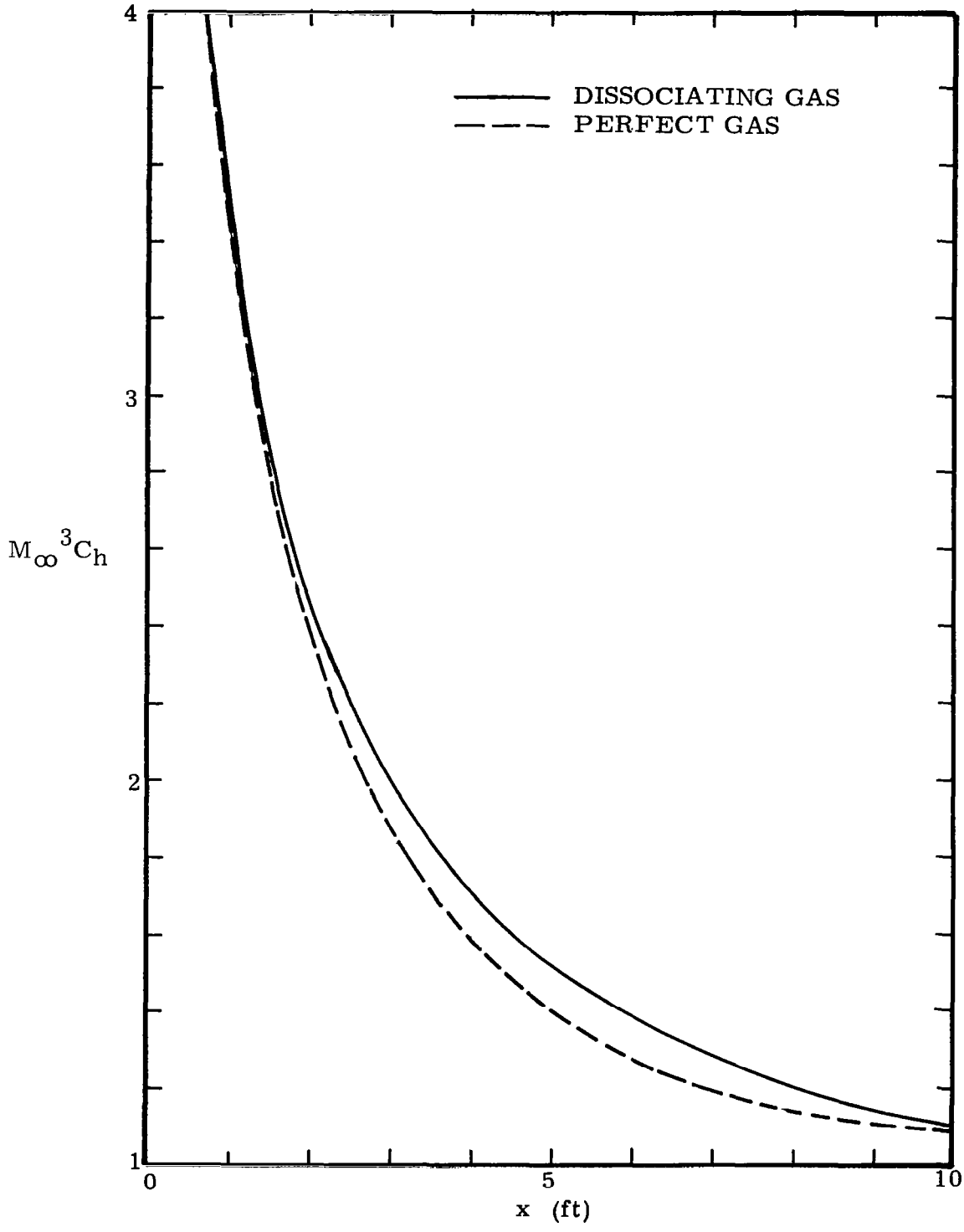

FIG. 22 HEAT TRANSFER ALONG A CATALYTIC FLAT PLATE

APPENDIX A

Momentum Integral Method

In the discussion of Section 2.4, it has been pointed out that if the one-parameter correlation is used, only one equation is required to obtain the ξ dependency of λ and $\varkappa$. Here we rewrite the momentum integral and the energy integral equations, Eqs. (2.15 and 2.18) as

$$f_{\eta\eta_b} = \Theta + 2\xi \frac{d\Theta}{d\xi} + \frac{H_e}{h_e} \frac{2\xi}{u_e} \frac{du_e}{d\xi} (\Delta + \Theta) \tag{2.15}$$

$$\frac{g_{\eta_b}}{P_r(1-g_b)} = \bar{\Lambda} + 2\xi \frac{d\bar{\Lambda}}{d\xi} \tag{2.18}$$

Multiply Eq. (2.15) by Θ and Eq. (2.18) by $\bar{\Lambda}$ and rearrange, results

$$\frac{d}{d\xi}(\xi\Theta^2) = \Theta f_{\eta\eta_b} - \frac{H_e}{h_e} \frac{2\xi}{u_e} \frac{du_e}{d\xi} \Theta^2 (1 + H_F) \tag{2.20}$$

$$\frac{d}{d\xi}(\xi\bar{\Lambda}^2) = \frac{\bar{\Lambda}\, g_{\eta_b}}{P_r(1-g_b)} \tag{2.21}$$

In the method of momentum integral (Ref. 3), the energy integral equation is ignored and the momentum integral equation alone is used. If the following relations are defined:

$$\bar{m} = \frac{H_e}{h_e} \frac{\xi}{u_e} \frac{du_e}{d\xi} \Theta^2 \tag{A.1}$$

$$l = \Theta f_{\eta\eta_b} \tag{A.2}$$

$$\bar{r} = \frac{\bar{\Lambda}\, g_{\eta_b}}{P_r(1-g_b)} \tag{A.3}$$

$$H_F = \frac{\Delta}{\Theta} \tag{A.4}$$

Then the momentum integral equation (2.20) can be written with the defanations of (A.1), (A.2) and (A.4) as

$$\frac{d}{d\xi}\left(\bar{m} \frac{h_e}{He} \frac{u_e}{u_{e\xi}}\right) = \bar{L} \tag{A.5}$$

where

$$\bar{L} = l - 2\bar{m}(1 + H_F) \tag{A.6}$$

Equation (A. 5) can be integrated if $\bar{L}$ is assumed as a function of $\bar{m}$ only, for a given surface temperature. This is the basic assumption of the one-parameter integral method and in Thwaites' or Cohen and Reshotko's approach (Refs. 1 and 3), the functional relation $\bar{L}(\bar{m})$ is provided by the exact similarity solutions. If a peicewise linear approximation for the function $\bar{L}(\bar{m})$ is used, such that

$$\bar{L} = \bar{A} - \bar{B}\,\bar{m} \tag{A. 7}$$

Then Eq. (A. 5) becomes a simple first order ordinary differential equation and can be integrated to yield $\bar{m}$

$$\bar{m} = \frac{He}{he}\frac{u_{e\xi}}{u_e}\left(\exp - \int_{u_{e_0}}^{u_e} \bar{B}'\frac{du_e}{u_e}\right)\left[C + \int_{\xi_0}^{\xi} \bar{A}\left(\exp \int_{u_{e_0}}^{u_e} \bar{B}'\frac{du_e}{u_e}\right)d\xi\right] \tag{A. 8}$$

where $\bar{B}' = \frac{He}{he}\bar{B}$

and the constant C is determined at $\xi = \xi_0$ as

$$C = \Theta_0^2\,\xi \tag{A. 9}$$

If the integration starts from the leading edge, then C = 0.

Once the dependency of $\bar{m}$ on x (or ξ) is known, the boundary layer characteristics follow directly from the correlations which are based on the similarity solutions.

Equation (A. 8) can be transformed back to the physical coordinates as

$$\bar{m} = -\frac{\gamma-1}{2\gamma}\frac{1}{u_e}P^{-\bar{\alpha}}\left(1-P^{\frac{\gamma-1}{\gamma}}\right)^{-\bar{\beta}}\frac{dP}{dx}\left[\Theta_0^2 u_{e_0} x_0 P_0^{\bar{\alpha}-1}\left(1-P_0^{\frac{\gamma-1}{\gamma}}\right)^{\bar{\beta}-1} + \int_{x_0}^{x} \bar{A}\,P^{\bar{\alpha}-1}\left(1-P^{\frac{\gamma-1}{\gamma}}\right)^{\bar{\beta}-1} u_e\,dx\right] \tag{A. 10}$$

where

$$\begin{aligned} \bar{\alpha} &= 2 - \frac{\gamma-1}{2\gamma}\bar{B} \\ \bar{\beta} &= 1 + \frac{\bar{B}}{2} \\ P &= p_e/p_s \end{aligned} \tag{A. 11}$$

The skin friction coefficient is given as

$$C_{f_b}\sqrt{Re_{x_b}} = \sqrt{\frac{2\rho_b u_e x/\mu_b}{\int_0^x \rho_b\mu_b u_e\,dx}}\; f_{\eta\eta_b} \tag{A. 12}$$

and the modified Reynolds' analogy gives

$$\frac{C_{f_1}}{C_{h_b}} = \frac{2 f_{\eta\eta_b}}{\frac{g_{\eta_b}}{1 - g_b}} \tag{A. 13}$$

where

$$C_{f_b} = 2\tau_b / \rho_b u_e^2$$
$$Re_{x_b} = \frac{\rho_b u_e x}{\mu_b} \tag{A. 14}$$
$$C_{h_b} = \frac{-q_b}{\rho_b u_b (H_e - H_b)}$$

are the skin friction coefficient, the local Reynolds number and the heat transfer coefficient respectively with reference to the surface conditions.

In the one-parameter method, however, the energy integral equation can also be used to solve the problem with a suitable correlation based on the similarity solutions. The results obtained by the momentum integral and the energy integral equations are not the same in general. This has been shown in Refs. 4 and 5 that only if the thicknesses $\bar{\Lambda}$ and Θ are proportional to each other over the entire range of consideration, that these two equations will yield a similar result.

The momentum integral equation (A. 5) is

$$\frac{d}{d\xi}\left(\bar{m}\frac{h_e}{H_e}\frac{u_e}{u_{e\xi}}\right) = 1 - 2\bar{m}(1 + H_F) \tag{A. 5}$$

and the energy integral equation (2. 21) can be written with the definations (A. 1) and (A. 3)

$$\frac{d}{d\xi}\left(\bar{m}\frac{h_e}{H_e}\frac{u_e}{u_{e\xi}}\frac{\bar{\Lambda}^2}{\Theta^2}\right) = \bar{r} \tag{A. 15}$$

or by expanding the left hand side,

$$\frac{d}{d\xi}\left(\bar{m}\frac{h_e}{H_e}\frac{u_e}{u_{e\xi}}\right) = \frac{\Theta^2}{\bar{\Lambda}^2}\bar{r} - \bar{m}\frac{h_e}{H_e}\frac{u_e}{u_{e\xi}}\frac{\Theta^2}{\bar{\Lambda}^2}\frac{d}{d\xi}\left(\frac{\bar{\Lambda}^2}{\Theta^2}\right) \tag{A. 16}$$

If $\bar{\Lambda}/\Theta$ is constant throughout the entire range, then the second term at the right hand side of Eq. (A. 16) becomes zero. For similarity solutions, the boundary layer characteristics do not depend on ξ , Eqs. (2. 15) and (2. 18) yield

$$\bar{r}\frac{\Theta^2}{\bar{\Lambda}^2} = \Theta f_{\eta\eta_b} - \frac{H_e}{h_e}\frac{2\xi}{u_e}\frac{du_e}{d\xi}\Theta^2(1 + H_F) \tag{A. 17a}$$

or

$$\bar{r}\frac{\Theta^2}{\bar{\Lambda}^2} = 1 - 2\bar{m}(1 + H_F) \tag{A. 17b}$$

Therefore, if $\bar{\Lambda}/\Theta$ is constant, then Eq. (A. 17b) shows immediately that Eq. (A. 7) and Eq. (A. 16) yield a similar result.

However, in general, these thicknesses $\bar{\Lambda}$ and Θ are not proportional to each other over the entire range of consideration. The variation of the ratio will appear in the second term at the right hand side of (A. 16) and will effect the computation of heat transfer. The discussion of taking into account of this point within the base of the one-parameter method is given in Section 2. 4.

APPENDIX B

Solution of the Pressure Interaction Problem by Iteration

The system of equations developed in the Section 4. 1 for the computation of the pressure interaction problem are rewritten here as

$$m = -\frac{\gamma-1}{2\gamma} A\left[\bar{\chi}^3 \frac{d}{d\bar{\chi}}\left(\frac{p_e}{p_\infty}\right)\right]\left(\frac{p_e}{p_\infty}\right)^{-\alpha}\int_{\bar{\chi}_0}^{\bar{\chi}} \left(\frac{p_e}{p_\infty}\right)^{\alpha-1} \frac{d\bar{\chi}}{\bar{\chi}^3} \tag{4.7}$$

$$\Delta^{*2} = -(\gamma-1)^2 A \frac{(1+H_F)^2}{1+Q^2}\left(\frac{p_e}{p_\infty}\right)^{-\alpha}\int_{\bar{\chi}_0}^{\bar{\chi}} \left(\frac{p_e}{p_\infty}\right)^{\alpha-1} \frac{d\bar{\chi}}{\bar{\chi}^3} \tag{4.8}$$

and the tangent-wedge relation

$$-\frac{1}{2}\bar{\chi}^3 \frac{d\Delta^*}{d\bar{\chi}} = \sqrt{\frac{2}{\gamma(\gamma+1)}} \frac{\frac{p_e}{p_\infty}-1}{\sqrt{\frac{p_e}{p_\infty}+\frac{\gamma-1}{\gamma+1}}} \tag{4.9}$$

In principle, a certain pressure distribution is assumed, which in turn yields the pressure gradient parameter m as a function of $\bar{\chi}$ and thus the value of $(1 + H_F)^2/(1 + Q^2)$. Then the displacement thickness Δ^* is computed. A new pressure distribution is then calculated by the tangent-wedge relation using the computed local displacement thickness. The procedure is then repeated until convergence is reached.

It is noted that the value of the parameter $(1 + H_F)^2/(1 + Q^2)$ varies only slightly through the whole pressure range of the problem, especially for a very cold surface (see Fig. 7). Thus a mean value is chosen for this parameter for a given total enthalpy ratio g_b and is held constant through the computation. If this is done, the pressure distribution can then be calculated by using Eqs. (4. 8) and (4. 9) only.

At the leading edge $x \to 0$, and $\bar{\chi} \to \infty$. It is difficult to choose the starting point $\bar{\chi}_0$ for the numerical integration and estimate the initial pressure near the singularity. Numerical instability did arise due to small errors in the initial estimation. Thus a further transformation is desirable so that the singularity at infinity is transformed back to the origin. Introduce the following transformation

$$\bar{z} = \frac{1}{\bar{\chi}^2} \tag{B.1}$$

$$P = \frac{p_e}{p_\infty} \tag{B.2}$$

then the Eqs. (4. 9) and (4. 8) reduce to

$$\frac{d\Delta^*}{d\bar{z}} = \sqrt{\frac{2}{\gamma(\gamma+1)}} \frac{\frac{1}{P}-1}{\sqrt{\frac{1}{P}+\frac{\gamma-1}{\gamma+1}}} \tag{B.3}$$

$$\Delta^{*2} = \frac{(\gamma-1)^2}{2} A \frac{(1+H_F)^2}{1+Q^2} P^\alpha \int_{\bar{z}_0}^{\bar{z}} P^{1-\alpha} d\bar{z} \tag{B.4}$$

The tangent-wedge relation can then be integrated to yield the displacement thickness

$$\Delta^* = \sqrt{\frac{2}{\gamma(\gamma+1)}} \int_{z_0}^{z} \frac{\frac{1}{P}-1}{\sqrt{\frac{1}{P}+\frac{\gamma-1}{\gamma+1}}}\, dz \tag{B. 5}$$

Eliminating the displacement thickness from the above equations, we obtain an expression suitable for iteration procedure

$$P(z) = \left[\frac{4}{\gamma(\gamma+1)(\gamma-1)^2}\,\frac{1+Q^2}{(1+H_F)^2}\,\frac{1}{A}\right]^{\frac{1}{\alpha}} \left[\frac{\left(\int_0^z \frac{\frac{1}{P}-1}{\sqrt{\frac{1}{P}+\frac{\gamma-1}{\gamma+1}}}\, dz\right)^2}{\int_0^z P^{1-\alpha}\, dz}\right]^{\frac{1}{\alpha}} \tag{B. 6}$$

The quantities in the first bracket and α are now all constant and depend only on the specified g_b. For a given initial pressure distribution, we can calculate a new $P(z)$ by performing two integrations inside the second bracket. In the present computation, the asymptotic solutions of the strong interaction are used as initial values for the iteration. The results show that only five iterations are needed to give accuracy up to five digits.

APPENDIX C

Method of Local Similarity

The local similarity method is based on the condition that the external flow and the body properties vary sufficiently slowly with the x-dependent variable ξ . If this is the case, then derivatives with respect to ξ of the boundary-layer dependent variables are small compared with the corresponding η derivatives. So that the right hand sides of the transformed boundary layer equations (2. 9) and (2. 10) can be neglected. Those terms on the left hand sides which are functions of ξ are assumed to take on their local values and the boundary layer equations are considered as ordinary differential equations in η with ξ as a parameter. Local similarity thus presents a "patching together" of local solutions in which the history of the flow is involved only in the ξ dependence of the definition of η in the transformation (Eq. 2.7a).

The limit of this approximation can be shown through the integrated boundary layer equations (see also Ref. 14). If we write Eqs. (2. 15) and (2. 16) in a slightly different form, namely

$$f_{\eta\eta_b} = \Theta\left[1 + 2\frac{\xi}{\Theta}\frac{d\Theta}{d\xi} + \frac{H_e}{h_e}\frac{2\xi}{u_e}\frac{du_e}{d\xi}(1+H_F)\right] \tag{2.15}$$

$$\frac{g_{\eta_b}}{P_r} = \Lambda\left[1 + \frac{2\xi}{\Lambda}\frac{d\Lambda}{d\xi}\right] \tag{2.16}$$

the derivatives of the boundary layer characteristics with respect to ξ appear only in the second term of both equations.

Thus if both

$$\frac{\xi}{\Theta}\frac{d\Theta}{d\xi} \ll 1$$

and

$$\frac{\xi}{\Lambda}\frac{d\Lambda}{d\xi} \ll 1$$

then these equations reduced to the following form with these two terms neglected

$$f_{\eta\eta_b} = \Theta\left[1 + \beta(1+H_F)\right] \tag{C. 1}$$

$$\frac{g_{\eta_b}}{P_r} = \Lambda \tag{C. 2}$$

where

$$\beta = \frac{H_e}{h_e}\frac{2\xi}{u_e}\frac{du_e}{d\xi} \tag{C. 3}$$

is a variable depending only on the external flow condition. In general β is a function of ξ . If β is assumed to take on its local value and be constant locally, then the above equations give nothing more than the relations of boundary layer characteristics for the similarity solutions at that local point. The error introduced by neglecting the logarithmic derivative terms can be estimated with thelp of the similarity solutions. We may write for

$$\frac{\xi}{\Theta}\frac{d\Theta}{d\xi} = \left(\frac{\xi}{\beta}\frac{d\beta}{d\xi}\right)\left(\frac{\beta}{\Theta}\frac{d\Theta}{d\beta}\right) \tag{C.4}$$

The first bracket at the right hand side contains the logarithmic derivative of β with respect to ξ . This term is determined completely by the external conditions. The second bracket contains the logarithmic derivative of the momentum thickness with respect to β and can be estimated with the help of similarity solutions. Thus if both terms are small, the error introduced by neglecting the ξ derivative term will be small and the local similarity method may provide a good approximation. Similarly we can estimate the order of magnitude of the logarithmic derivative of Λ with respect to ξ in the energy integral equation. Therefore, we can see that for cases where the logarithmic derivative of θ and Λ is much less than unity, the method of local similarity can be used.

The local similarity concept has been applied to a number of problems with success. The application of this method to the boundary layer problem with a self-induced pressure field was given in Ref. 14. With the integral method formulated herein and the use of the local similarity concept, solutions in closed form can be obtained for the pressure interaction problem.

Two-Dimensional Flow

The boundary layer displacement thickness was defined by

$$\delta^* = \int_0^\delta \left(1 - \frac{\rho u}{\rho_e u_e}\right) dy \tag{3.4}$$

Through the transformation (2.7a)

$$\delta^* = \frac{\sqrt{2\xi}}{\rho_e u_e}\int_0^\infty \left(\frac{\rho_e}{\rho} - f_\eta\right) d\eta \tag{3.4a}$$

in terms of external flow conditions

$$\delta^* = \frac{\sqrt{2C}}{\sqrt{Re_{x\infty}}}\,\frac{\left[x\int_0^x \frac{\rho_e}{\rho_\infty}\,dx\right]^{\frac{1}{2}}}{\frac{\rho_e}{\rho_\infty}}\,I(x) \tag{3.4b}$$

where

$$I(x) = \int_0^\infty \left(\frac{\rho_e}{\rho} - f_\eta\right) d\eta$$

The derivative of the displacement thickness with respect to x is thus

$$\frac{d\delta^*}{dx} = \frac{\sqrt{C}}{\sqrt{2 Re_{x\infty}}} \left(\frac{p_e}{p_\infty}\right)^{-1} \left(\frac{\int_0^x \frac{p_e}{p_\infty} dx}{x} \right)^{\frac{1}{2}} I(x) \left[1 - \frac{x}{p_e}\frac{dp_e}{dx} + \frac{x}{\bar{\lambda}}\frac{d\bar{\lambda}}{dx} + \frac{x}{I}\frac{dI}{dx} \right] \qquad (C.5)$$

where

$$\bar{\lambda} = \frac{\int_0^x \frac{p_e}{p_\infty} dx}{\frac{p_e}{p_\infty} x}$$

Here again, we assume that an effective body is formed by the original body and the additional thickness due to the growth of the boundary layer. The flow inclination at the outer edge of the boundary layer thus consists of the geometric slope and the slope of the displacement thickness of the boundary layer.

The quantity $\bar{\lambda}$ (x) depends only on the external pressure distribution. For flows over a slender body, the quantity $\bar{\lambda}$ (x) is a slowly varying function of x. Thus the logarithmic derivative of it is small in magnitude compared with terms of order unity. The order of magnitude of the logarithmic derivative of I can be estimated with the help of the similarity solutions. If we write

$$\frac{x}{I}\frac{dI}{dx} = \left(\frac{x}{\beta}\frac{d\beta}{dx}\right)\left(\frac{\beta}{I}\frac{dI}{d\beta}\right) \qquad (C.6)$$

where β is the pressure gradient parameter defined by Eq. (C.3). We know from the similar solutions that I is a slowly varying function of β, and if β changes only slowly along x, we can conclude that this logarithmic derivative of I is small in comparison with order of unity.

Thus if we neglect all terms with order of magnitude much smaller than unity from Eq. (C.5), we have

$$\frac{d\delta^*}{dx} = \frac{\sqrt{C}}{\sqrt{2 Re_{x\infty}}} \left(\frac{p_e}{p_\infty}\right)^{-1} \left(\frac{\int_0^x \frac{p_e}{p_\infty} dx}{x} \right)^{\frac{1}{2}} I(x) \left[1 - \frac{x}{p_e}\frac{dp_e}{dx} \right] \qquad (C.7)$$

If we further assume that $p \propto x^n$ locally, and I takes the value from the similarity solution corresponding to the local value of n, then the right hand side of Eq. (C.7) is now an explicit function of n and x. From the assumption $p \propto x^n$, we can write (Ref. 14)

$$n = \frac{x}{p_e}\frac{dp_e}{dx} = \left(\frac{K^2}{p_e}\frac{dp_e}{dK^2}\right)\left(\frac{x}{K^2}\frac{dK^2}{dx}\right) \qquad (C.8)$$

where K is the hypersonic similarity parameter

$$K = M_\infty \left(\theta_b + \frac{d\delta^*}{dx}\right) \qquad (C.9)$$

The first bracket on the right hand side of Eq. (C. 8) relates the pressure field p_e and the hypersonic similarity parameter K. This term is concerned solely with the inviscid flow field and theories in inviscid flow should be able to provide the required relation. The second bracket consists of the relation between the change of K along x, i.e., the growth of the boundary layer along x. Thus from Eq. (C. 9)

$$\frac{\chi}{K^2}\frac{dK^2}{d\chi} = \frac{2\chi}{\theta_b}\frac{d\theta_b}{d\chi} + \frac{2\chi}{\theta_b}\frac{d^2\delta^*}{d\chi^2}$$

From Eq. (C. 7) we can show that

$$\chi\frac{d^2\delta^*}{d\chi^2} = -\left(\frac{n+1}{2}\right)\frac{d\delta^*}{d\chi}$$

and from Eq. (C. 9)

$$\frac{d\delta^*}{d\chi} = \frac{K - K_{\theta_b}}{M_\infty} \qquad \text{(C. 10)}$$

where, $K_{\theta_b} = M_\infty \theta_b$

Therefore

$$\frac{\chi}{K^2}\frac{dK^2}{d\chi} = -(n+1)\frac{K - K_{\theta_b}}{K} \qquad \text{(C. 11)}$$

where, the term $d\ln\theta_b / d\ln\chi$ is neglected for a slender body. Hence

$$n = \left(\frac{K^2}{p_e}\frac{dp_e}{dK^2}\right)\left[-(n+1)\left(1 - \frac{K_{\theta_b}}{K}\right)\right]$$

Solving for n yields

$$n = \frac{-\left(\frac{K^2}{p_e}\frac{dp_e}{dK^2}\right)\left(1 - \frac{K_{\theta_b}}{K}\right)}{1 + \left(\frac{K^2}{p_e}\frac{dp_e}{dK^2}\right)\left(1 - \frac{K_{\theta_b}}{K}\right)} \qquad \text{(C. 12)}$$

The relation of pressure to the local flow inclination is provided by the tangent-wedge relation as

$$\frac{K^2}{p_e}\frac{dp_e}{dK^2} = \frac{\frac{\gamma}{2}K^2\left[\left(\sqrt{\left(\frac{\gamma+1}{2}\right)^2 + \frac{4}{K^2}} + \frac{\gamma+1}{2}\right) - 2\left(\left(\frac{\gamma+1}{4}\right)^2 + \frac{4}{K^2}\right)^{-\frac{1}{2}}\frac{1}{K^2}\right]}{1 + \frac{\gamma}{2}K^2\left[\left(\left(\frac{\gamma+1}{2}\right)^2 + \frac{4}{K^2}\right)^{\frac{1}{2}} + \frac{\gamma+1}{2}\right]} \qquad \text{(C. 13)}$$

By using K as a parameter, n can be computed from the Eq. (C. 12). The pressure can then be calculated from the tangent-wedge relation, which gives the relation of p_e/p_∞ and K.

$$\frac{p_e}{p_\infty} = 1 + \frac{\gamma}{2}K^2\left[\sqrt{\left(\frac{\gamma+1}{2}\right)^2 + \frac{4}{K^2}} + \frac{\gamma+1}{2}\right] \qquad \text{(C. 14)}$$

The relation between the parameter K and the distance x is provided by the boundary layer thickness relation. If the expression for the boundary layer displacement thickness δ^* obtained by the integral method is used, Eq. (3. 6)

$$\delta^{*2} = \frac{C x M_\infty^4}{Re_{x\infty}} \frac{(\gamma-1)^2}{2} A \frac{(1+H_F)^2}{1+Q^2}\left(\frac{p_e}{p_\infty}\right)^{-\alpha}\int_0^x \left(\frac{p_e}{p_\infty}\right)^{\alpha-1} dx \qquad \text{(3. 6)}$$

Equation (C. 10), with the assumption $p \propto x^n$, yields in closed form

$$K - K_{\theta_b} = \frac{\gamma-1}{2}\sqrt{\frac{A}{2}} \frac{1+H_F}{\sqrt{1+Q^2}} \frac{1-n}{[n(\alpha-1)+1]^{\frac{1}{2}}}\sqrt{\frac{p_\infty}{p_e}}\,\bar{\chi} \qquad \text{(C. 15)}$$

where $\bar{\chi} = \dfrac{\sqrt{C}M_\infty^3}{\sqrt{Re_{x\infty}}}$ is the interaction parameter.

Thus a functional relation of p_e/p_∞ and $\bar{\chi}$ is finally formed through (C. 14) and (C. 15). The skin friction coefficient follows immediately as

$$M_\infty^3 C_f = \sqrt{\frac{2}{A}}\,\bar{\chi}\,(n(\alpha-1)+1)^{\frac{1}{2}}\sqrt{\frac{p_e}{p_\infty}}\sqrt{1+Q^2}\,l \qquad \text{(C. 16)}$$

where $\sqrt{1+Q^2}\,l$ is now a function of the pressure gradient parameter m, where

$$m = -\frac{\gamma-1}{2\gamma} A \frac{n}{n(\alpha-1)+1} \qquad \text{(C. 17)}$$

The heat transfer coefficient can then be calculated through the modified Reynolds analogy once m and the skin friction coefficient are known, or directly as

$$M_\infty^3 C_h = \frac{1}{2}\sqrt{\frac{2}{A}}\,\bar{\chi}\,(n(\alpha-1)+1)^{\frac{1}{2}}\sqrt{\frac{p_e}{p_\infty}}\sqrt{\frac{1+Q^2}{Q^2}}\,\bar{r} \qquad \text{(C. 18)}$$

Hence by using K as a parameter, n and p_e/p_∞ can be computed from Eqs. (C. 12), (C. 13) and (C. 14) respectively. For a flat plate $\theta_b = 0$, and here the quantities can be computed once and for all. The numerical value of these functional relations for a flat plate are listed in Table V. For a body with specified surface temperature, the relation between the parameter K and the interaction parameter $\bar{\chi}$ is given by Eq. (C. 15). Skin

friction and heat transfer can then be computed from Eqs. (C. 16) and (C. 18) respectively.

Since this method refers only to local conditions, the formulation can also be applied to cases with surface temperature varying along the body. In such cases, the boundary layer parameters A, α , $(1+H_F)/(1+Q^2)$, etc. are chosen to correspond to the local g_b along the surface.

The solutions obtained by the foregoing formulation are compared with solutions obtained by using the integral method through several examples. The details of a discussion is given in Sec. 4. 3.

Axisymmetric Flow

The local similarity method can be readily applied for axisymmetric flow in a similar way as for two-dimensional case. Due to lack of information on similarity solutions with transverse curvature effect, only the case with negligible transverse curvature effect is considered here. In this case, all necessary information can be obtained through the Mangler transformation from the two-dimensional formulation.

The boundary-layer displacement-thickness integral has been shown to be in the following form for slender bodies with a constant surface temperature distribution

$$\delta^{*2} = \frac{2\chi M_c^4}{Re_{xc}} \frac{(\gamma-1)^2}{2} A \frac{(1+H_F)^2}{1+Q^2} \frac{1}{r_b^2} \left(\frac{p_e}{p_c}\right)^{-\alpha} \int_0^{\chi} \left(\frac{p_e}{p_c}\right)^{\alpha-1} r_b^2 \, d\chi \tag{4.29}$$

where, the subscript c refers to conditions on the body surface when the boundary layer is absent and r_b is the radius of the body measured from the axis of symmetry. For conical body,

$$\delta^{*2} = \frac{2\chi M_c^4}{Re_{xc}} \frac{(\gamma-1)^2}{2} A \frac{(1+H_F)^2}{1+Q^2} \frac{1}{\chi^2} \left(\frac{p_e}{p_c}\right)^{-\alpha} \int_0^{\chi} \left(\frac{p_e}{p_c}\right)^{\alpha-1} \chi^2 \, d\chi \tag{C. 19}$$

The induced pressure due to the local flow inclination is approximated by the tangent-cone relation. If

$$K_c = M_\infty \theta_e = M_\infty \left(\theta_c + \frac{d\delta^*}{d\chi}\right) \tag{C. 20}$$

then for $K_e \gg 1$, we use Lees' results (Ref. 26) for slender cones when the conical shock wave is not too far away from the cone surface. The relation is in the form

$$\frac{p_e}{p_\infty} - 1 = \frac{2\gamma}{\gamma+1}(K_s^2 - 1) + \gamma(K_s - K_e)^2\left[\frac{\gamma+1}{(\gamma-1)+\frac{2}{K_s^2}}\right]$$

$$K_s = \frac{\gamma+1}{\gamma+3}K_e + \sqrt{\left(\frac{\gamma+1}{\gamma+3}K_e\right)^2 + \frac{2}{\gamma+3}} \qquad \text{(C. 21)}$$

where $K_s = M_\infty \theta_s$, θ_s is the half angle of the conical shock and $K_e = M_\infty \theta_e$, $K_c = M_\infty \theta_c$.

The relation of K_s and K_e can be approximated by the form (Ref. 26)

$$\frac{K_s}{K_e} = \sqrt{\frac{\gamma+1}{2} + \frac{1}{K_e^2}} \qquad \text{(C. 22)}$$

Following the approach of the two-dimensional case, we can assume again that $p \propto x^n$. By taking n to be a constant locally, we can derive the variation of n as

$$n = \frac{-\frac{K_e^2}{p_e}\frac{dp_e}{dK_e^2}\left(1 - \frac{K_c}{K_e}\right)}{1 + \frac{K_e^2}{p_e}\frac{dp_e}{dK_e^2}\left(1 - \frac{K_c}{K_e}\right)} \qquad \text{(C. 23)}$$

The term $\frac{K_e^2}{p_e}\frac{dp_e}{dK_e^2}$ is given by the tangent-cone relation

$$\frac{K_e^2}{p_e}\frac{dp_e}{dK_e^2} = \frac{\frac{\gamma(\gamma+1)}{8}K_e^2}{1 + \frac{2\gamma}{\gamma+1}\left[\frac{\gamma+1}{8}\left(1 + \frac{\gamma+1}{2}K_e^2\right)^2 - \frac{3}{4}\right]} \qquad \text{(C. 24)}$$

Thus by using Ke as a parameter, we can calculate the value of n along the body from Eqs. (C. 23) and (C. 24). The pressure distribution is calculated by the tangent-cone relation Eq. (C. 21). The relation between Ke and the interaction parameter $\bar{\chi}_c$ can be derived from the boundary-layer displacement-thickness integral (C. 19) as

$$K_e - K_c = \frac{\gamma-1}{2}\sqrt{\frac{A}{2}}\frac{1+H_F}{\sqrt{1+Q^2}}\frac{1-n}{\left[n(\alpha-1)+3\right]^{\frac{1}{2}}}\sqrt{\frac{p_c}{p_e}}\,\bar{\chi}_c \qquad \text{(C. 25)}$$

Here p_c is the pressure on the cone surface when the viscosity effect is absent. The pratio of p_c/p_∞ can be obtained from standard conical flow solutions (Ref. 27).

Similarly, the pressure gradient parameter m is given as

$$m = -\frac{\gamma-1}{2\gamma}A\frac{n}{n(\alpha-1)+3} \qquad \text{(C. 26)}$$

and the skin-friction coefficient as

$$M_c^3 C_f = \sqrt{\frac{2}{A}}\,\bar{x}_c\,(n(\alpha-1)+3)^{\frac{1}{2}}\sqrt{\frac{p_e}{p_c}}\sqrt{1+Q^2}\,I \qquad \text{(C. 27)}$$

The heat-transfer coefficient can then be calculated through the modified Reynolds analogy once m and the skin friction coefficient is known, or directly as

$$M_c^3 C_h = \frac{1}{2}\sqrt{\frac{2}{A}}\,\bar{x}_c\,(n(\alpha-1)+3)^{\frac{1}{2}}\sqrt{\frac{p_e}{p_c}}\sqrt{\frac{1+Q^2}{Q^2}}\,\bar{r} \qquad \text{(C. 28)}$$

NASA-Langley, 1965 CR-284